UNIVERSITY OF CALIFORNIA, SAN DIEGO
SCRIPPS INSTITUTION OF OCEANOGRAPHY
VISIBILITY LABORATORY
SAN DIEGO, CALIFORNIA 92152

OCEAN COLOR ANALYSIS

Seibert Q. Duntley, Roswell W. Austin, Wayne H. Wilson
Catharine F. Edgerton, and Steven E. Moran

Approved for public release; distribution unlimited.

SIO Ref. 74-10
April 1974

Naval Research Laboratory
Washington, D. C. 20390
Contract N00014-69-A-0200-6033

National Oceanographic and Atmospheric Agency
Washington, D. C. 20233
Grant No. 04-3-158-64

Final Technical Report

Approved:

S. Q. Duntley

Seibert Q. Duntley, Director
Visibility Laboratory

Approved for Distribution:

William A. Nierenberg

William A. Nierenberg, Director
Scripps Institution of Oceanography

CONTENTS

PREFACE

This report is divided into three parts covering the different phases of the effort on Contract N00014-69-A-0200-6033 and Grant No. 04-3-158-64, as follows:

1. A STUDY OF THE DETECTION OF OCEAN CHLOROPHYLL FROM EARTH ORBIT.

The initial phase of this study was carried through in support of NASA's preliminary design of the sensors and orbital parameters for the Earth Observatory Satellite (EOS) for sensing changes in ocean chlorophyll. The results were reported formally at the Fourth Annual Earth Resources Program held in January 1972 at the Manned Spacecraft Center. (See p. 102, Vol. IV of the PROCEEDINGS.) Since that time, new measurements have been made of the optical properties of many pure phytoplankton cultures. Improved computational techniques have been applied to the problem to refine the analysis and extend the scope of its applicability.

2. A STUDY OF THE INHERENT SPECTRAL RADIANCE SIGNATURES OF THE OCEAN SURFACE.

The need for this study became obvious in the process of reducing and analyzing the surface truth data which the Visibility Laboratory had obtained in support of remote sensing experiments. It has not been feasible to measure all of the necessary environmental parameters with sufficient spectral detail in the brief time of an overpass of an aircraft or satellite. In order to obtain the best assessment of the variables in the minimum time, we have taken the approach that we would sample all of the variables at a few selected wavelengths and interpolate between these observations to obtain the complete spectral character of the required optical parameters. The information necessary for these interpolations that was available in the literature was sparse, and much of it of doubtful quality or applicability. Consequently, a measurement program was instituted which had as its objectives: to understand and determine the spectral nature of the variables involved in the generation and propagation of the remotely sensed optical signal, to obtain a measure of the absolute magnitudes of these variables and the range of magnitudes which occur with various atmospheric conditions, water color characteristics, and solar zenith angles, and to improve the equipment and techniques used in the acquisition of surface truth data.

The results reported here show the status of this study at the end of the present contract. Useful methodology and data have been generated and are presented. In addition, valuable experience has been acquired relative to the performance of and operational techniques for the instruments used in the acquisition of surface truth data. The study will be continuing and these results represent a sample of the type of data which is expected to be forthcoming.

3. STUDY OF THE REFLECTANCE CHARACTERISTICS OF WHITECAPS, FOAM, AND SPRAY.

This study has been underway since May 1969, having been initiated under Naval Oceanographic Office Contract No. N62306-69-A-0072.0003. For the first two years the major effort was devoted to acquiring carefully controlled and processed aerial photographs of the ocean surface under a variety of documented windspeed conditions, and to obtaining the equipment and generating the techniques for scanning these films. Since then the effort on this study has consisted mainly of computer-assisted scanning and statistical analysis of the data from selected frames of this photography, and the writing of computer software for the proper reduction of the data to sea surface reflectances. The effort of the last two years has been at a low level because of project priorities and because of lengthy delays in acquiring both camera calibration information and suitably processed duplicate prints of some of the photography. The results presented here are preliminary and may be revised when the analysis of the total body of data for the other windspeeds is completed.

1. DETECTION OF OCEAN CHLOROPHYLL FROM EARTH ORBIT

Seibert Q. Duntley
Wayne H. Wilson
Catharine F. Edgerton

1.1 INTRODUCTION

At the outset, this study was undertaken to aid in the optimization of the Earth Observatory Satellite for ocean sensing. The work was initiated in April 1971 and because of rigid EOS time requirements, the investigation was of limited scope. During the past year a more detailed study was performed. Measured vertical distributions of chlorophyll in the ocean were used in improved radiative transfer calculations. Special phytoplankton were grown which more accurately represented those in the ocean, and spectrophotometric techniques for measuring those cultures were improved. Other refinements included allowances for sea-surface curvature.

1.2 OBJECTIVE

The objective was the determination of the magnitude of the optical signature of ocean chlorophyll available to any remote sensor in earth orbit. The study had several goals, and all of them were achieved. First, it was desired to ascertain whether commercially significant concentrations of chlorophyll-A pigments in the ocean would produce a sufficient optical signal at orbital altitudes to operate optical remote sensors, such as those being planned for the Earth Observatory Satellite, on clear and hazy days. Second, it was desired to explore the effect of solar altitude on these optical signals, because this is an important matter in choosing the best orbit for an oceanographic satellite. Third, it was desired to find the best orientation for the field of view for a remote sensor in orbit in order to optimize its ability to detect ocean chlorophyll.

1.3 DISCUSSION

In investigative terms, the problem was translated into a study of apparent orbital contrasts of the sea surface in the presence of chlorophyll. To compute such contrasts, a determination of both the inherent surface and apparent orbital sea radiances, with various amounts of chlorophyll, was required. Drawing upon an existing bank of atmospheric data and an existing generalized sea radiance computer program, both developed by the Visibility Laboratory, the staff was able to coordinate a customized computer process for this study. Data from both the blue and green portions of the spectrum were incorporated, since chlorophyll in sea water causes distinct reflectance changes in those spectral regions. Atmospheric input parameters consisted of two fully documented days: one clear and one hazy. Sea condition inputs included a range of sea states, with and without white water. The output was then analyzed to determine the best sun zenith angle and viewing azimuth for optimizing the sensitivity of the sensor for detecting chlorophyll concentrations from orbit.

Many uncertainties were avoided by using actual experimental oceanographic, atmospheric, and lighting data. These were obtained on board ships and from aircraft. The only use of mathematical modeling was in connection with the enrichment of chlorophyll above the concentration found in the ocean water that was used as a base and which previously had been measured *in situ*. Richer waters were simulated by using laboratory spectrophotometric measurements of living cultures of ocean phytoplankton in radiative transfer calculations which predicted the optical properties of ocean waters containing concentrations of chlorophyll-A pigments covering the entire range of commercial importance beginning with arid* water, where the concentration is 0.1 mg/m^3 or less, and extending to higher concentrations characteristic of highly productive ocean water.

OCEANOGRAPHIC DATA

The oceanographic data used in this study were obtained from measurements made by John E. Tyler and Dr. Raymond C. Smith in the southern part of the Gulf of California near Islas Tres Marias during 1968.[1] These data were used for a number of reasons. First, they represent typical oceanic water which is clear, blue, and arid. The chlorophyll-A pigment concentration of the water was 0.112 mg/m^3 as measured by a biologist from Scripps Institution of Oceanography at the time of the optical measurements. This concentration represents the upper boundary of arid water from a commercial standpoint. This water, however, was not meant to represent the clearest, relatively sterile oceanic water which might be found, for example, in the Sargasso Sea. This base water was chosen after careful consideration to be typical of an arid but biologically mature oceanic water. This means that, though the level of chlorophyll-A pigment concentration at the time of measurement was low, indications from the optical measurements were that the water had been more productive in the past. The evidence for this conclusion may be found from an inspection of the diffuse reflection coefficient in the blue region of the spectrum (400-500 nm). The coefficient at 460 nm is a factor of 2 to 3 lower than the similar reflection coefficient of waters found in the Sargasso Sea or any other extremely clear oceanic waters. A study of the unpublished and published data of Tyler and Smith[2] indicates that this large decrease in the reflection coefficient in the blue region occurs in any biologically active water. The amount of decrease is not in any clear manner dependent on the current level of productivity. It is in all likelihood due to the "yellow" substances and detritus produced by any mature phytoplankton crop. It would thus remain even after a crop had bloomed and faded. Given a region of ocean where crops are continually blooming and fading, the average background reflectance would thus not be the clearest blue water but rather this arid but biologically mature water.

* "arid" is used here in the sense of "devoid of interest and life" (Webster's Third New International Dictionary, Unabridged, 1970).

BASE WATER

The living cultures used in this study were in their blooming stages when measured in order to have the highest optical density for measurement purposes. Thus, they did not have the background absorption due to the dissolved "yellow" substances. This background was supplied by the base water. Second, the base water data were taken under ideal experimental conditions: sky unclouded, water calm, temperature in the top 45 meters isothermal within 1/2°C, and the beam attenuation coefficient relatively constant over the depths of measurement. Third, both upwelling and downwelling irradiances between 400 and 650 nm were obtained for a number of depths. This allowed a complete description of the water in terms of both the reflectance coefficient and the diffuse attenuation coefficient. These two coefficients were needed in the study in order to completely describe the two independent phenomena, scattering and absorption, which govern the propagation of an optical signal through the water. Figure 1 shows the spectral reflectance of the water as measured beneath the water surface while the spectral diffuse attenuation coefficients for irradiance are plotted in Figure 2. The figures were obtained from Tyler and Smith [1] and have been smoothed in order to remove the higher frequency noise that was present in the data.

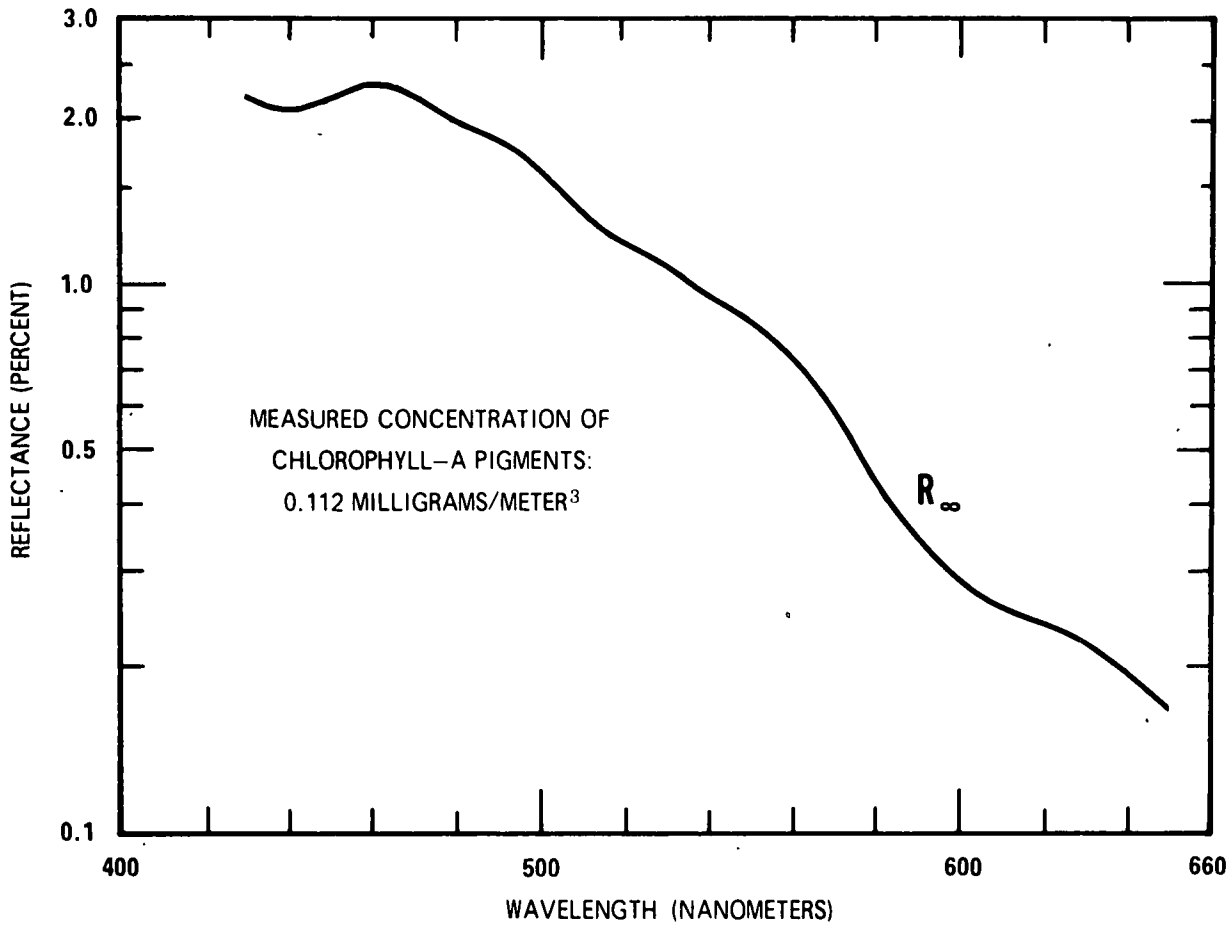

Fig. 1. Subsurface reflectance of deep clear ocean water measured at Islas De Las Tres Marias, south of the Gulf of California, 1968. J. E. Tyler and R. C. Smith

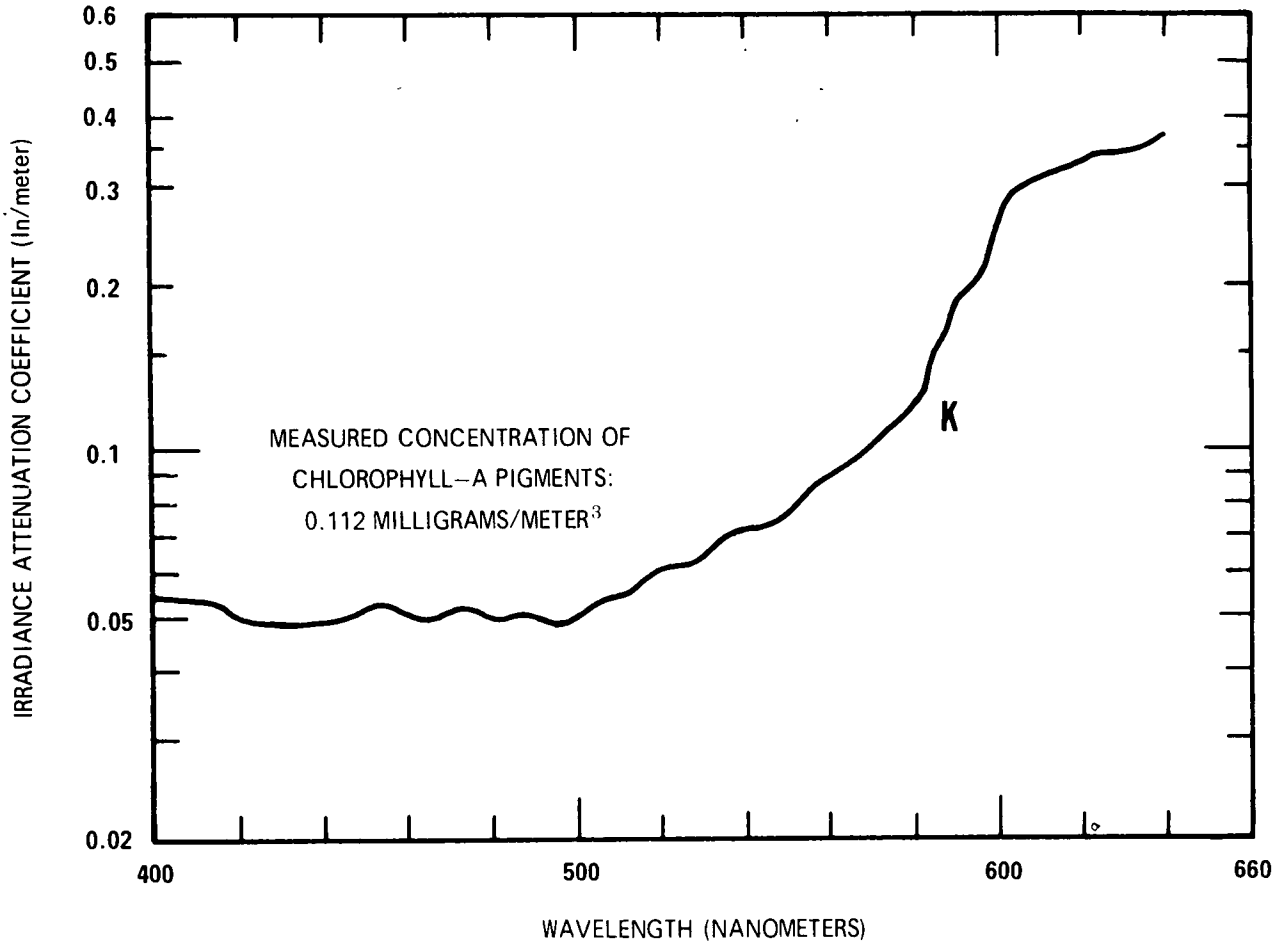

Fig. 2. Irradiance attenuation coefficient of clear ocean water measured at Islas De Las Tres Marias, south of the Gulf of California, 1968. J. E. Tyler and R. C. Smith

From Figures 1 and 2 it was possible to calculate the spectral diffuse backscattering coefficients and the spectral diffuse absorption coefficients of the ocean water at Islas Tres Marias by a previously published method.[3] The results are shown in Figures 3 and 4. These coefficients are linearly related to the concentration of chlorophyll-A pigments. Thus, corresponding coefficients for known concentrations of laboratory cultures of ocean phytoplankton can be added to those in Figures 3 and 4 in order to predict the optical properties of ocean water containing any arbitrary concentration of chlorophyll-A pigments.

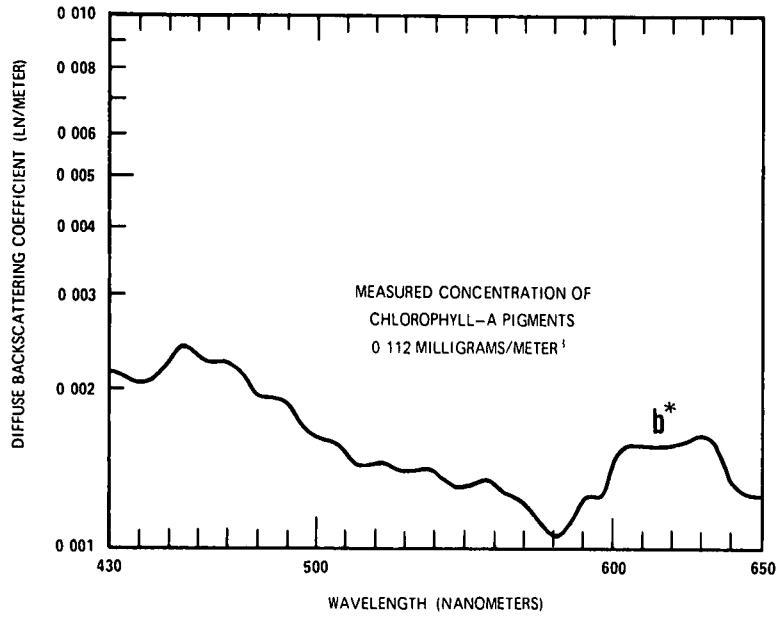

Fig. 3. Diffuse backscattering coefficient of clear ocean water calculated from measurements at Islas De La Tres Marias, south of the Gulf of California, 1968.

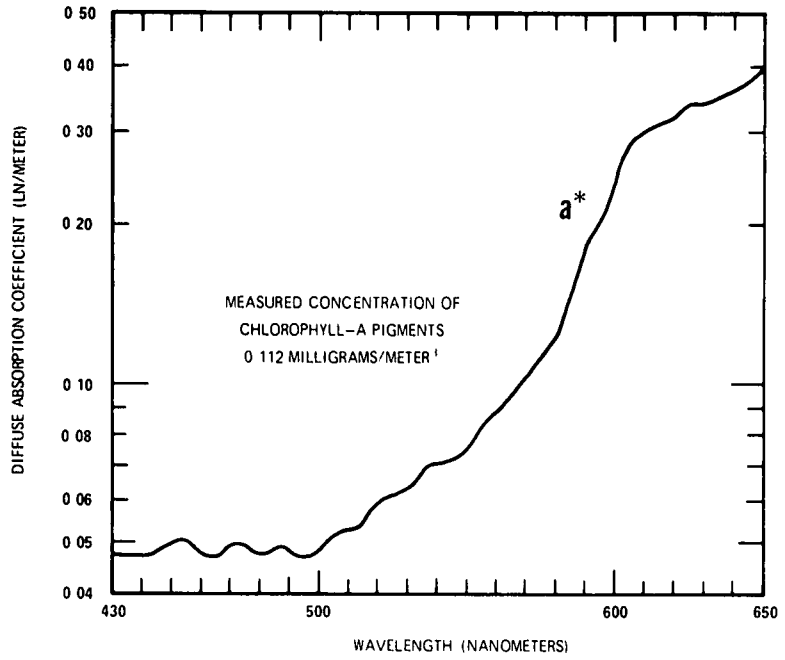

Fig. 4. Diffuse absorption coefficient of clear ocean water calculated from measurements at Islas De La Tres Marias, south of the Gulf of California, 1968.

PHYTOPLANKTON SAMPLES

Nine living laboratory cultures of typical oceanic and coastal phytoplankton were obtained from the Marine Research Group at the Scripps Institution of Oceanography. After optical measurements had been made of these samples, they were analyzed for chlorophyll-A pigment concentration. Dr. Dale A. Keifer, a marine biologist, collaborated on this aspect of the study, and his assistance is gratefully acknowledged. The phytoplankton samples used in the study represented a broad spectrum of plants commonly found in oceanic and coastal waters. Phytoplankton populations found in commercial fishing grounds are usually a mixture of some of these samples. However, at any given time, one type of species is usually dominant, while another is fading and still another is beginning to bloom. Any one of the samples can become dominant. Table I lists the samples that were measured.

Table I

Sample	Species
1B	Nitzschia closterium
2B	Lauderia borealis
4B	Gymnodinium species
2C	Monochrysis lutheri
4C	Cyclotella nana
5C	Skelotonema costatum
1D	Gonyaulax polyedra
2D	Gymnodinium splendens
8D	Coccolithus huxleyi

Though calculations of the spectral signature at the water surface were completed for all of the samples, the two which were representative of the boundaries associated with the optical properties were chosen for the extensive calculations necessary for the determination of the spectral signal at orbital altitude. These samples are Monochrysis lutheri (2C) found in estuaries and coastal waters and Coccolithus huxleyi (8D), a general ocean type.

Sample 1D, Gonyaulax polyedra, the phytoplankton responsible for the so-called "red tide" presented experimental problems because of its low concentration and fast settling rate. It was extremely difficult to grow in the laboratory to higher concentrations. The accuracy of its results was probably lower than that of the other cultures. It was included, however, because of its distinctive *in situ* optical property and not because of any beneficial connection with fisheries. On the contrary it usually has a quite deleterious effect.

SPECTRAL MEASUREMENTS

The spectral diffuse reflectance and the spectral diffuse optical density of the various living cultures were measured using the original Hardy recording spectrophotometer.[4] The measurements were made for two different thicknesses, one and two centimeters. The cultures were optically dense enough so that there was no direct beam transmittance through the spectrophotometer cells. Only diffuse light was transmitted, even through the one centimeter thickness.

Typical data for the spectral diffuse reflection and spectral diffuse optical density as measured on the Hardy spectrophotometer are illustrated in Figures 5, 6, 7, and 8. These data have been corrected for wavelength nonlinearities, neutral density filters, spectrophotometric cell boundary reflections and scale calibrations.

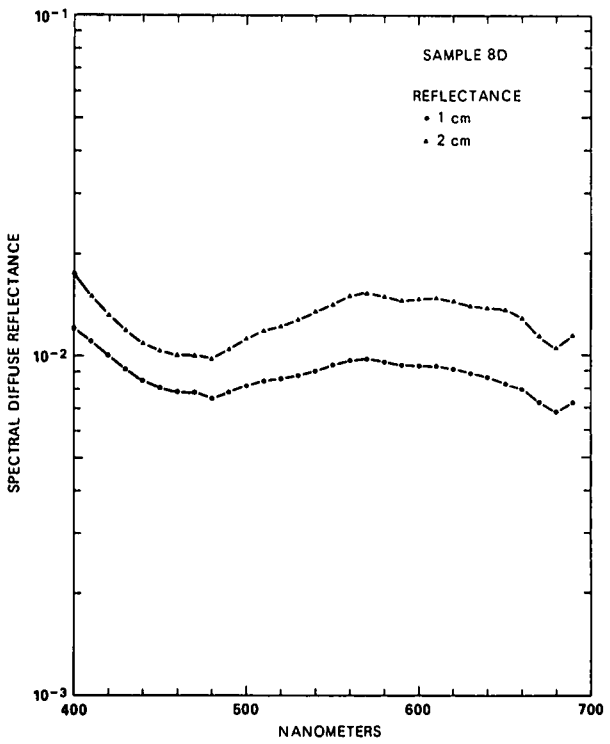

Fig. 5. Spectral diffuse reflection – of 1 cm thickness of lot culture *Coccolithus huxleyi* (Sample 8D).

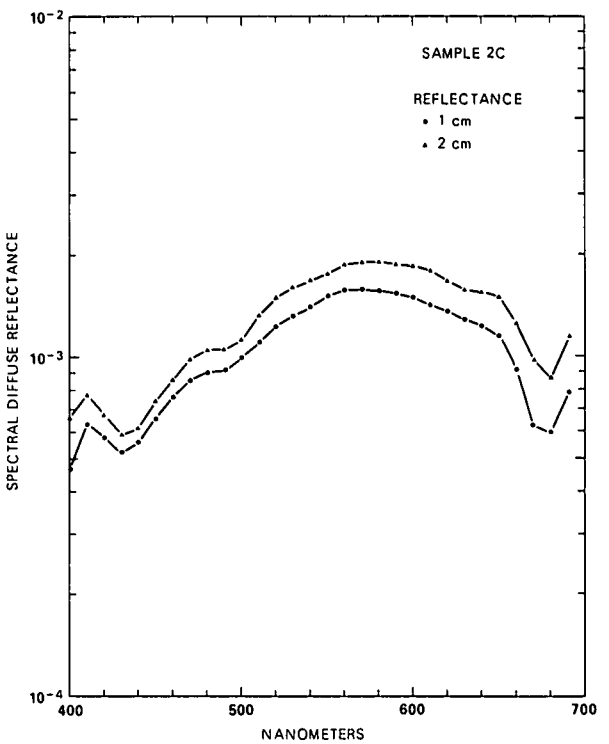

Fig. 6. Spectral diffuse reflection – of 1 cm thickness of lot culture *Monochrysis lutheri* (Sample 2C).

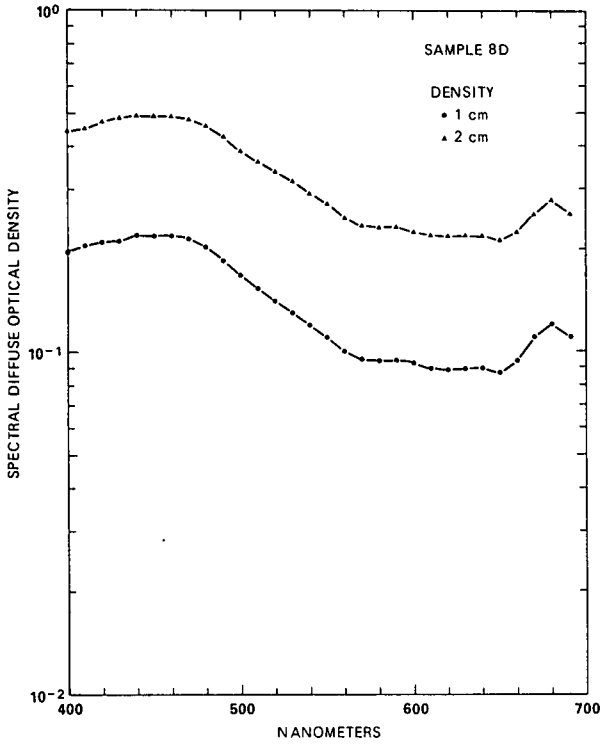

Fig. 7. Spectral diffuse optical density – of 1 cm thickness of lot culture (Sample 8D).

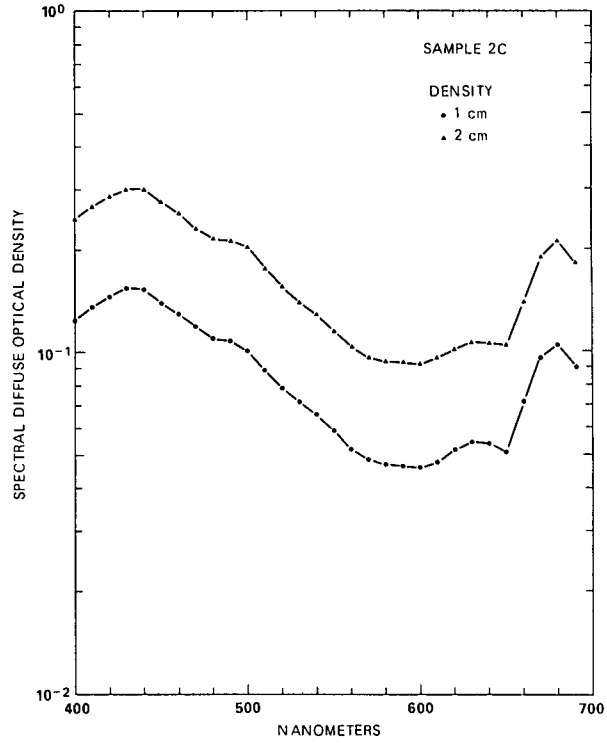

Fig. 8. Spectral diffuse optical density – of 1 cm thickness of lot culture (Sample 2C).

The spectral diffuse backscattering coefficient, b^*, and the spectral diffuse absorption coefficient, a^*, were then calculated from the diffuse reflection and optical density for each of the samples. These calculations were programmed for and computed on an IBM 360/44. This computation followed the iterative procedure for calculating a^* and b^* from two different thickness measurements as outlined in reference 3. The resulting coefficients for the samples are shown in figures 9 and 10 for unit concentration of chlorophyll-A pigments.

The samples were then added individually in appropriate concentrations to the corresponding optical coefficients for the arid ocean water measured at Islas Tres Marias. No attempt was made to artificially construct mixtures of the cultures. This was in keeping with the view of the marine biologists that at any one time one species was dominant. It was felt also that more information could be gleaned from the data by observing the results of using the boundary cases alone.

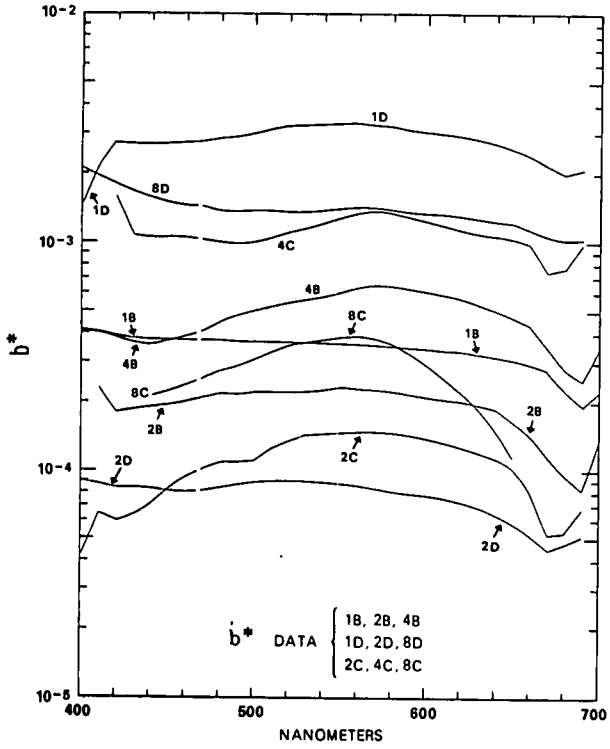

Fig. 9. Spectral diffuse backscattering coefficient of ocean phytoplankton calculated from spectrophotometric data on lot cultures.

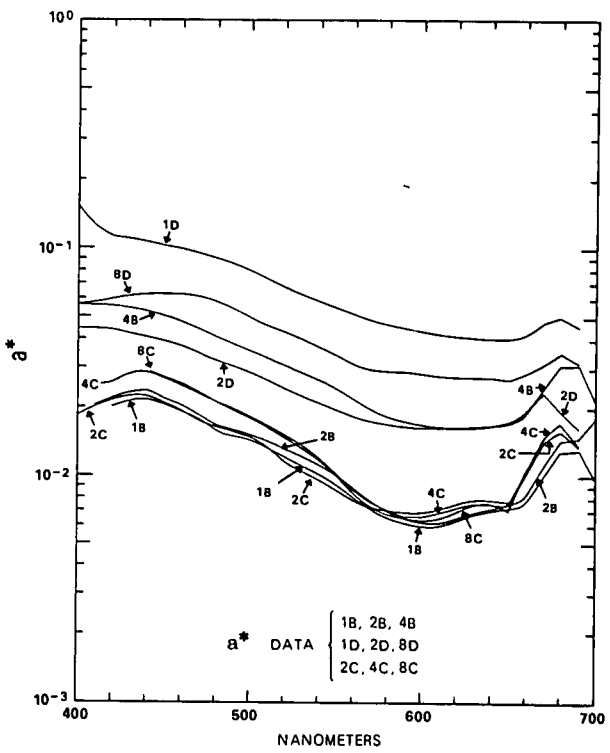

Fig. 10. Spectral diffuse absorption coefficient of ocean phytoplankton calculated from spectrophotometric data on lot cultures.

SPECTRAL EFFECTS OF OCEAN CHLOROPHYLL

The spectral diffuse backscattering coefficient and spectral diffuse absorption coefficient computed by the above method were then used as input to a two-flow radiative transfer calculation patterned after reference 3. For the first phase of this part of the study, it was assumed that there was an optically infinitely thick layer of water lying just below the water surface with the given concentration of phytoplankton sample. This procedure enabled the subsurface reflectance, R_{∞}, of the ocean water to be calculated for a number of concentrations of chlorophyll-A pigment. Figures 11a through 11h show curves of R_{∞} for the species in Table I with the exception of Sample 1D, Gonyaulax polyedra. Because this "red-tide" plankton species represents a special case, not desirable for commercial fisheries, it is shown separately in Fig. 12. In each figure, four curves are shown representing chlorophyll-A concentrations of 0.1 (curve A), 0.3 (curve B), 0.70 (curve C), and 1.75 milligrams per cubic meter (curve D). The curves marked A in each of the figures are identical and are for the base water. They represent the measurements obtained by Tyler and Smith at Islas Tres Marias. Visual observations at the time of those measurements were that the water color was deep blue. Table II is a listing of the reflectances as a function of wavelength for all species at a chlorophyll-A concentration of 0.70 milligrams per cubic meter.

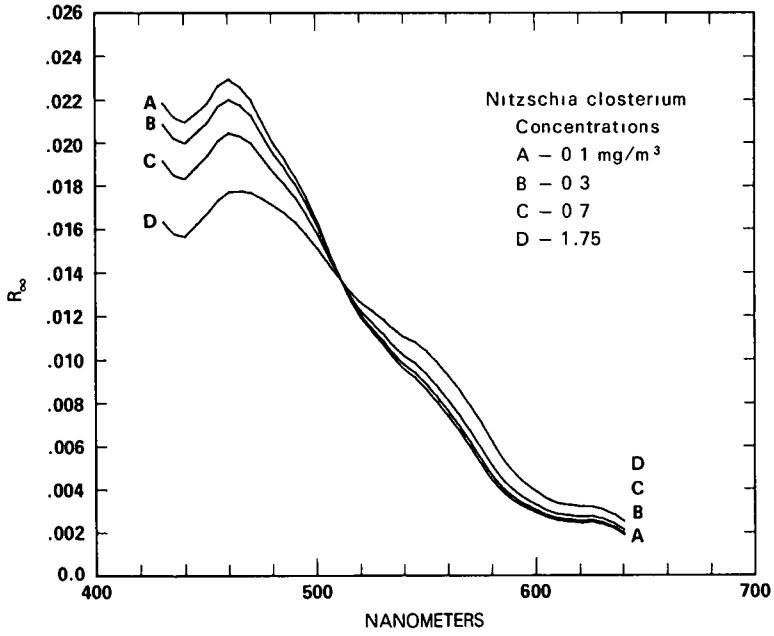

Fig. 11a

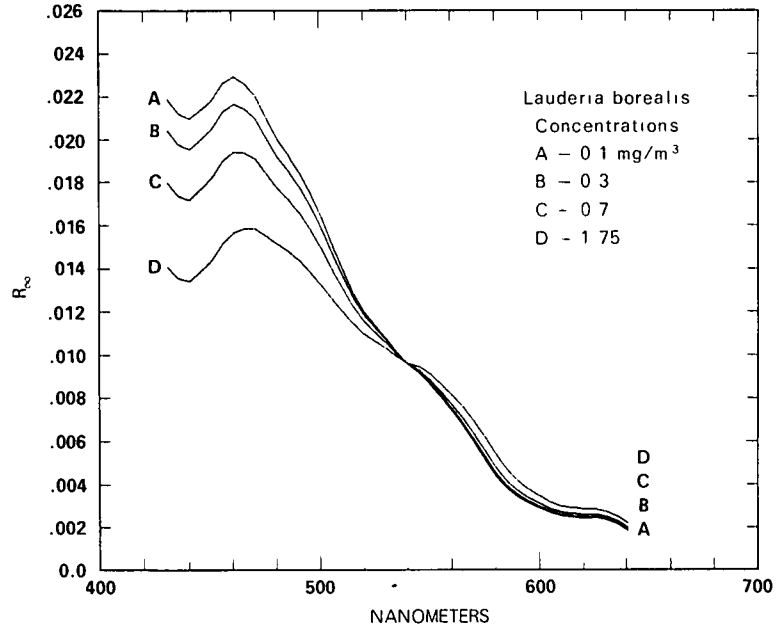

Fig. 11b

Fig. 11. Subsurface spectral reflectance for various concentrations of chlorophyll-A pigment.

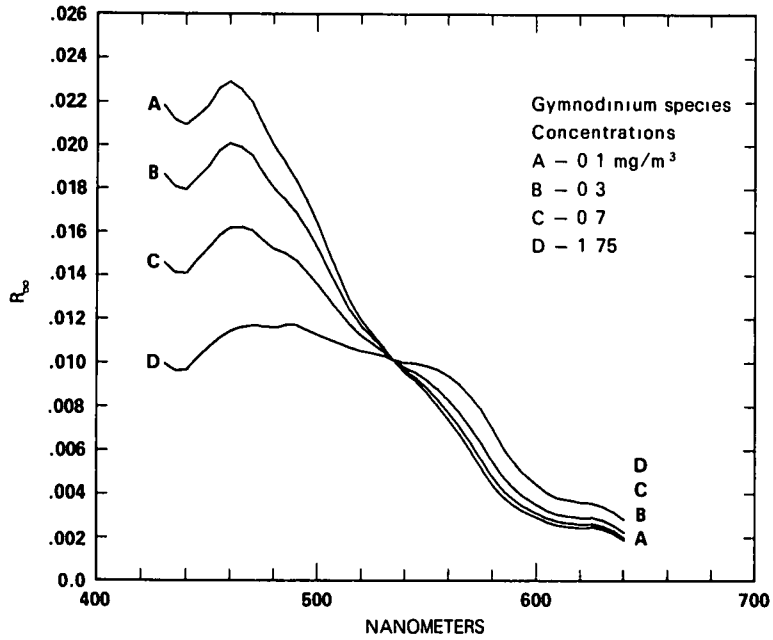

Fig. 11c

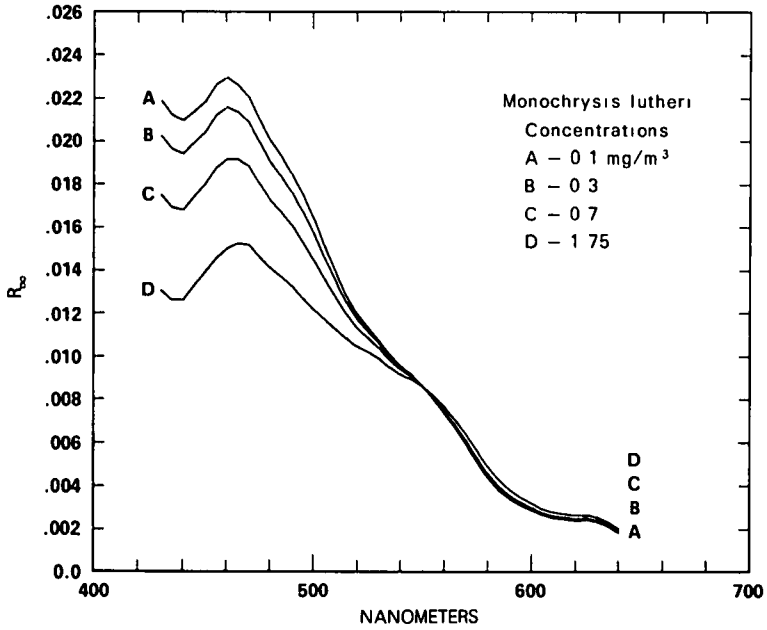

Fig. 11d

Fig. 11 (cont.) Subsurface spectral reflectance for various concentrations of chlorophyll-A pigment.

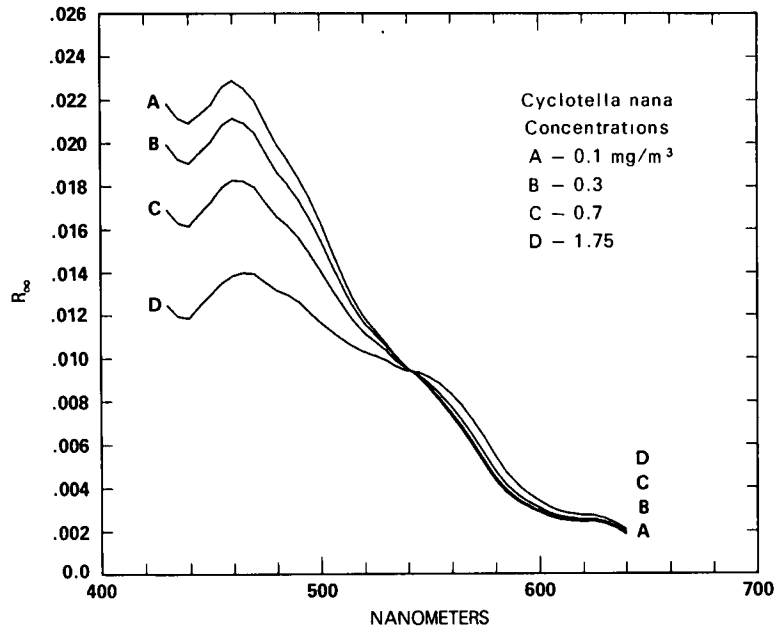

Fig. 11e.

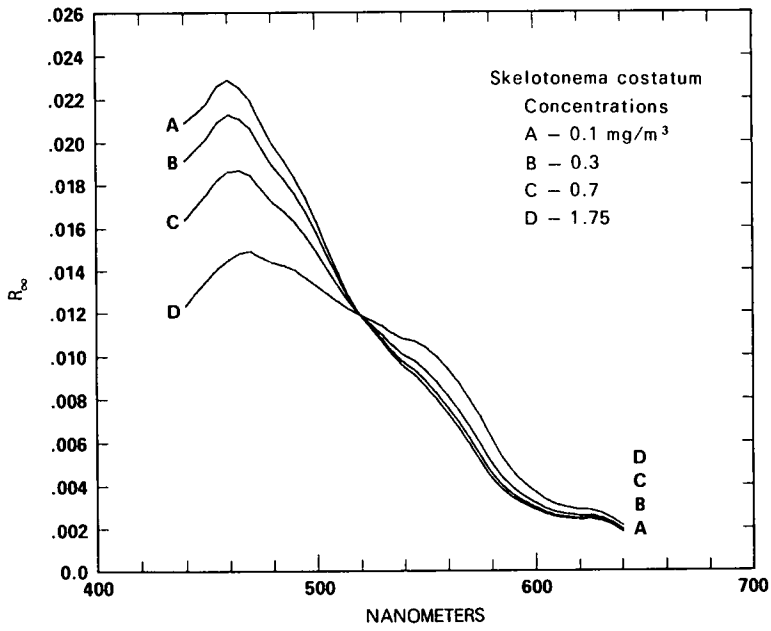

Fig. 11f

Fig. 11 (cont.) Subsurface spectral reflectance for various concentrations of chlorophyll-A pigment.

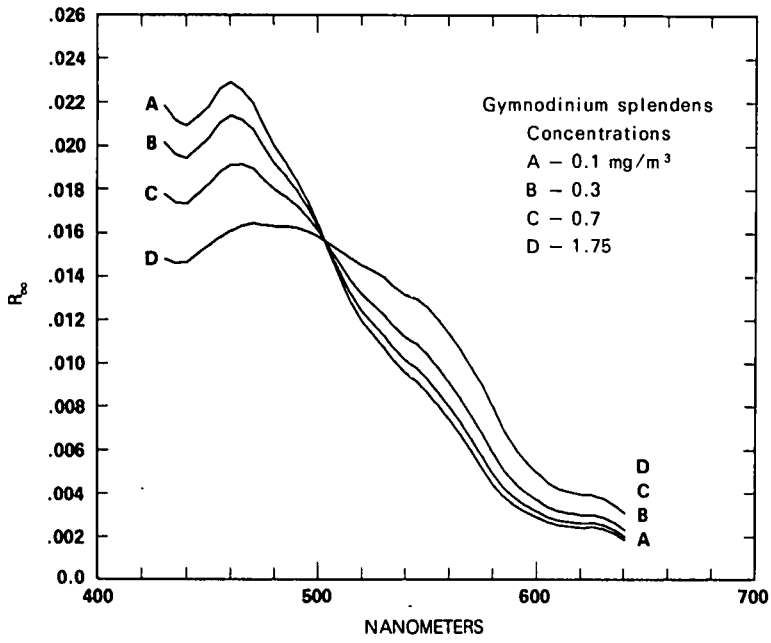

Fig. 11g

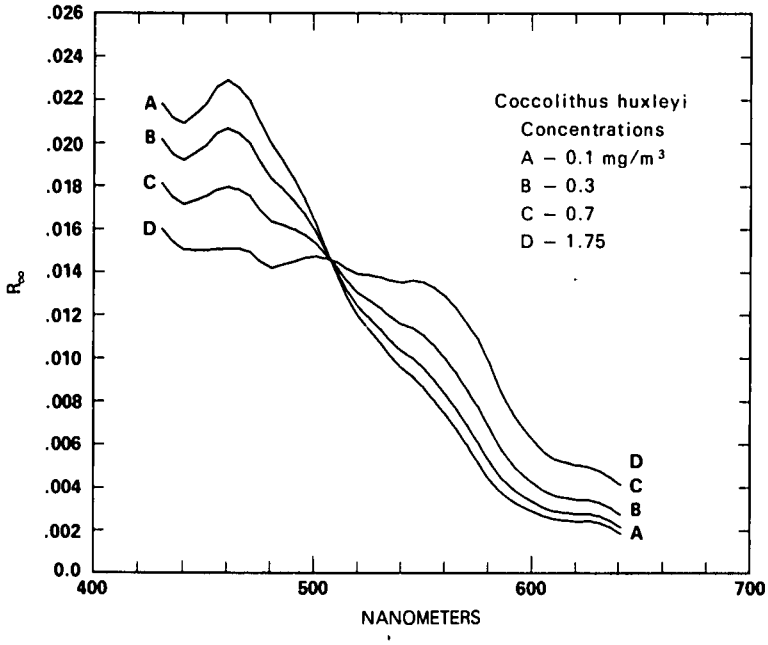

Fig. 11h

Fig. 11 (cont.) Subsurface spectral reflectance for various concentrations of chlorophyll-A pigment.

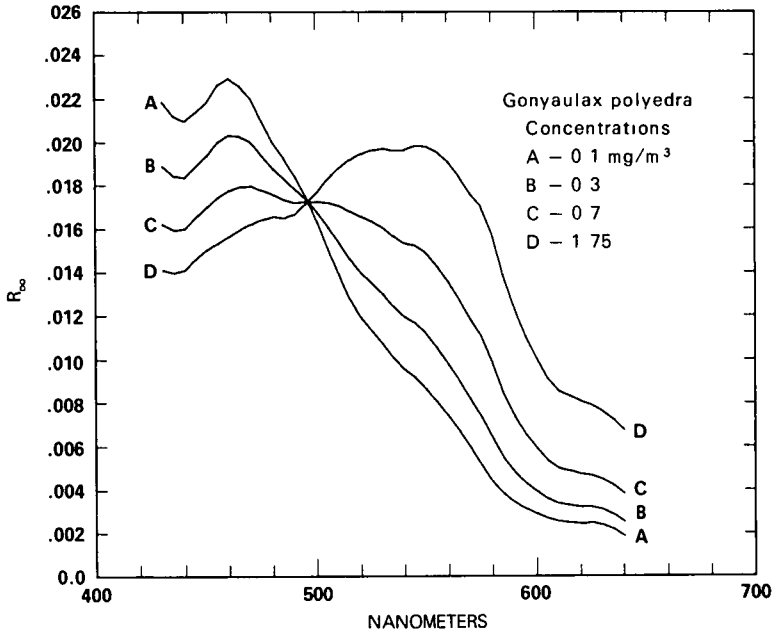

Fig. 12. Subsurface spectral reflectance for various concentrations of chlorophyll-A pigment. (Red tide)

Table II

REFLECTANCE FOR CHLOROPHYLL CONCENTRATION 0.700 MILLIGRAMS/CUBIC METER.

WAVELENGTH (NM)	SAMPLES 1B	2B	4B	2C	4C	8C	1D	2D	8D
430.	1.9086E-02	1.7913E-02	1.4532E-02	1.7437E-02	1.6894E-02	2.1794E-02	1.6160E-02	1.8117E-02	1.7752E-02
440.	1.8286E-02	1.7133E-02	1.4068E-02	1.6775E-02	1.6140E-02	1.6402E-02	1.5951E-02	1.7170E-02	1.7333E-02
450.	1.9294E-02	1.8144E-02	1.5204E-02	1.7944E-02	1.7249E-02	1.7574E-02	1.6951E-02	1.7516E-02	1.8211E-02
460.	2.0378E-02	1.9357E-02	1.6147E-02	1.9092E-02	1.8273E-02	1.8630E-02	1.7707E-02	1.7938E-02	1.9095E-02
470.	1.9926E-02	1.9043E-02	1.6037E-02	1.8786E-02	1.7958E-02	1.8477E-02	1.7921E-02	1.7553E-02	1.8947E-02
480.	1.8596E-02	1.7665E-02	1.5167E-02	1.7193E-02	1.6600E-02	1.7215E-02	1.7542E-02	1.6333E-02	1.7952E-02
490.	1.7418E-02	1.6515E-02	1.4641E-02	1.5997E-02	1.5601E-02	1.6295E-02	1.7159E-02	1.5980E-02	1.7224E-02
500.	1.5758E-02	1.4889E-02	1.3518E-02	1.4393E-02	1.4088E-02	1.4890E-02	1.7196E-02	1.5360E-02	1.6049E-02
510.	1.3833E-02	1.3025E-02	1.2275E-02	1.2716E-02	1.2495E-02	1.3269E-02	1.7029E-02	1.4212E-02	1.4521E-02
520.	1.2210E-02	1.1483E-02	1.1198E-02	1.1281E-02	1.1190E-02	1.1907E-02	1.6532E-02	1.3007E-02	1.3152E-02
530.	1.1181E-02	1.0519E-02	1.0497E-02	1.0363E-02	1.0362E-02	1.1004E-02	1.6029E-02	1.2330E-02	1.2222E-02
540.	1.0133E-02	9.5551E-03	9.7331E-03	9.3747E-03	9.4779E-03	1.0057E-02	1.5291E-02	1.1563E-02	1.1172E-02
550.	9.3393E-03	8.8319E-03	9.1819E-03	8.6192E-03	8.8381E-03	9.3659E-03	1.4843E-02	1.1064E-02	1.0400E-02
560.	8.1212E-03	7.6792E-03	8.2682E-03	7.4990E-03	7.7813E-03	8.2017E-03	1.3539E-02	9.9731E-03	9.0917E-03
570.	6.6924E-03	6.3290E-03	7.0187E-03	6.1315E-03	6.4179E-03	6.7527E-03	1.1827E-02	8.5275E-03	7.5700E-03
580.	5.0730E-03	4.7648E-03	5.4581E-03	4.5785E-03	4.8175E-03	5.0846E-03	9.8646E-03	6.7822E-03	5.8465E-03
590.	3.8928E-03	3.6802E-03	4.1765E-03	3.5594E-03	3.6917E-03	3.8533E-03	7.3751E-03	5.1360E-03	4.4467E-03
600.	3.2404E-03	3.0878E-03	3.4610E-03	2.9978E-03	3.0747E-03	3.1796E-03	5.9048E-03	4.2057E-03	3.6683E-03
610.	2.8162E-03	2.6907E-03	2.9969E-03	2.6193E-03	2.6674E-03	2.7370E-03	4.9885E-03	3.6147E-03	3.1547E-03
620.	2.6992E-03	2.5816E-03	2.8614E-03	2.5075E-03	2.5361E-03	2.5937E-03	4.7231E-03	3.4478E-03	3.0006E-03
630.	2.6191E-03	2.5061E-03	2.7573E-03	2.4415E-03	2.4569E-03	2.5015E-03	4.4836E-03	3.3137E-03	2.8911E-03
640.	2.0994E-03	1.9969E-03	2.2182E-03	1.9359E-03	1.9458E-03	1.9665E-03	3.8230E-03	2.7505E-03	2.3250E-03

Radiative transfer theory[3] shows that the spectral diffuse reflectance R of macroscopically homogeneous, optically deep water is governed at each wavelength by the ratio of its diffuse back-scattering coefficient b^* to its diffuse absorption coefficient a^*, as follows:

$$R = \frac{(b^*/a^*)}{1 + (b^*/a^*) + \sqrt{1 + 2(b^*/a^*)}} .$$

Ordinarily, $b^*/a^* < 1$.

The spectral reflectance of arid water (Fig. 1) results from combined effects of a^* and b^*, since both vary with optical wavelength across the spectrum. When any type of phytoplankton is added to such water, the spectral reflectance rises in the green and falls in the blue region of the spectrum. The rise in the green is caused by the fact that all of the phytoplankton of commercial importance are "armored"; that is to say, each microscopic organism has a translucent protective case or shell. In different species these shells may be either calcaceous, silacaceous, or cellulosic, but all of them scatter light throughout the visible spectrum, thereby increasing b^* in the above equation.

In the green, the absorption coefficient a^* is not changed appreciably by the addition of phytoplankton because chlorophyll does not absorb green light appreciably. Thus, the green reflectance R increases with b^*.

In the blue, chlorophyll absorbs so strongly that the addition of phytoplankton causes the absorption coefficient a^* to increase much more than does the back-scattering coefficient b^*. Thus, R is decreased in the blue region of the spectrum (See, for example, Fig. 11h).

HINGE POINT

Between the blue and green (at wavelength 505 nanometers in Fig. 11h) the ratio of b^*/a^* for Coccolithus huxleyi (sample 8D) is the same as the ratio of b^*/a^* for the base water. Thus, addition of this phytoplankton does not alter the reflectance of optically deep water at that wavelength. This produces a "hinge point" in the family of curves in Fig. 11h.

The hinge point has a different wavelength for each of the nine species of phytoplankton we measured. Since only one species at a time dominates an ocean plankton bloom, identification of species may be possible by remote sensing if the spectroradiometric time history of a bloom can be measured.

Sets of spectral reflectance curves which do not exhibit a common hinge point usually represent different species measured at different locations or at different times. Movement of the hinge point can also result, however, from differences in the base water. For example, sediments in suspension scatter light strongly, thereby increasing b^* throughout the spectrum, but they ordinarily have only weak effects on a^*. Thus, an addition of suspended sediments tends to raise the spectral reflectance of ocean water at all wavelengths, much as does cream when added to coffee. Consequently, the presence of sediments can be distinguished from chlorophyll-bearing phytoplankton by the shape of their respective spectral reflectance curves.

MATURITY OF PHYTOPLANKTON BEDS

Growing phytoplankton shed their cases periodically and grow new ones. Thus, biologically mature water contains an accumulation of discarded cases, as well as phytoplankton which have died. All of this particulate detrital material sinks gradually despite convective mixing and the action of water waves. Nevertheless, any mature phytoplankton bed contains a significant amount of such material, which behaves optically somewhat like a sediment. Although quantitative data are somewhat sparse, it appears that the quantity of detrital material ordinarily exceeds the amount of living matter by a considerable factor in the productive phytoplankton beds of the sea.

Decomposing organic material produces pale yellow solutes which increase a^*, primarily in the violet and ultraviolet spectral regions. This "yellow stain" lowers the spectral reflectance R_∞ curves throughout the ultraviolet, violet and blue in a manner readily distinguishable from the spectral effects of living chlorophyll. The base water selected for the study described in this report was biologically mature in the sense that it contained a typical amount of "yellow stain."

STRATIFICATION OF CHLOROPHYLL IN THE OCEAN

The Food Chain Research Group of the Institute of Marine Resources, University of California, San Diego, has in its file thousands of measured depth profiles of chlorophyll-A pigment at a wide variety of ocean locations. Two of these are shown in Fig. 13. Obviously, their shapes are very dissimilar, but no more so than many hundreds of other profiles in the collection. Virtually any conceivable shape of profile can be found in the file except, perhaps, one that does not vary with depth. The two shown in Fig. 13 are not extreme cases in any sense. Ocean chlorophyll occurs in stratified patterns with seemingly limitless variety.

In order to calculate by radiative transfer methods the subsurface spectral reflectances R_∞ of the data shown in Fig. 13, the profiles were approximated by layers of constant chlorophyll-A pigment concentration*, as shown in Fig. 14a and 14b. Integration of the total chlorophyll-A in a vertical column extending to a depth of 70 meters shows that the ocean at Station No. 5 contained 143 milligrams of chlorophyll-A pigment per square meter of ocean surface. The corresponding quantity at Station No. 6C was 55 milligrams per square meter. Thus, the ocean at Station No. 5 contained 2.6 times more total chlorophyll-A pigment than it did at Station No. 6C.

AMBIGUITY OF THE OPTICAL SIGNATURES

Radiative transfer calculations described at the beginning of the preceding entitled "Spectral Effects of Ocean Chlorophyll" produced the spectral diffuse reflectance curves in Fig. 15 for the two chlorophyll-A profiles given by Figs. 14a and 14b. Despite a factor of 2.6 in total integrated milligrams of chlorophyll-A pigments per square meter of ocean surface, the curves are indistinguishable in the green and differ but

* The species population of the water column was assumed to be mixed and was composed of 38 percent dinoflagellates (Sample 2D), 12 percent coccolithophorids (Sample 8D), and 50 percent diatoms (Sample 4C). These ratios approximated the actual populations measured at these stations.

slightly in the blue and in the red. These small differences, moreover, are in *reverse directions* from those that would be expected if the chlorophyll-A pigments were uniformly distributed in the water column. (See Figs. 11 and 12) A very small alteration of the thickness of the upper layers in Fig. 14 will produce *identical* curves of subsurface spectral diffuse reflectance without changing the factor 2.6 in total integrates chlorophyll-A pigments. *Thus, the subsurface spectral diffuse reflectance is wholly ambiguous as a measure of the total chlorophyll-A pigments present,* even to a spectroradiometer located just below the water surface.

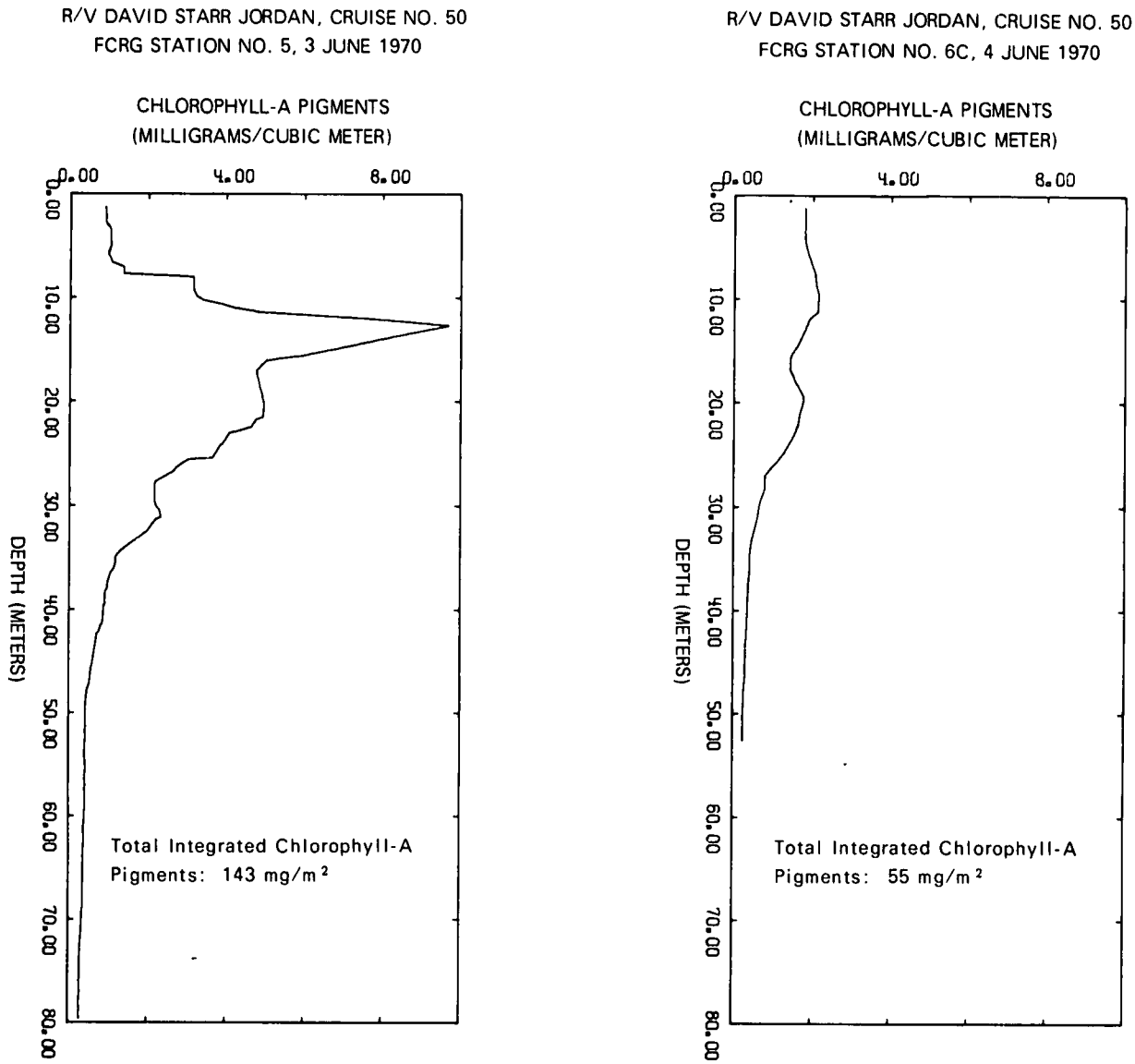

Fig. 13. Chlorophyll-A Pigment Depth Profiles measured *in situ* in waters near San Diego. (From Research on the Marine Food Chain Progress Report, July 1970 – June 1971, Institute of Marine Resources, Report 71-10, Part III Data Records, "Unpublished Manuscript".)

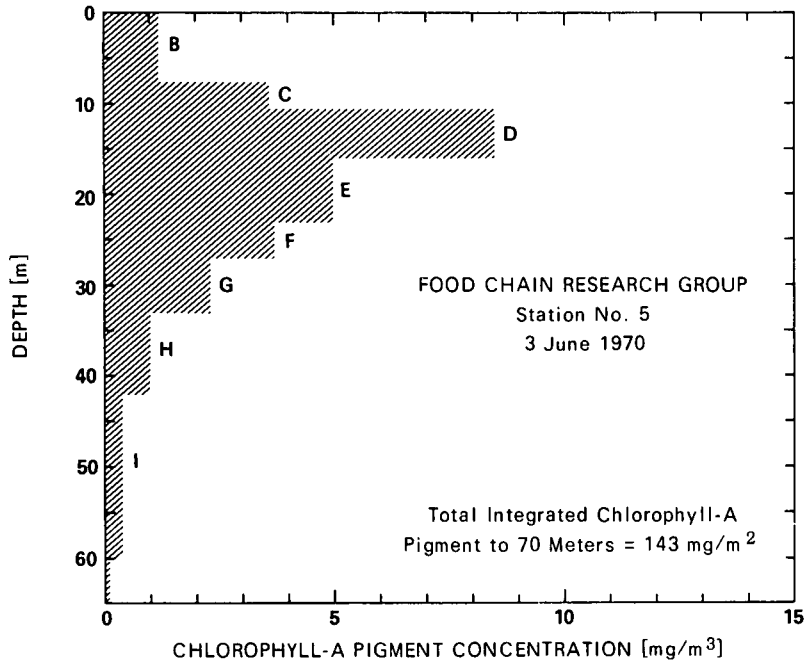

Fig. 14a

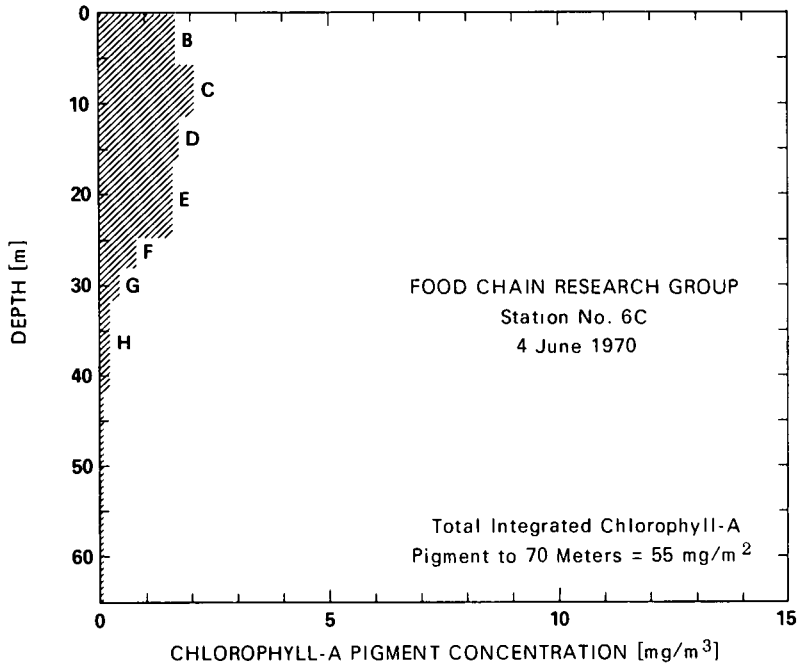

Fig. 14b

Fig. 14. The measured chlorophyll-A depth profiles shown in Fig. 13 have been approximated by uniform layers having constant chlorophyll-A concentration. The total integrated chlorophyll-A pigments in Figures 13a and 14a are the same. This is also true of Figures 13b and 14b.

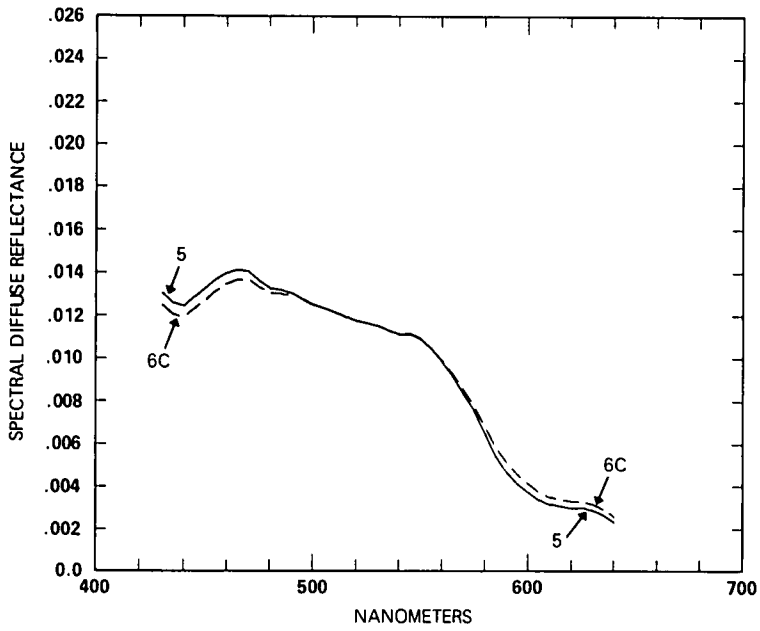

Fig. 15. Subsurface spectral diffuse reflectance at Station 5 (solid line) and Station 6C (dashed line) calculated from Fig. 14. Unlike the non-stratified cases represented by Figs. 11a through 11h and Fig. 12, the greater total integrated chlorophyll-A concentration (143 mg/m^2) at Station 5 produces a lower blue reflectance and a higher red reflectance than does the smaller concentration (55 mg/m^2) at Station 6C.

Another aspect of ambiguity is illustrated by Figs. 16a and 16b, wherein the previously described two-flow radiative transfer method was used to add layers consecutively underneath previous layers until the whole column corresponded to the actual profile measured. Thus, layer B was placed on top of the base water A, layer C was then placed under B and above A, etc. At each step the reflection signature at the top was computed. Figs. 16a and 16b show the results of this calculation. In Fig. 16a, for example, the spectral reflectance was not changed by the addition of layers E, F, G, and H. They were hidden by layers A, B, C, and D.

ADDITIONAL COMPLICATIONS

It is sometimes said that a few phytoplankton near the surface of the ocean where sunlight is plentiful are worth many times that number at a greater depth, because of the exponential-like decrease of daylight due to absorption by water molecules. The efficiency of photosynthesis by phytoplankton is, however, greater in dim light. Thus, the attenuation of daylight with depth is at least partially compensated. Organic productivity due to photosynthesis in the sea is an amazingly complicated matter that is presently undergoing intense research by scores of marine biologists throughout the world. Correlation between the remotely measureable optical signature of ocean chlorophyll and total organic productivity in the sea is far from being established. From the standpoint of optical remote sensing of marine resources, the ambiguity of the spectral signature of chlorophyll is only one part of a remarkably difficult problem.

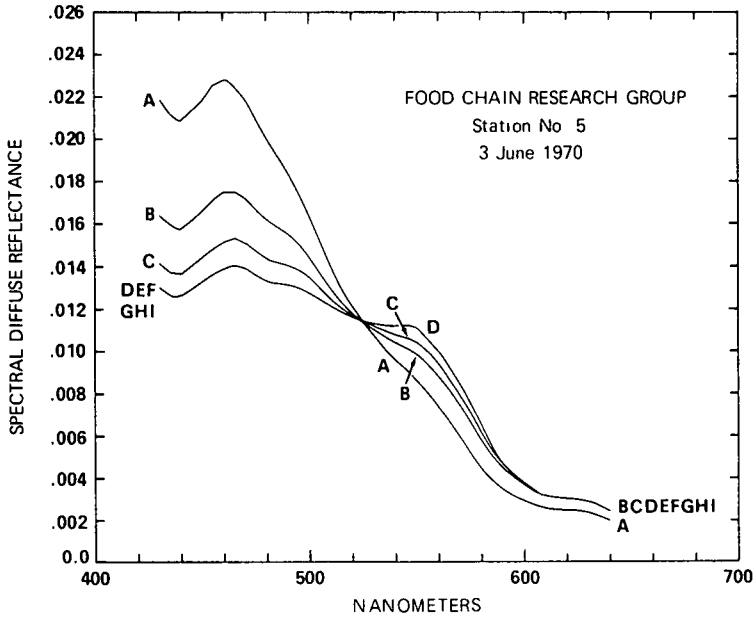

Fig. 16a

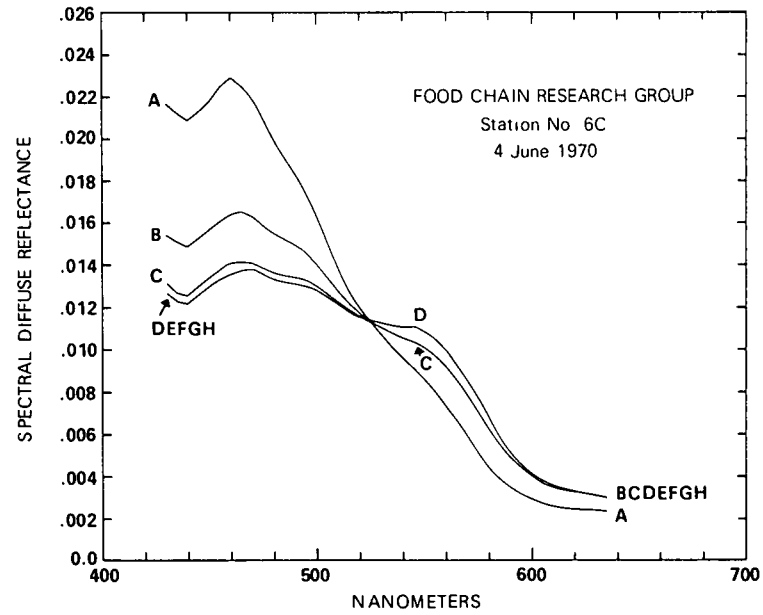

Fig. 16b

Fig. 16. Computed Subsurface Spectral Diffuse Reflectance.
Curve A: base water (infinitely deep)
Curve B: layer B from Fig. 14a, b above base water
Curve C: layers B and C above base water
Curve DEFGHI: all layers in Fig. 14a, b

RECOMMENDATION

The detection of a strong chlorophyll-A signal from some ocean location should result in a visit to that spot by a ship equipped to measure vertical profiles of chlorophyll-A pigment concentration and/or total organic productivity in the water column. A time history of the vicinity can then be made by a remote sensor, from which it may be possible to infer the probability of fish in commercial abundance.

ATMOSPHERIC DATA

Having predicted the spectral reflectance characteristics for ocean waters containing a range of chlorophyll concentrations that are of importance to ocean food chain productivity it remained to use this information to predict the chlorophyll signal that would reach remote sensors in orbit. For many years, the Visibility Laboratory has engaged in a data collection program to obtain exactly the type of information that was needed to accomplish this. These measurements have been made from aircraft, spacecraft, ships, and ground stations. Figures 17 and 18 show the facilities which were employed to collect the atmospheric data that were used in the calculations described in this paper. Figure 17 is a photograph of the specially instrumented C-130 aircraft which is used in the atmospheric data collection program conducted by the Visibility Laboratory under the auspices of the Air Force Cambridge Research Laboratories. This airplane has been extensively modified, both inside and out, for the determination of optical and meteorological parameters. It is equipped, for example, with scanners which map the skies above and below the airplane. At low altitude over the ocean the lower scanner maps the water surface and records the manner in which sunlight and skylight are reflected. All of the optical sensors in the aircraft combine to measure contrast attenuation by the lower atmosphere along any path of sight, inclined upward or downward. This information is supplemented by data taken at sea level with the instrument shown in Figure 18 called a contrast reduction meter. It has the capability of determining from a ground station the reduction of contrast throughout the total atmosphere, that is to say, from the surface of the earth to orbital altitude.

Fig. 17. Instrumented C-130 aircraft.

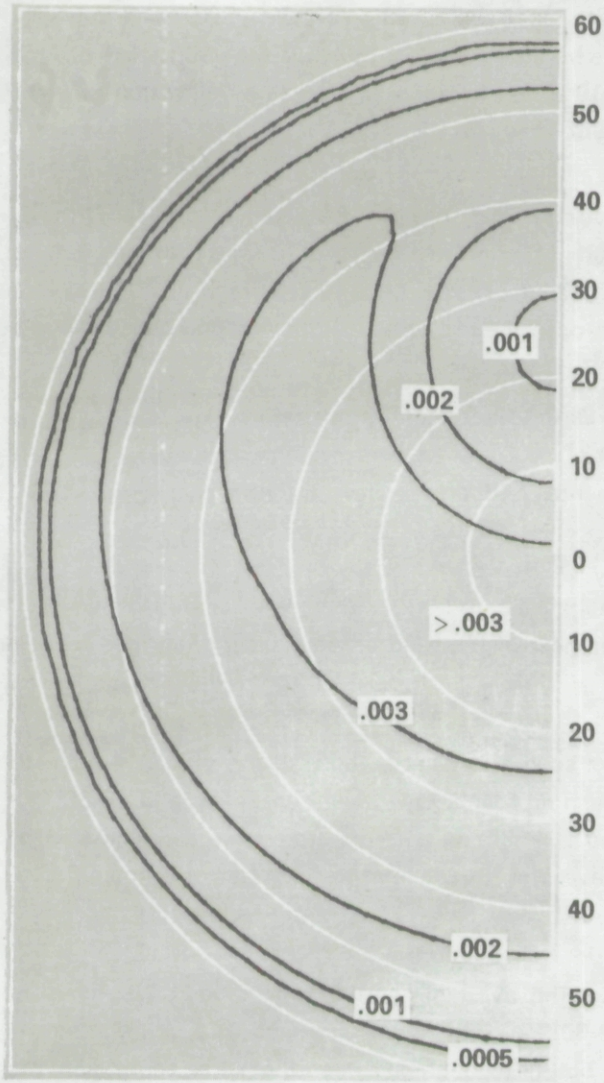

Fig. 19. Apparent Orbital Contrast

Green (560 nm)
Chlorophyll-A – 0.30 mg/m^3
Sample – Coccolithus huxleyi (8D)
Clear Day
Windspeed – 10 Knots
Solar Zenith Angle – 30.9°

Note: The chlorophyll-A concentration used for calculating the subsurface spectral reflectance was taken as uniform throughout the upper 50 meters of the ocean. The results presented also apply, of course, to any other vertical distribution of chlorophyll-A which produces the same optical effect (see comments under "Ambiguity").

Figure 19 is a plot of the apparent orbital contrast of a sample of Coccolithus huxleyi (8D) at a concentration of 0.3 mg/m^3 throughout the top 50 meters. This apparent orbital contrast was computed by first calculating the apparent spectral radiance signal available at orbital altitude from a water mass without any phytoplankton (N_B) and the signal from a water mass with the desired phytoplankton concentration (N_T). The apparent orbital contrast is thus

$$C = \frac{N_T - N_B}{N_B} .$$

In these calculations all variables except for the change in phytoplankton concentration were kept constant.

Numerous calculations were made for a variety of subsatellite local sun zenith angles, phytoplankton concentrations and atmospheric conditions.

Figure 19 depicts an occasion where the subsatellite local sun zenith angle was 30.9° and therefore the solar reflection point on the ocean surface is seen to be approximately 30° from the nadir. The observing wavelength was 560 nm and a surface windspeed of 10 knots (5.14 m/sec), a value below that required to produce whitecaps, was assumed over the whole field of view.

The calculation has been based on data for a cloud-free, clear day that was measured in the vicinity of San Diego on 2 September 1964. The air mass was unstable, continental, tropical. The National Weather Service Office reported "visibility" 10 to 20 miles (16 to 32 km), temperature 72°F to 76°F, (22°C to 24°C), relative humidity 50 to 64 percent. Local meteorologists described it as a "mild Santa Ana condition."

The ocean color sensors planned by NASA for the Earth Observatory Satellite are expected to have a sensitivity sufficient to detect a change in optical input of 0.001 when a sensor element passes from arid water to water containing significant chlorophyll-A pigments. That is to say, the effective spectral contrast threshold of the sensor is 0.001.

The contours of apparent orbital contrast in Figure 19 indicate that for the conditions specified above changes in optical input of greater than 0.001 occur over most of the field of view except near the subsolar reflection point and near the horizon.

On 2 September 1964 optical data were taken from soon after sunrise until nearly sunset. From the Visibility Laboratory's data bank six solar altitudes, ranging from a high solar zenith angle of 24.3° to a low sun with a solar zenith angle of 70.6°, were selected. These six solar zenith angles are compared by the curves in Figure 20. They represent orbital signal levels in the plane of the sun for a chlorophyll concentration of 0.30 mg/m^3 for sample 8D.

Several conclusions can be drawn from Figure 20. The available optical signal was greatest in the case of the curve representing a solar zenith angle of 30.9°. The signal level and its angular extent is almost but not quite as good when the sun is at 24.3°, but it is degraded when the solar zenith angle is 42.0°. It is clear that, for the conditions which these curves represent, to maximize the signal the solar zenith should be 30° or less. For the same concentration of sample 2C shown in Figure 21 for green light the signal is not of sufficient strength to be seen. However, it is much greater in the blue (456 nm) as will be shown later.

The field of view planned for the sensors on the Earth Observatory Satellite is 50° degrees in angular diameter. It is clear from Figure 19 that it would be better to place the field of view off the nadir, away from the sun. For example, the 50° field of view might be chosen to extend from 5° toward the sun to 45° away from the sun. Studies of similar curves for other azimuths and different atmospheric and wind speed conditions seem to make this choice of field of view appear to be wise for many circumstances. Figure 22 A-F shows a series of polar plots for the sample 8D in the green (560 nm). These were analyzed in the same manner as for Figure 19. Figure 22B is the same as Figure 19. These plots show the values and curves for sun zenith angles from 24.3 to 70.6 degrees. Comparison of the plots show how the signal changes with the sun angle in all azimuths. Again, the signal is strongest at 30.9, almost as strong at 24.3 and then when the sun reaches 42 degrees the signal begins to degrade. The wind speed for all these cases was 10 knots (5.14 m/sec).

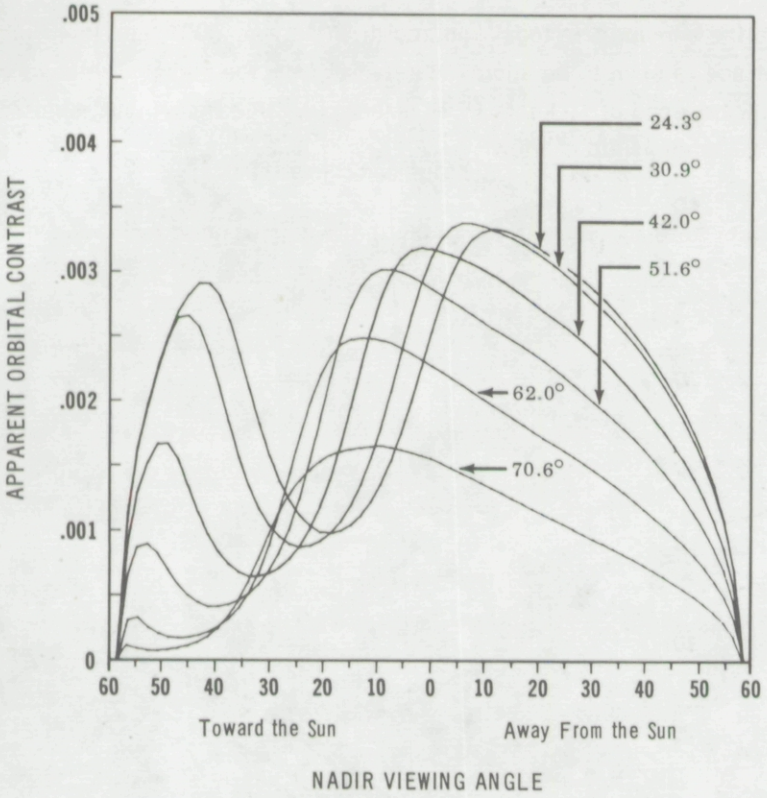

Fig. 20

Apparent Orbital Contrast Values Through Azimuth of Sun for Various Solar Angles

Green (560 nm)

Chlorophyll-A Concentration – 0.3 mg/m³ Uniform Upper 50 Meters

Sample – Coccolithus huxleyi (8D)

Clear Day

Windspeed – 10 Knots

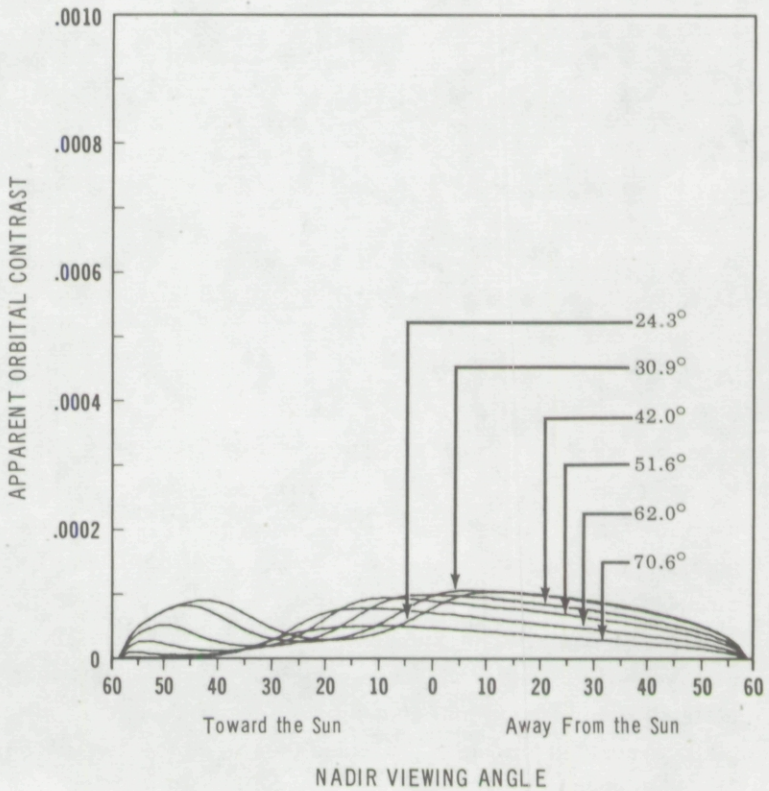

Fig. 21

Apparent Orbital Contrast Values Through Azimuth of Sun for Various Solar Angles

Green (560 nm)

Chlorophyll-A Concentration – 0.3 mg/m³ Uniform Upper 50 Meters

Sample – Monochrysis lutheri (2C)

Clear Day

Windspeed – 10 Knots

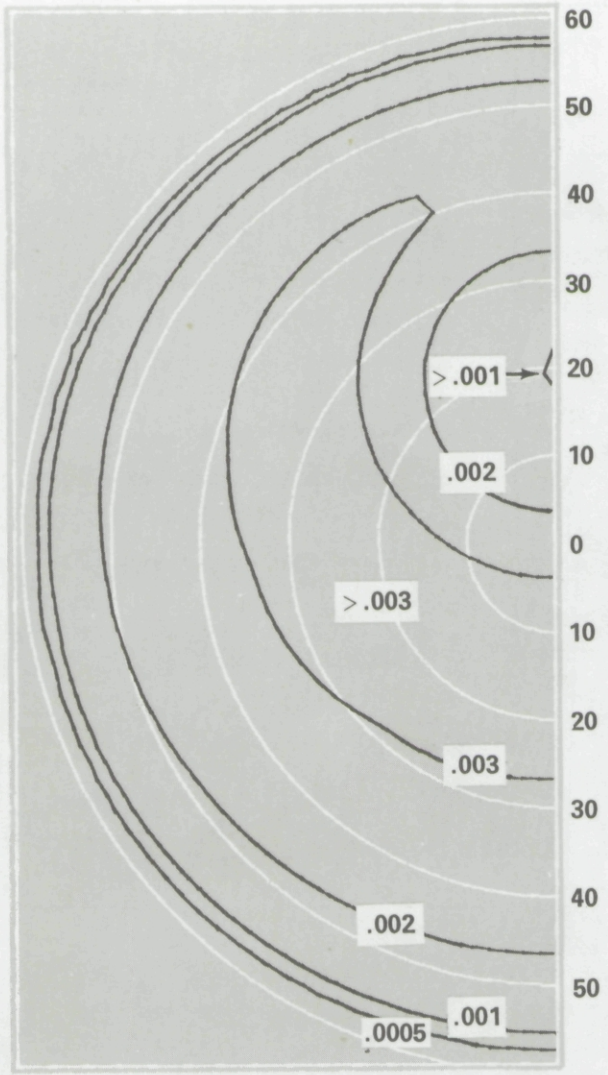

Fig. 22a. Apparent Orbital Contrast

Green (560 nm)
Chlorophyll-A – 0.30 mg/m³, Uniform
Sample – Coccolithus huxleyi (8D)
Clear Day
Windspeed – 10 Knots
Solar Zenith Angle – 24.3°

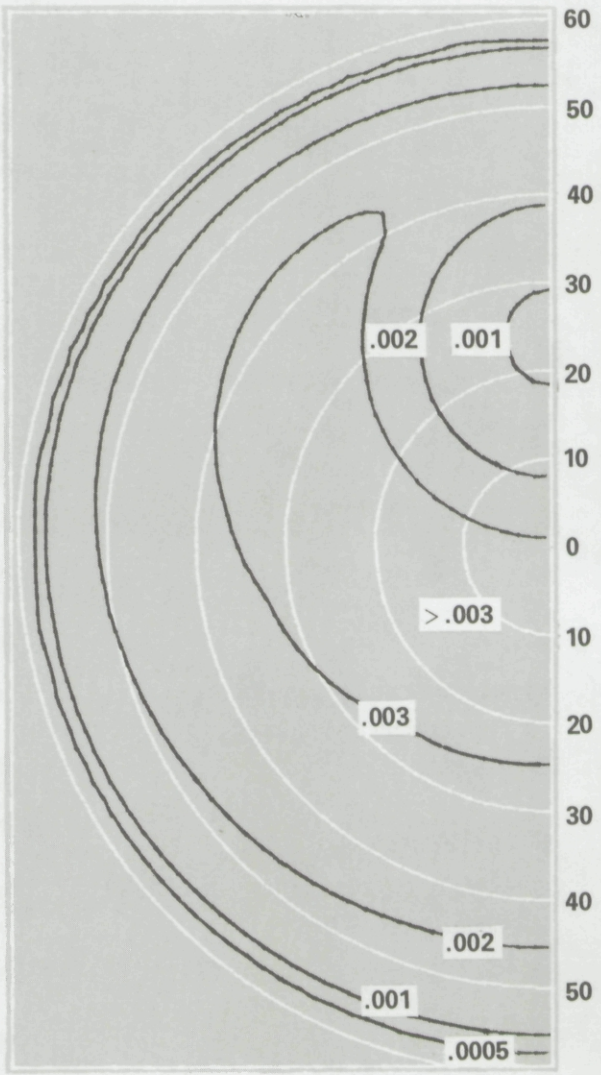

Fig. 22b. Apparent Orbital Contrast

Green (560 nm)
Chlorophyll-A – 0.30 mg/m³, Uniform
Sample – Coccolithus huxleyi (8D)
Clear Day
Windspeed – 10 Knots
Solar Zenith Angle – 30.9°

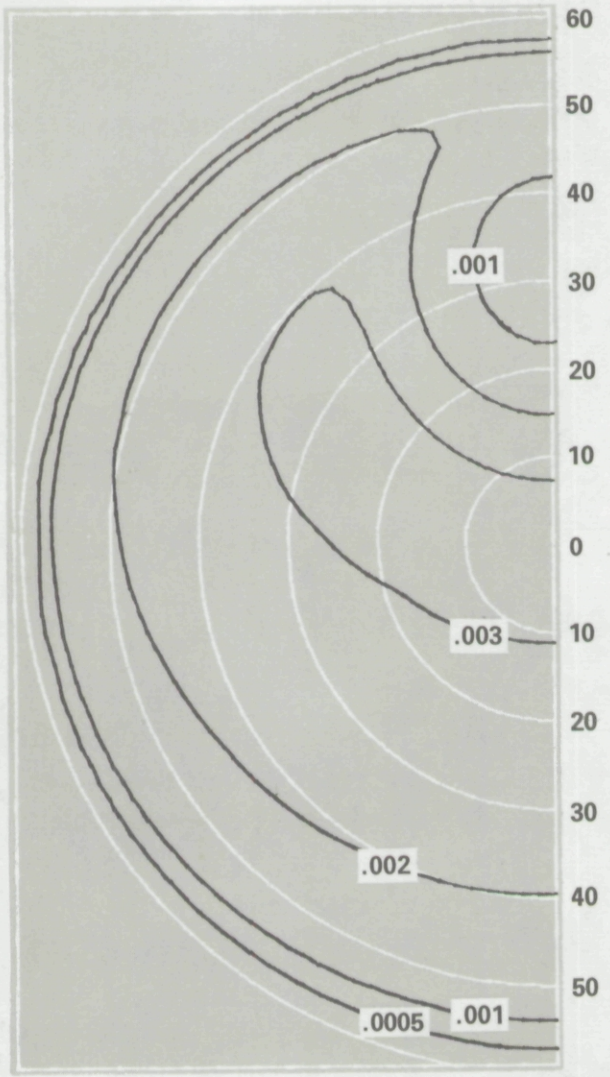

Fig. 22c. Apparent Orbital Contrast

Green (560 nm)
Chlorophyll-A – 0.30 mg/m^3, Uniform
Sample – Coccolithus huxleyi (8D)
Clear Day
Windspeed – 10 Knots
Solar Zenith Angle – 42.0°

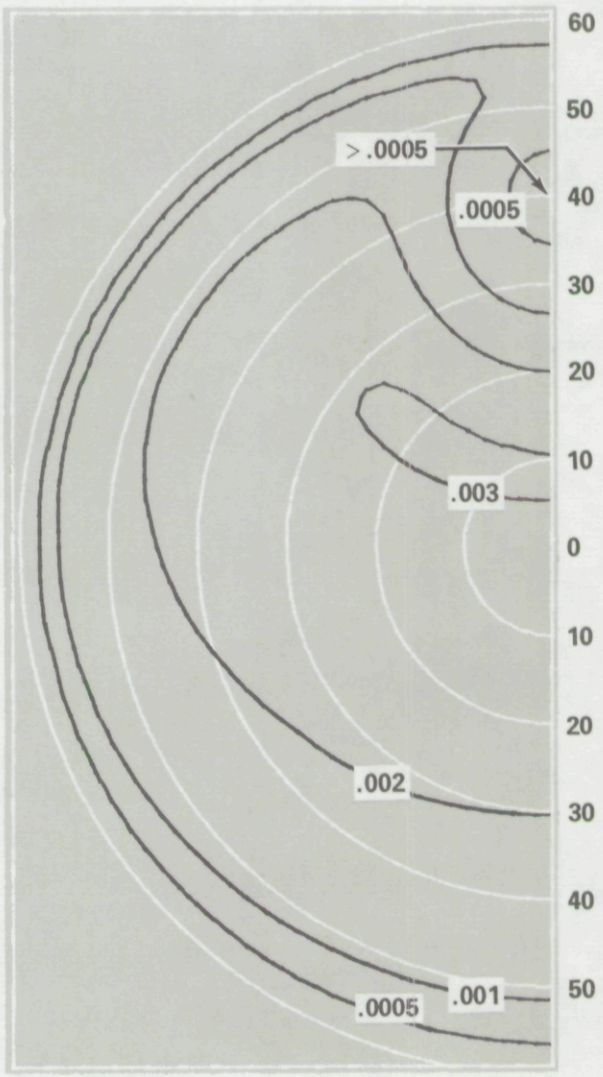

Fig. 22d. Apparent Orbital Contrast

Green (560 nm)
Chlorophyll-A – 0.30 mg/m^3, Uniform
Sample – Coccolithus huxleyi (8D)
Clear Day
Windspeed – 10 Knots
Solar Zenith Angle – 51.6°

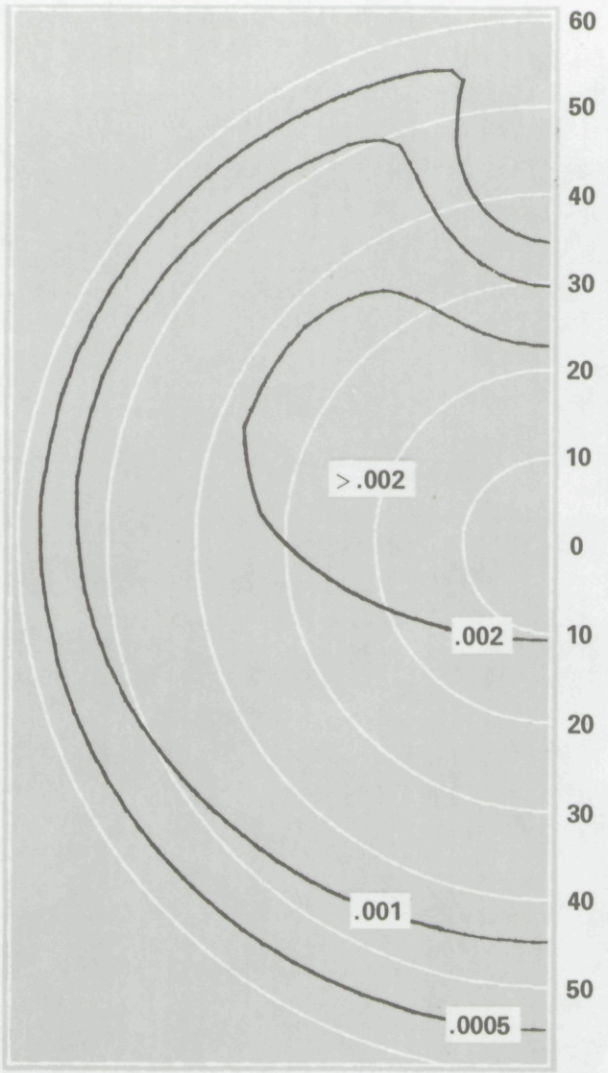

Fig. 22e. Apparent Orbital Contrast

Green (560 nm)
Chlorophyll-A – 0.30 mg/m³, Uniform
Sample – Coccolithus huxleyi (8D)
Clear Day
Windspeed – 10 Knots
Solar Zenith Angle – 62.0°

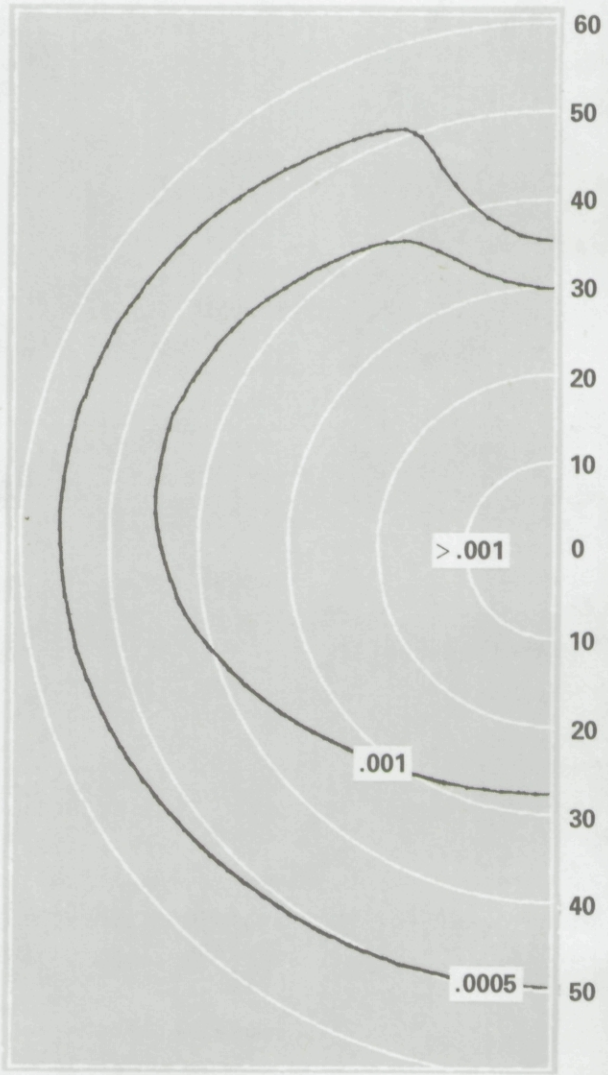

Fig. 22f. Apparent Orbital Contrast

Green (560 nm)
Chlorophyll-A – 0.30 mg/m³, Uniform
Sample – Coccolithus huxleyi (8D)
Clear Day
Windspeed – 10 Knots
Solar Zenith Angle – 70.6°

Not all fair weather is as clear as was the day represented by Figs. 19 and 20. A more common, hazier, blue sky occasion was measured near San Diego on 30 July 1964. The results of the computations for that day are shown in Fig. 23. There was a stable maritime polar air mass over the sea on that day and the sky contained 0.2 to 0.3 scattered clouds. The "visibility" was officially reported as 10 miles (16 km). The sea level temperature was 71° to 73°F (22° to 23°C) and the relative humidity was 60 to 68 percent. Although the sky was blue overhead the horizon appeared gray because of low-level atmospheric haze.

Figure 23 shows that for 560 nm the apparent orbital contrast for phytoplankton concentrations of 0.3 mg/m^3 for sample 8D still has values over 0.001 in the region of the field of view specified above. Though the atmospheric optical properties of the hazy day has lowered the apparent orbital contrast of the sea surface over the whole field of view, the conclusions with respect to the aiming of the field of view of the orbital sensor are still valid.

Figures 19 through 23 relate to chlorophyll detection by means of green light at 560 nm. Figures 11a through 11h show, however, that in terms of the subsurface reflectance of ocean water the magnitude of the optical radiance for a given chlorophyll-A pigment concentration is greater in the blue region of the spectrum that it is in the green. Scattering of light by the atmosphere, on the other hand, ordinarily attenuates the blue optical signal to a greater extent than it does the green. There has been considerable speculation, therefore, concerning whether the blue signal can be used at orbital altitudes. One result of this study is that on both the clear and the hazy days the blue chlorophyll signal (contrast) at orbit was greater than the green signal. Figures 24 and 25 show the apparent orbital contrast through the azimuth of the sun, for the two samples, Coccolithus huxleyi and Monochrysis lutheri, for a range of sun zenith angles on the clear day.* For each of the samples it can be seen that the signal for 31° solar zenith is very similar to that for 24°, but that the 31° curve is slightly higher particularly at the nadir. Figures 26a through 26f is a series of polar plots similar to Fig. 22 but for the blue region (456 nm). Again, a comparison of the plots shows how the signal changes with sun angle in all azimuths. Even on the hazy day the blue signal was, *on the average*, greater than the green signal. This is illustrated by Figs. 27a and 27b which show the apparent orbital contrast under conditions for a sun zenith angle about 31 degrees. Figure 27a is for the species Coccolithus huxleyi (Sample 8D) and shows the variations through the azimuth of the sun for a chlorophyll-A concentration of 0.3 mg/m^3, in the green region on clear and hazy days for a wind speed of 10 knots (5.14 m/sec). The same variations are shown for the blue region. A line is drawn at the threshold of 0.001 and it is evident that the signal is well above threshold for this sample on the clear day for both wavelengths. On the hazy day the signal, though less than the signal for the clear day, is above or near the threshold in the direction of optimum viewing. Figure 27b is for the species Monochrysis lutheri (Sample 2C) under the same conditions. The signal is well below threshold for all of the cases involving the green signal. However, the signal is above or near threshold for the blue signal even on the hazy day.

The apparent orbital contrasts obtained in this study were computed assuming that the atmosphere is cloud-free and uniform in its optical properties throughout the entire field of view. Obviously, that circum-

* The values of apparent orbital contrast for the blue (456 nm) are negative; this means that the region of the ocean containing the chlorophyll-A segment is darker than the base water in this spectral region.

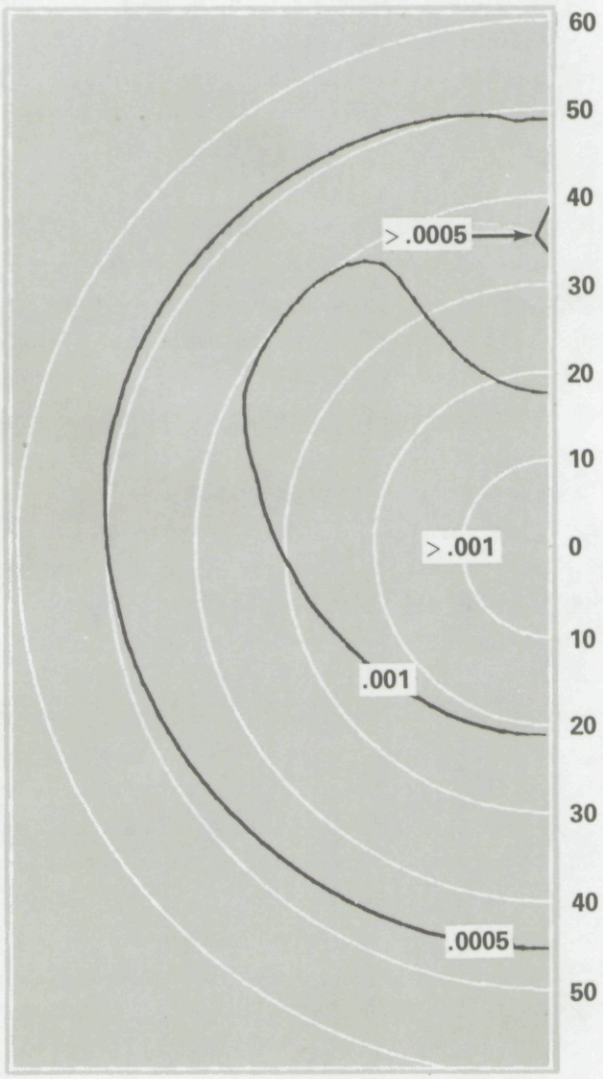

Fig. 23. Apparent Orbital Contrast

Green (560 nm)
Chlorophyll-A – 0.30 mg/m³, Uniform
Sample – Coccolithus huxleyi (8D)
Hazy Day
Windspeed – 10 Knots
Solar Zenith Angle – 32.4°

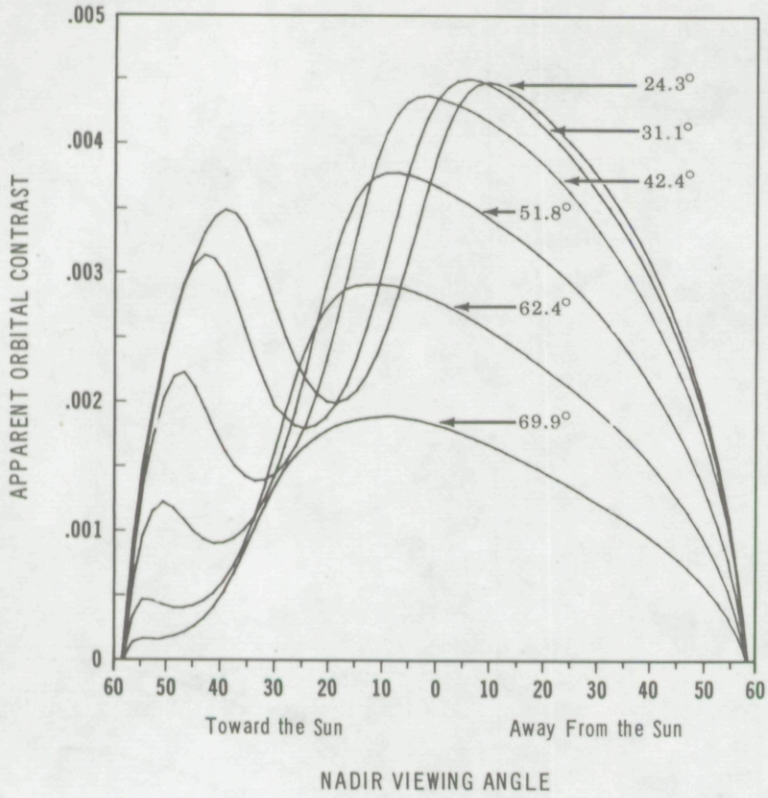

Fig. 24

Apparent Orbital Contrast Values Through Azimuth of Sun for Various Solar Angles

Blue (456 nm)

Chlorophyll-A Concentration – 0.3 mg/m³ Uniform Upper 50 Meters

Sample – Coccolithus huxleyi (8D)

Clear Day

Windspeed – 10 Knots

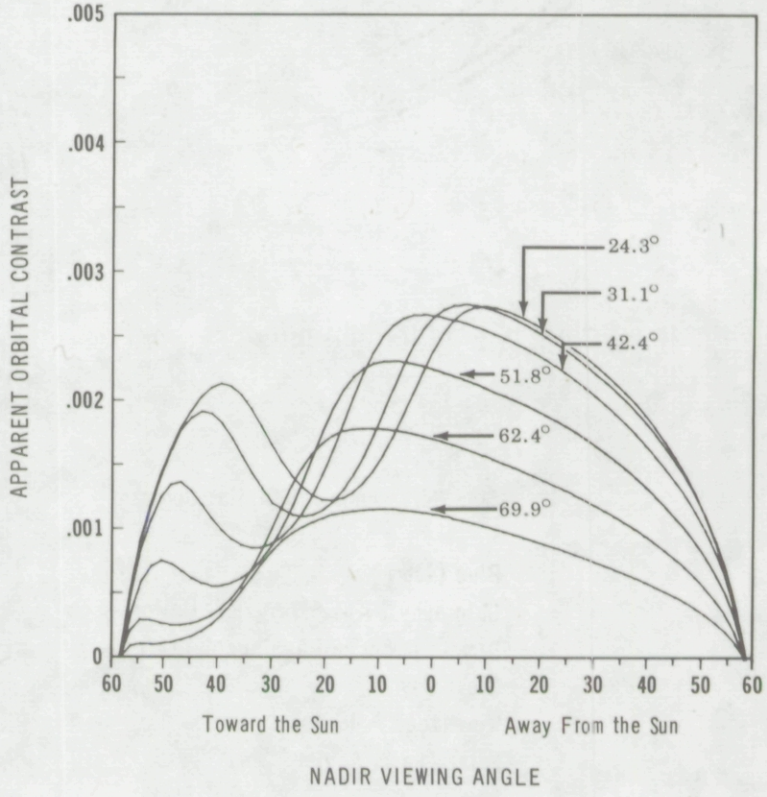

Fig. 25

Apparent Orbital Contrast Values Through Azimuth of Sun for Various Solar Angles

Blue (456 nm)

Chlorophyll-A Concentration – 0.3 mg/m³ Uniform Upper 50 Meters

Sample – Monochrysis lutheri (2C)

Clear Day

Windspeed – 10 Knots

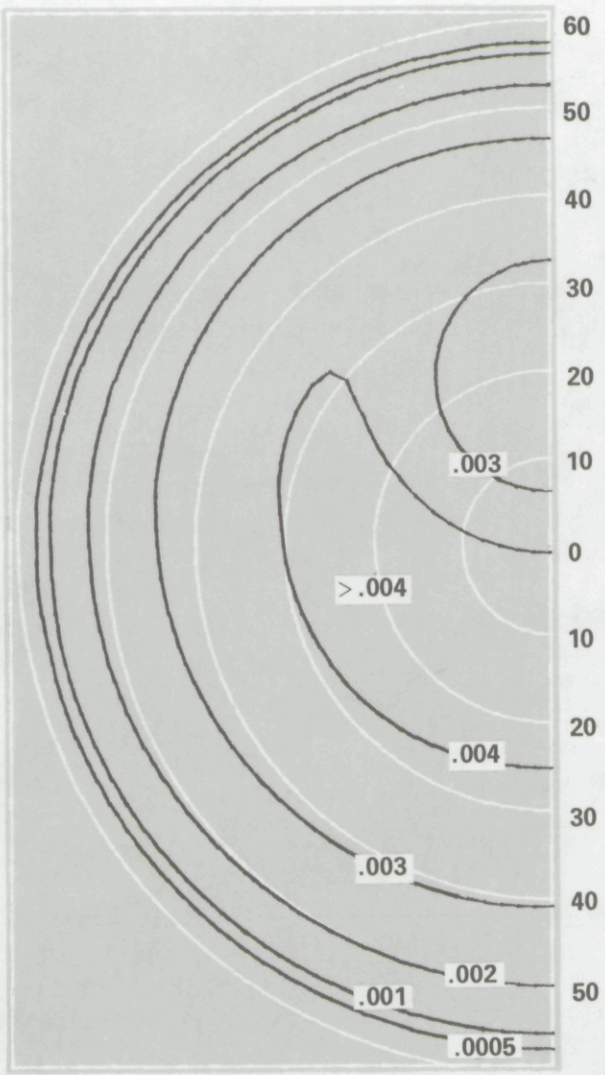

Fig. 26a. Apparent Orbital Contrast

Blue (456 nm)
Chlorophyll-A – 0.3 mg/m³, Uniform
Sample – Coccolithus huxleyi (8D)
Clear Day
Windspeed – 10 Knots
Solar Zenith Angle – 24.3°

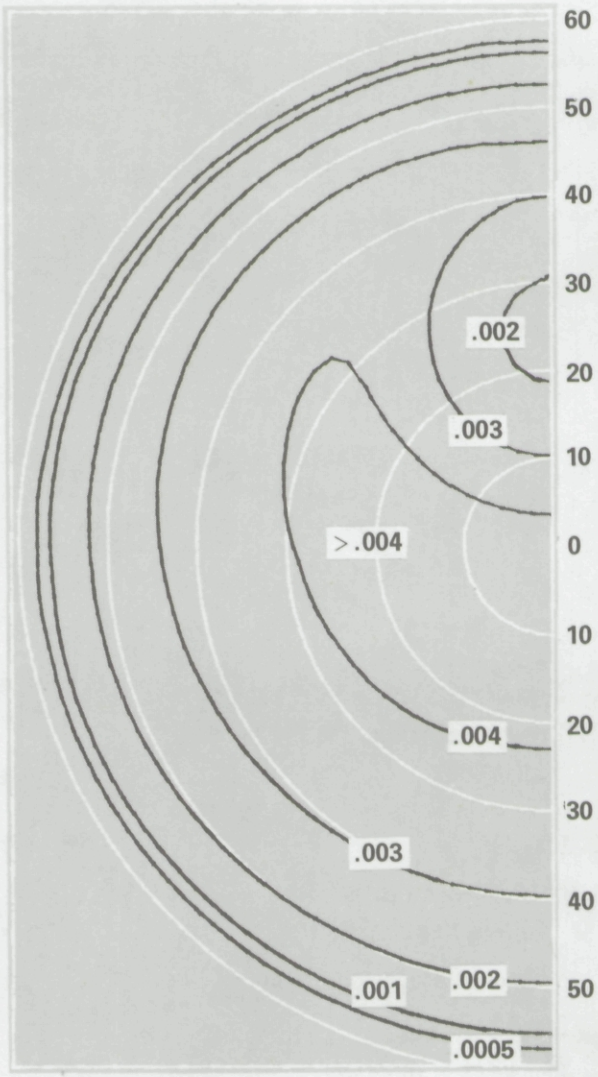

Fig. 26b. Apparent Orbital Contrast

Blue (456 nm)
Chlorophyll-A – 0.3 mg/m³, Uniform
Sample – Coccolithus huxleyi (8D)
Clear Day
Windspeed – 10 Knots
Solar Zenith Angle – 31.1°

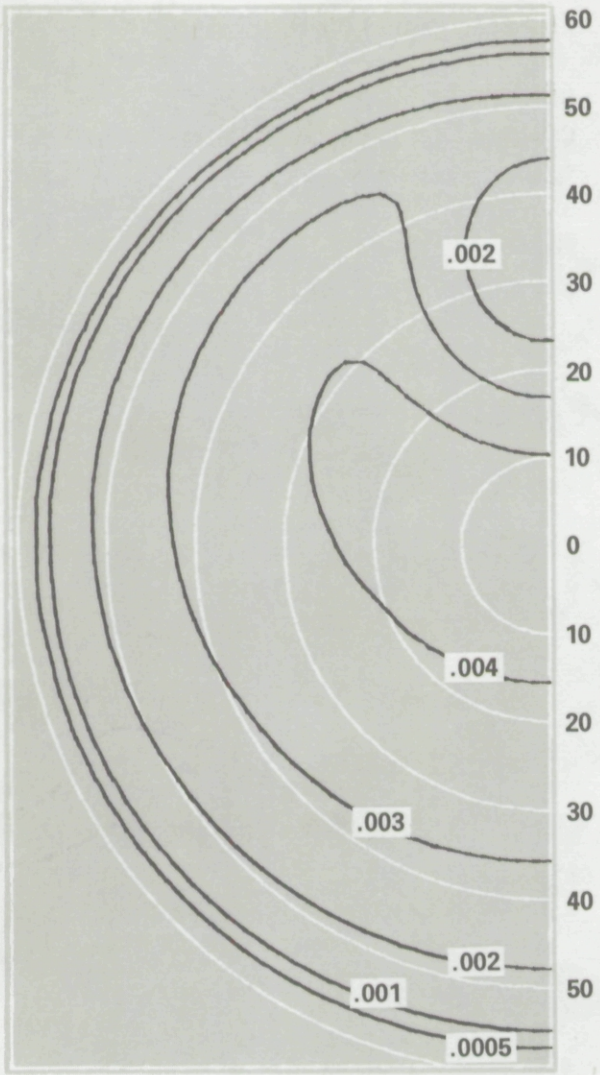

Fig. 26c. Apparent Orbital Contrast

Blue (456 nm)
Chlorophyll-A – 0.3 mg/m³, Uniform
Sample – Coccolithus huxleyi (8D)
Clear Day
Windspeed – 10 Knots
Solar Zenith Angle – 42.4°

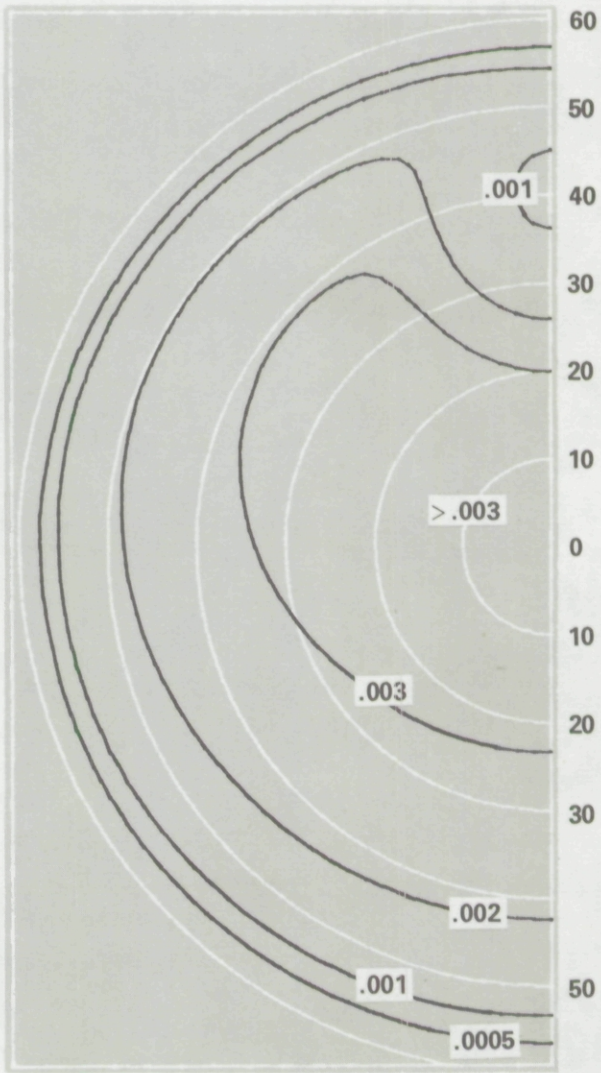

Fig. 26d. Apparent Orbital Contrast

Blue (456 nm)
Chlorophyll-A – 0.3 mg/m³, Uniform
Sample – Coccolithus huxleyi (8D)
Clear Day
Windspeed – 10 Knots
Solar Zenith Angle – 51.8°

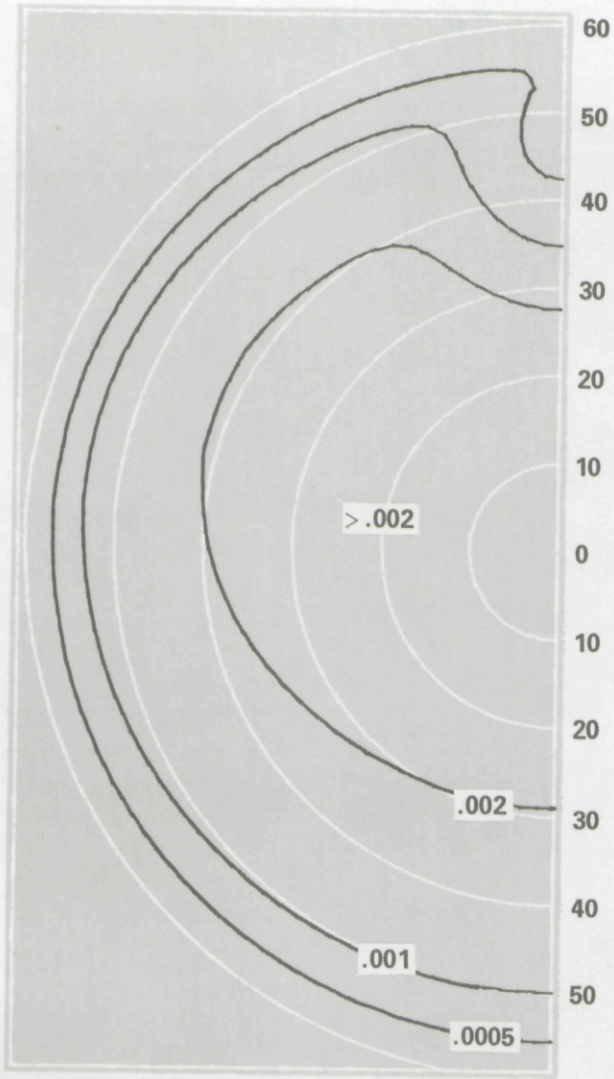

Fig. 26e. Apparent Orbital Contrast

Blue (456 nm)
Chlorophyll-A – 0.3 mg/m³, Uniform
Sample – Coccolithus huxleyi (8D)
Clear Day
Windspeed – 10 Knots
Solar Zenith Angle – 62.4°

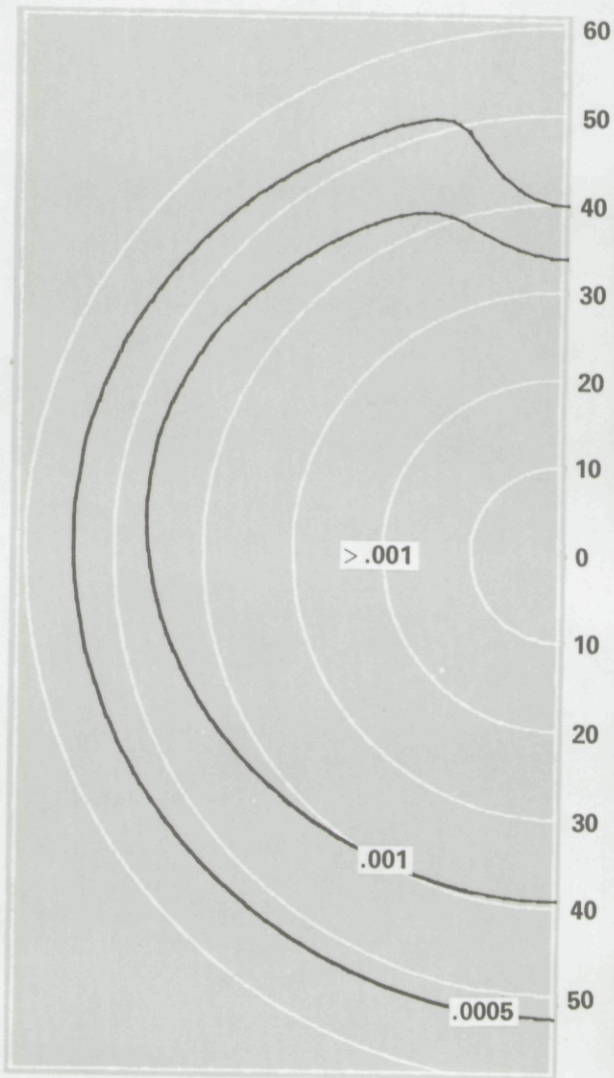

Fig. 26f. Apparent Orbital Contrast

Blue (456 nm)
Chlorophyll-A – 0.3 mg/m³, Uniform
Sample – Coccolithus huxleyi (8D)
Clear Day
Windspeed – 10 Knots
Solar Zenith Angle – 69.9°

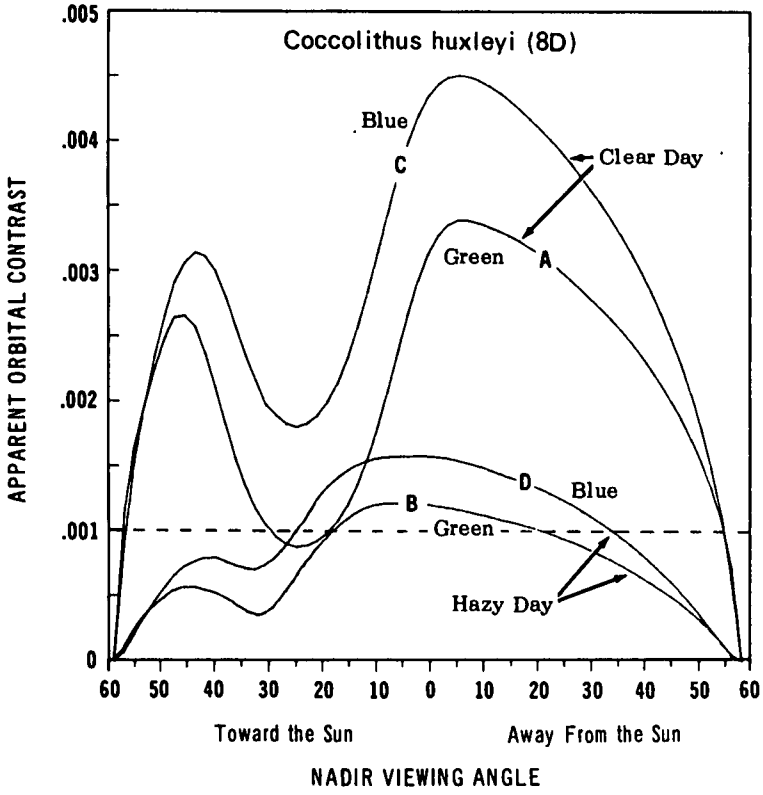

Fig. 27a.

Fig. 27

Comparison of the apparent orbital contrast of the ocean surface in the sun-nadir plane using blue light and using green light. Curves for both clear and hazy day conditions are shown. Phytoplankton species, Coccolithus huxleyi (Sample 8D) for Fig. 27a and Monochrysis lutheri (Sample 2C) for Fig. 27b have been added to the base water to bring the total chlorophyll-A concentration to 0.3 mg/m^3. Windspeed is 10 knots. The contrast of the water containing the sample is negative in the blue and positive in the green relative to the base water background.

A – Green (560 nm)
Clear, 30.9°

B – Green (560 nm)
Hazy, 32.4°

C – Blue (456 nm)
Clear, 31.1°

D – Blue (456 nm)
Hazy, 32.8°

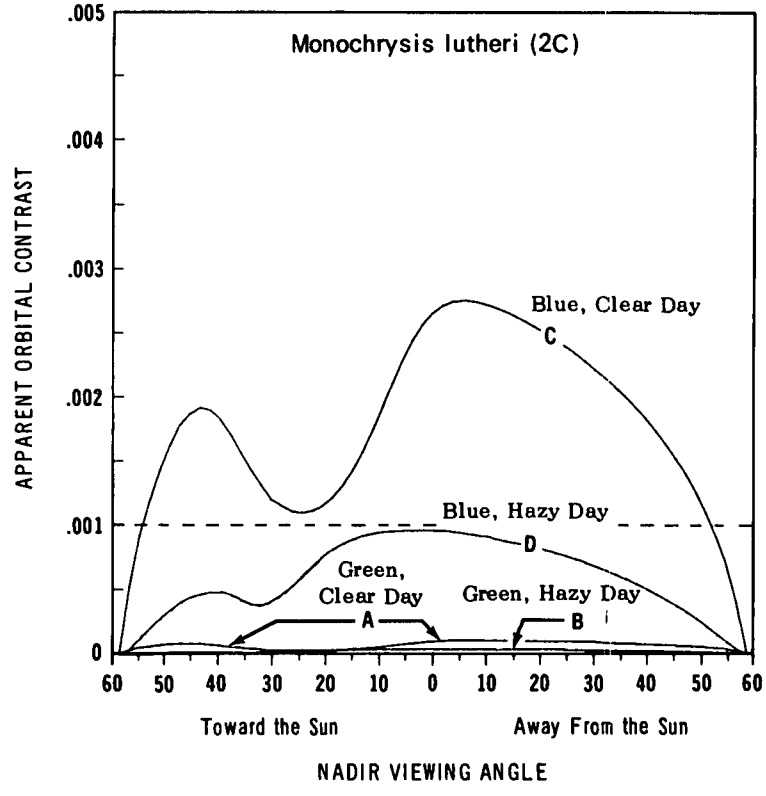

Fig. 27b.

stance rarely, if ever, exists. Our computer software and data bank can, however, readily produce corresponding plots for any meteorological condition that may be selected in the future. It appears to be significant that the optimum viewing direction and local sub-satellite solar zenith angle differ little with respect to the clear or hazy days. It seems probable, therefore, that variations in the atmospheric properties throughout the field of view (neglecting, of course, clouds or storms) will have little effect on the choice of optimum viewing conditions.

The fact that the size of the sun glitter pattern increases with wind-surface wind speed suggests that the optimum viewing direction should be moved as far away from the solar reflection point as possible without omitting the region of highest apparent orbital contrast.

Optical effects due to small scale surface wind speed variations, slicks, etc., can be treated by our present software although continuing study of the inherent properties of these phenomena may be needed.

REFERENCES

1. J. E. Tyler and R. C. Smith, *Measurements of Spectral Irradiance Underwater*, (Gordon and Breach Science Publishers, New York, 1970).

2. J. E. Tyler, R. C. Smith, and C. R. Goldman, "Optical Properties and Color of Lake Tahoe and Crater Lake," Limnol. Oceanog., **18**, 189 (1973).

3. S. Q. Duntley, J. Opt. Soc. Am. **32**, 61 (1942).

4. A. C. Hardy, J. Opt. Soc. Am. **25**, 305 (1935).

5. J. I. Gordon, "Directional Radiance (luminance) of the Sea Surface," S.I.O. Ref. 69-20 (1969).

2. INHERENT SPECTRAL RADIANCE SIGNATURES OF THE OCEAN SURFACE

R. W. Austin

2.1 INTRODUCTION

In the design and evaluation of systems for the remote sensing of ocean color it is necessary to know the magnitude of the spectral radiance available at the sensor. The basic physical principles involved in the generation of signal at the ocean surface and its transmission through the atmosphere are well known. However, the magnitudes of the various component parts of this signal and the manner in which they vary with wavelength, solar zenith angle, water type, sea state, etc., are not adequately documented with measurements which will allow the investigator to predict apparent spectral radiances with adequate precision.

We will, in what follows, formulate an approach to synthesizing the spectral radiance signal which reaches the sensor, show how the components of this signal may be expected to vary, and how these variations, in turn, will affect the magnitude of the spectral radiance. Examples of data are provided: some acquired as "surface truth" for remote sensing experiments and some obtained specifically to increase the data bank available for this study when it became obvious that insufficient data of suitable quality existed. The measurement program is expected to continue and the data presented herein should be considered as provisional samples, hopefully usable as they are here reported, but to be expanded to include other atmospheric conditions, solar zenith angles, etc. Other bodies of data on underwater spectral radiance which have recently become available will also be incorporated into the data bank as the study progresses. In addition, ongoing research programs of the Laboratory will be contributing new information in such related areas as the angular distribution of underwater radiance, the measured and computed spectral reflectances of various ocean waters, ocean surface reflectance due to wind-generated white water, bottom reflectances, and atmospheric optical data obtained over the oceans.

The present study will be specifically restricted to the problem of the nadir radiance and we will not consider the contribution to this radiance from sunglitter. The extension to other paths of sight and the generalization of the ocean surface reflectance problem to include glitter are topics that will be treated in the follow-on study.

2.2 DISCUSSION

The upwelling radiance signal, available for the remote sensing of ocean color, originates from the interaction of the downwelling light field with the ocean surface, the body of water and the ocean bottom. Attention will be restricted in the present discussion to the case where the water is of such a depth that the effect of the existence of the bottom may be neglected.

SURFACE REFLECTED RADIANCE

The smooth or wind-roughened water surface specularly reflects a fraction of the radiance of the sky. If wind-generated white water is present, an additional radiance will be added which represents a fraction of the total downwelling irradiance. We will not consider the white water contribution at this time, as it is the subject of a separate study and preliminary indications are that the results of this study may reduce the presently accepted effective reflectance of this component by a significant amount. In any case, for many of the lower windspeed conditions commonly encountered, white water will have a small or negligible effect on the inherent radiance of the ocean surface.

The radiance, N_r, due to the surface reflectance is simply,

$$N_r = r_d N_s \,, \tag{1}$$

where r_d is the fresnel reflectance of the surface for downwelling radiance and N_s is the radiance of the sky in the angular region specularly reflected by the surface (see Fig. 1). The reflectance is a function of the index of refraction of the water, the viewing angle, and, since the wind affects the statistics of wave slopes on the ocean surface, it is also a function of windspeed. The index of refraction does not vary sufficiently with wavelength to result in any appreciable wavelength dependence of the reflectance. Table I presents reflectance values for various observation angles and windspeeds. Note that for all windspeeds shown and observation angles out to 40° from the nadir, the reflectances fall between .0211 and .0291. Thus, for viewing angles in this range the surface reflectance is small and shows no major dependence on either angle or windspeed. The radiance of the sky, on the other hand, varies with location in the sky, increasing in the proximity of both the sun and the horizon. Consequently the reflectance values in Table I can only be used to determine the reflected radiance when the region of the sky being reflected is suitably uniform. This situation occurs when the windspeed is low or when the reflected sky is away from the horizon and sun.

Table I

Time-Averaged Air/Water Surface Reflectance From Above

Observation Angle θ_a	Windspeed (m/s)			
	0	4	10	16
0°	0.0211	0.0211	0.0212	0.0212
10°	0 0211	0.0212	0.0213	0.0214
20°	0.0213	0.0214	0.0217	0.0220
30°	0.0222	0.0226	0 0232	0.0239
40°	0 0253	0.0262	0.0276	0.0291
50°	0.0346	0.0366	0.0394	0.0420
60°	0 0610	0.0646	0.0686	0.0709
70°	0.1354	0.1365	0.1316	0 1247
80°	0.3502	0 2919	0.2371	0.2046
90°	1.0000	0.4934	0.3642	0 3002

For sea water, refractive index $n_w = 1.341$

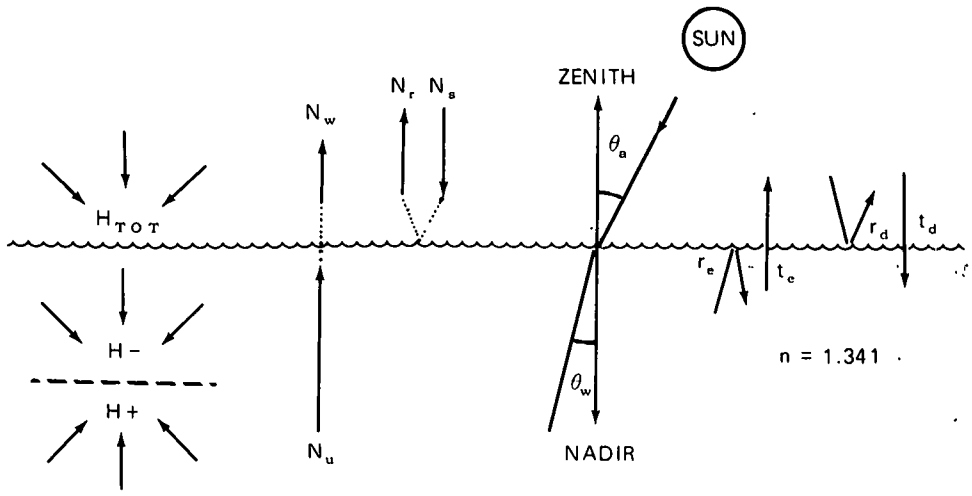

N_s = Zenith Radiance
N_r = Reflected Portion of Zenith Radiance
N_u = Nadir Underwater Radiance
N_w = Portion of N_u Propagated Upwards Through the Surface
$H_\odot$ = Irradiance at Sea Level Due to Sun Only
H_S = Irradiance at Sea Level Due to Sky Only
H_+ = Upwelling Underwater Irradiance
H_- = Downwelling Underwater Irradiance
r_e, t_e = Emergent Reflectance and Transmittance of Sea Surface From Water to Air
r_d, t_d = Downwelling Reflectance and Transmittance of Sea Surface From Air to Water

$$N_o = N_w + N_r \qquad N_r = r_d N_s \qquad R_w = \frac{\pi N_w}{H_{TOT}} \qquad N_w = \frac{t_e}{n^2} N_u \qquad H_{TOT} = H_S + H_\odot \qquad R_\pm = \frac{H_+}{H_-}$$

Fig. 1 . Schematic representation of concepts and symbols relating to the development of the inherent spectral radiance of the ocean.

Figure 2a shows measurements of spectral radiance of the zenith sky for three solar zenith angles, 64°, 49°, and 24°. Figure 2b shows the same information for a position 90 degrees from the sun in the sun-zenith plane. The latter curves show a greater wavelength dependence than the former, in agreement with the subjective impression that the sky is generally whiter at the zenith and bluer at right angles to the sun.

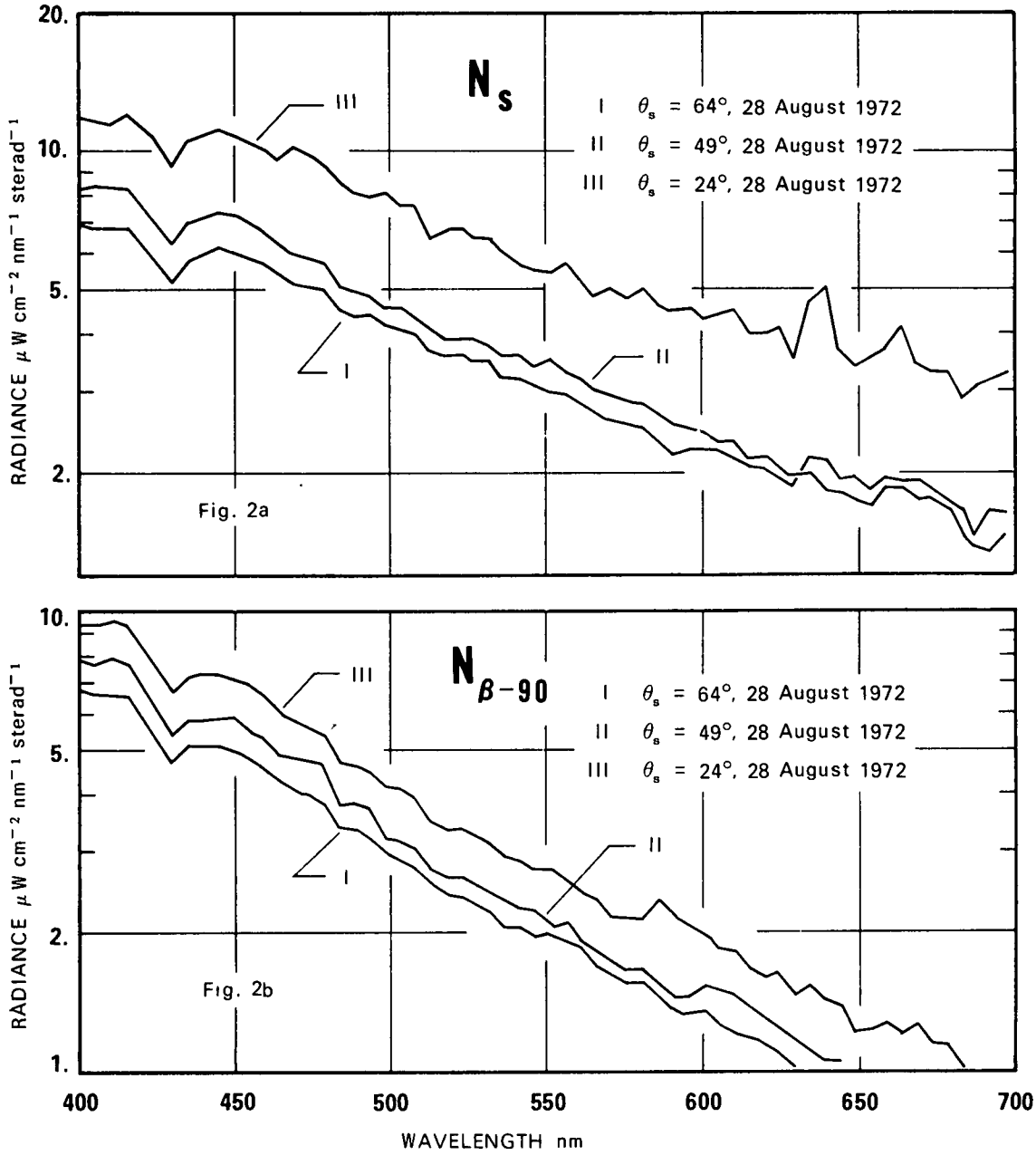

Fig. 2 Spectral radiance N_s of the sky at the zenith, and at a point 90° from the sun in the sun-zenith plane $N_{\beta-90}$, for three solar zenith angles θ_s. No smoothing has been performed on the curves. Spectral bandwidth was 5.9 nm or less. Angular field of view of spectroradiometer was 0.6° x 4.6°.

The measurements presented in Fig. 2 were obtained with the Scripps underwater spectroradiometer (Tyler and Smith, 1970), which was configured and calibrated to measure spectral radiance in air. It was operated on the roof of the Visibility Laboratory in San Diego, 0.4 nautical miles from the ocean, on six days in July and August, 1972, when clear-sky conditions prevailed. Spectral radiances of the sky at these two positions in the sky were obtained on 19 occasions, for solar zenith angles ranging from 14° to 64°. The data shown in Fig. 2a and 2b were obtained on 28 August 1972.

The component, N_r, of the surface radiance due to the ocean surface reflectance will have the same spectral behaviour as the sky radiance but will be reduced in magnitude by the appropriate reflectance, obtained from Table I.

WATER REFLECTED RADIANCE

The second component of radiance returned upward from the ocean, is that due to the interaction of the downwelling irradiance with the body of water itself. It is this component, denoted as N_w, that contains the spectral signature or water color information. In a manner similar to that used in the treatment of surface-reflected radiance, we may define a reflectance, R_w, for the water such that

$$N_w = R_w \frac{H_{tot}}{\pi} . \qquad (2)$$

This is the reflectance that a perfectly diffuse surface must have in order to return a radiance N_w for an incident irradiance H_{tot}. Note that R_w is an exterior reflectance, i.e., it does not in its construct require the measurement or knowledge of anything below the surface of the water. It does of course vary with wavelength, type of water, and to some extent, with the angular distribution of the radiance constituting H_{tot}. The determination of R_w by the direct measurement of N_w and H_{tot} has proven to be difficult from shipboard due to the noise introduced by surface waves. Measurements of R_w have been made from aircraft (Clarke and Ewing, 1973), although there may be difficulties in some circumstances in identifying the particular patch of water being measured and distinguishing the surface and atmospheric effects from water effects.

The approaches that will now be developed to determine N_w, and consequently R_w, utilize existing underwater data obtained in various types of water, or specific measurements of the underwater spectral radiance, N_u. Whereas more attention is concentrated on radiances at or near the nadir, the techniques can be extended to include other observation angles.

In passing upward through the surface, flux contained within an incremental solid angle $d\Omega_w$ in water will be spread into a larger solid angle $d\Omega_a = n^2 d\Omega_w$. Therefore, N_u, the emerging subsurface radiance, having the units of power/area · solid angle, will decrease by a factor of $1/n^2 = 0.555$ by virtue of this refraction effect at the surface. There is, in addition, an emergent transmittance, t_e, due to the fresnel reflectance at the surface of $t_e = 1 - r_e = 0.979$. Table II provides values for r_e for various windspeeds and angles of observation (measured underwater). The nadir radiance above the surface is then,

Table II

Time-Averaged Air/Water Surface Reflectance From Below

Observation Angle θ_w	Windspeed (m/s)			
	0	4	10	16
0°	0.0211	0.0211	0.0213	0.0217
10°	0 0211	0.0213	0.0218	0.0228
20°	0.0218	0.0227	0.0255	0.0334
30°	0.0265	0 0325	0.0613	0.0961
35°	0 0350	0.0602	0 1234	0.1686
40°	0.0588	0.1559	0.2367	0 2741
45°	0.1529	0 3801	0 4065	0.4131
50°	1 0000	0.6718	0.5988	0.5629
55°	1.0000	0.8905	0 7715	0.7055
60°	1.0000	0.9807	0.8967	0.8277

For sea water, refractive index $n_w = 1.341$

$$N_w = \frac{t_e}{n^2} N_u = 0.544\, N_u \,. \tag{3}$$

Adding Eq. (1) and (3), an expression for the total inherent radiance, N_o, leaving the surface may be obtained, i.e.,

$$N_o = N_w + N_r = \frac{t_e}{n^2} N_u + r_d N_s \,, \tag{4}$$

or if the reflectance, R_w, and the total downwelling irradiance on a horizontal plane, H_{tot}, are known or can be estimated, we can combine Eq. (1) and (2) to obtain

$$N_o = \frac{R_w}{\pi} H_{tot} + r_d N_s \,. \tag{5}$$

Here attention is called to the differences between the downwelling specular reflectance r_d appropriate to the zenith sky radiance and the effective diffuse reflectance R_w returning a portion of the incident irradiance. The fresnel reflectance, r_d, is essentially constant with wavelength while the water reflectance, R_w, varies with wavelength in significantly different ways for different waters.

From Eq. (2) and (3) we find that

$$R_w = \frac{\pi t_e}{n^2} \cdot \frac{N_u}{H_{tot}} . \qquad (6)$$

Measurements of N_u have been obtained with the Scripps underwater spectroradiometer on various occasions and selected data are herein combined with measurements of H_{tot} obtained with the same instrument operating as a spectral irradiance meter. The latter measurements were obtained on the same occasions as the sky radiances presented in Fig. 2. Data having comparable solar zenith angles were selected and combined to obtain the curves of R_w versus wavelength plotted in Fig. 3. These curves show markedly different shapes for waters that were low (II), intermediate (I), and moderately high (III) in chlorophyll concentration. The Munsell hue determinations for the water color at the three stations were 10B (Blue), 10BG (Blue Green), and 10G (Green) which might be expected from the shapes of these curves. Note also that the reflectance magnitudes are very low. Values from 1 percent to 2 percent at the wavelengths of maximum reflectance are found.

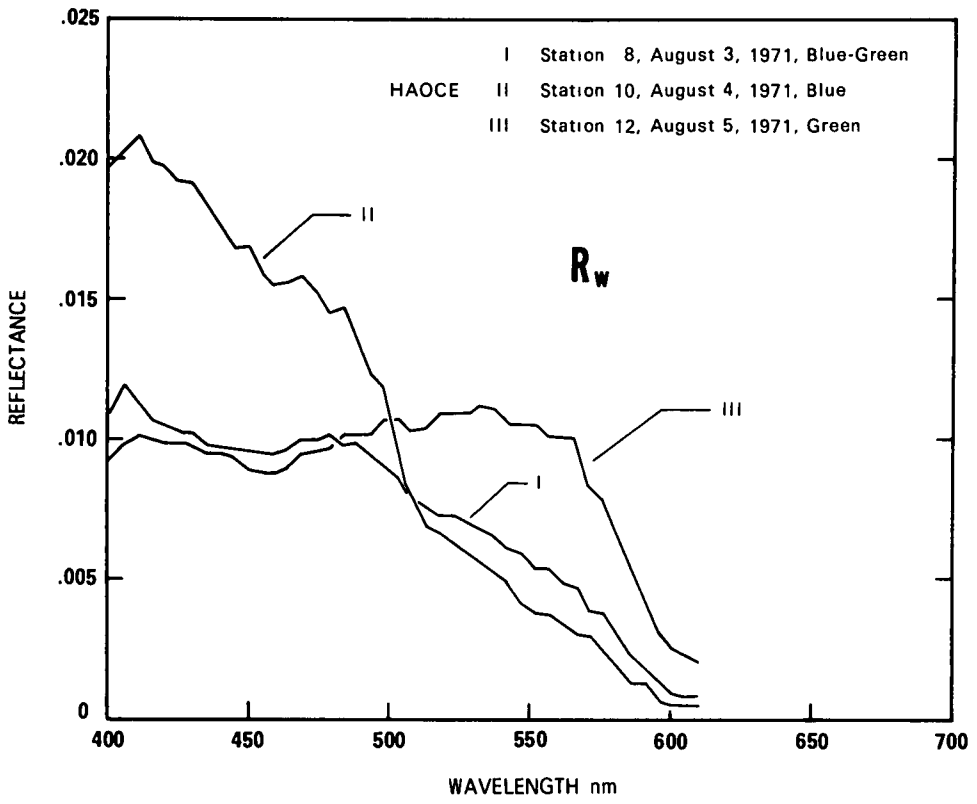

Fig. 3 Irradiance reflectance indicating the ratio of the upwelling underwater radiance available immediately above the ocean surface to the total downwelling irradiance H_{TOT} on the surface.

The data used for N_u are shown in Fig. 4. They were derived as follows. Measurements of the upwelling spectral radiance were obtained, at depths of 2.2 meters and 7.7 meters, every 5 nanometers throughout the visible spectrum. The measurements on each of the three days were obtained over a period of less than one hour. The solar zenith angles, θ_s, given in the legends apply to the midtime of the data acquisition period. The attenuation coefficient, K, at each wavelength was obtained from the radiance values at the two depths using the relation,

$$K = \frac{1}{Z_2 - Z_1} \ln \frac{N_1}{N_2} = \frac{1}{5.5} \ln \frac{N_{2\,2}}{N_{7\,7}} .$$

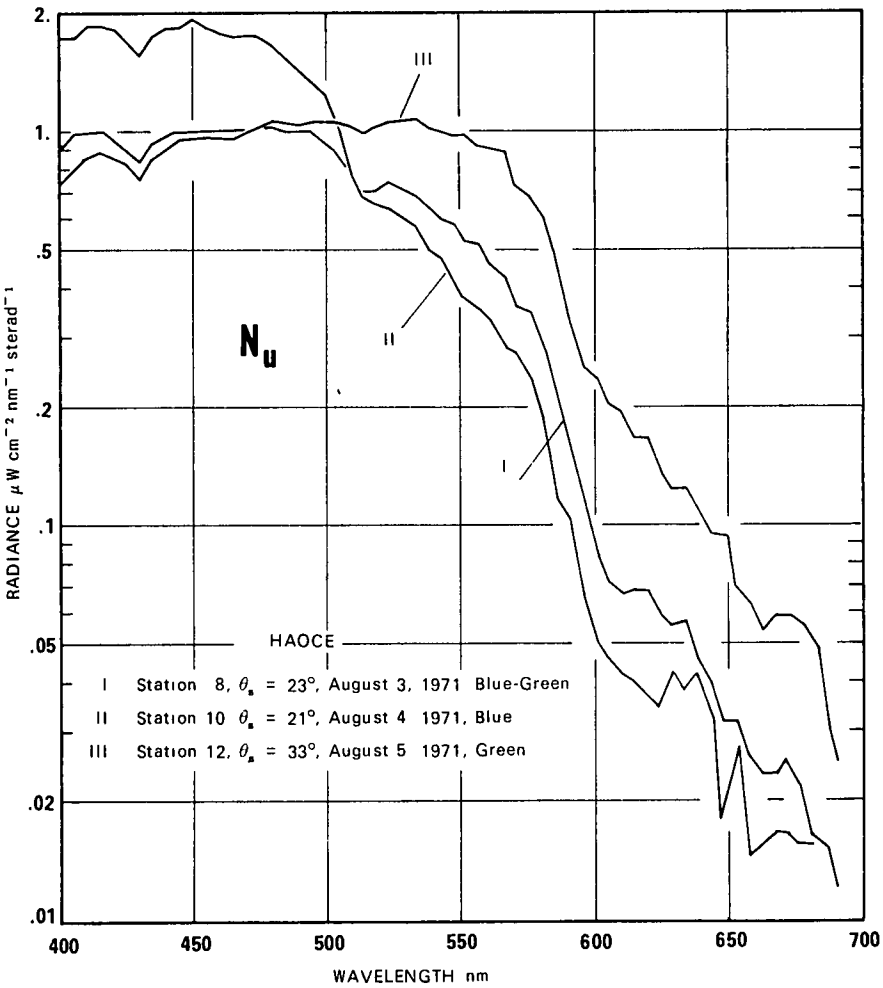

Fig. 4 Underwater nadir radiance immediately below the ocean surface, for three ocean waters of distinctly different color.

The radiance immediately under the surface was then computed assuming this same attenuation coefficient also applied to the upper 2.2 meters of water. These measurements were obtained in Southern California coastal waters in support of a high altitude ocean color experiment (HAOCE) conducted by the Laboratory for Meteorology and Earth Sciences of the Goddard Space Flight Center.

DOWNWELLING SPECTRAL IRRADIANCE

Figure 5 shows downwelling spectral irradiance data measured at four solar zenith angles on 28 August 1972. The overhead sky was cloudless, but variable maritime haze occurred during the day with visibilities reported as 2, 3, 4, and 5 miles at the time of measurement, for curves I through IV, respectively. The measurements were taken with the spectroradiometer fitted with an irradiance collector (cosine weighting function). The system was calibrated against a standard of spectral irradiance traceable to NBS. The illuminances, E_{tot}, represented by these four H_{tot} curves were calculated by performing the integration,

$$E_{tot} = 680 \int_{\lambda} H_{tot}(\lambda) \cdot V(\lambda)\, d\lambda .$$

The results were compared with values from illumination tables (Brown 1952) for the same solar zenith angles and were found to be generally higher than those tabulated. Although values in excess of Brown's can be obtained under certain conditions, other factors indicate that certain operational conditions may have precluded maintaining the expected measurement accuracy in the field. Subsequent to these measurements corrective modifications to the instrument, its calibration and operational procedure have been initiated; however, no new data are yet available. The data are presented without any attempt at smoothing or correcting obviously anomalous points. In this way the reader may judge the precision of the measurements.

Figure 5 also shows three curves of downwelling spectral irradiance from the sky with the contribution from the sun removed. This was accomplished by occulting the sun with a small disk casting a shadow on the irradiance collector. These measurements were obtained immediately following the H_{tot} measurements and can be considered as contemporaneous data. It may be noted that these curves are not significantly dependent on solar zenith angle. In fact, the curve for $\theta_s = 64°$ is not shown because it almost completely overlapped that for $\theta_s = 49°$. The sky irradiance component H_s may vary with the type of day, however, and might be expected to be somewhat lower and sloping more steeply downward with increasing wavelength on days with clear blue skies while being somewhat higher and flatter on more hazy days.

The component of the downwelling irradiance due to the sun $H_\odot$ is, of course, the difference between H_{tot} and H_s; thus

$$H_\odot = H_{tot} - H_s .$$

We may define a dimensionless ratio $y = H_s/H_{tot}$ between the two measured irradiances. It follows that

$$\frac{H_\odot}{H_{tot}} = 1 - y .$$

These ratios are useful indicators of the condition of the sky, i.e., hazy or clear, and will be used as parameters in the following paragraphs. In Fig. 6, 1 – y versus wavelength has been plotted. Its shape

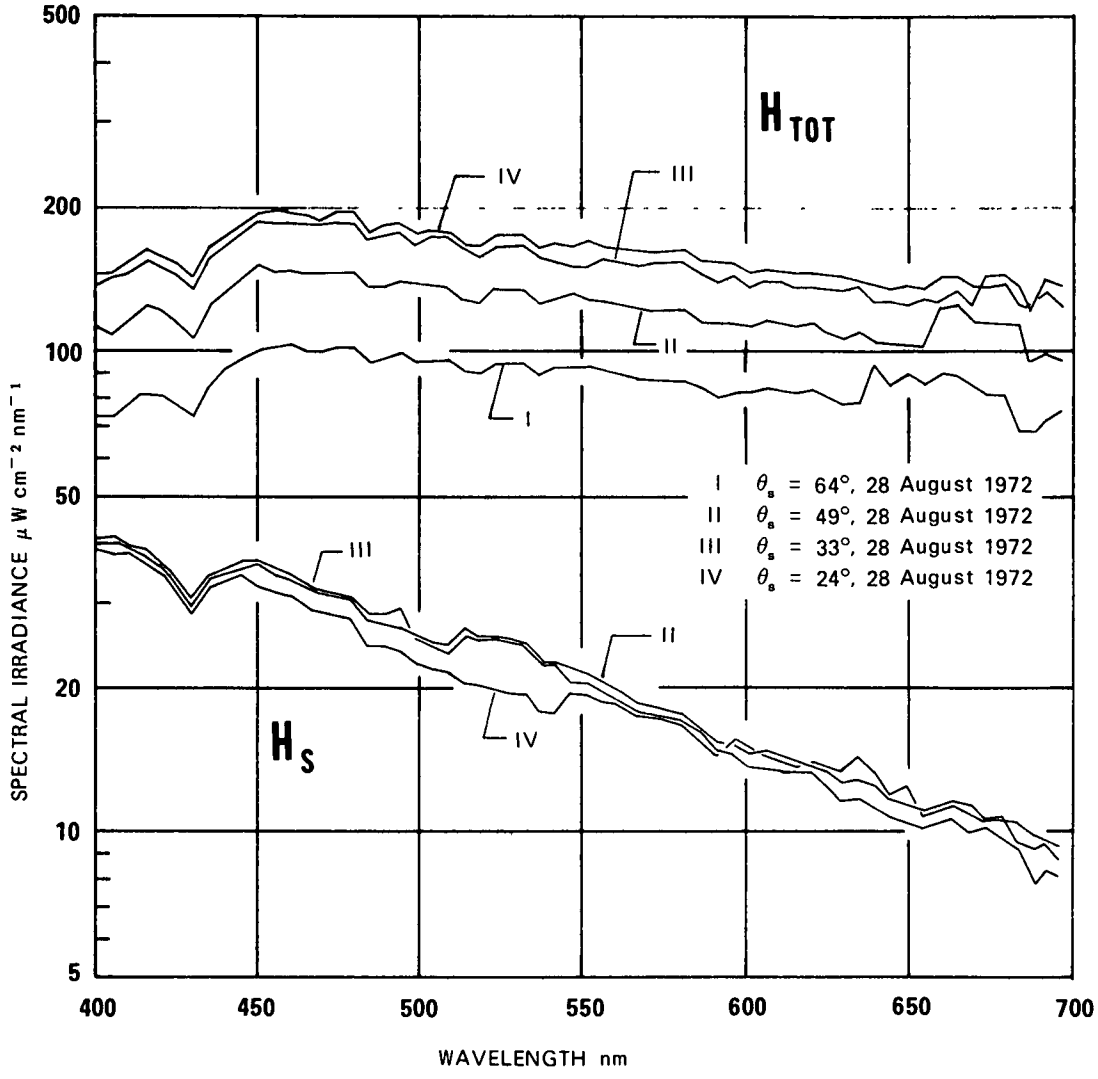

Fig. 5 Downwelling spectral irradiance measured on cloudless hazy day in San Diego, California. H_{TOT} is total downwelling irradiance. H_s is that contribution to the total downwelling irradiance from the sky without the sun. H_s for $\theta_s = 64°$ not shown but did not differ significantly from H_s for $\theta_s = 49°$.

reflects the relatively greater contribution of the sky irradiance to the total at the shorter wavelengths. This is also seen by the different slopes of the H_{tot} and H_s curves in Fig. 5. It may also be noted in Fig. 6 that the $1 - y$ curve for $\theta_s = 21°$ is appreciably higher in the red than that for $\theta_s = 24°$. The difference is more than would be expected for a 3° change in zenith angle and is attributable to the fact that 21 August was a much less hazy day than 28 August. Visibilities at the time of the measurements for curve I were reported to be 20 miles, vice 4 and 5 miles for curves II and III.

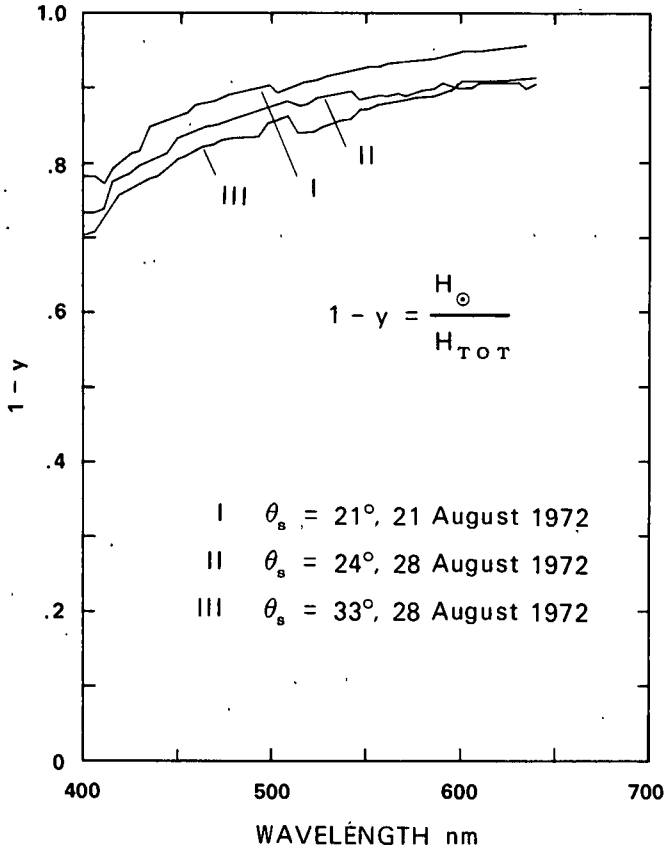

Fig. 6 Ratio of solar to total spectral irradiance for three solar zenith angles.

SUB-SURFACE IRRADIANCE REFLECTANCE

Having first approached the determination of N_w or R_w through direct measurement of N_u and H_{tot}, we will now present another approach which allows the utilization of an additional body of data. A

frequently used concept in optical oceanography is the underwater irradiance ratio, $R_{\pm}$. It will be defined here as the ratio of the upwelling to the downwelling horizontal irradiances at any depth, i.e.,

$$R_{\pm} = \frac{H_{+}}{H_{-}} . \tag{7}$$

Existing tabulations of $R_{\pm}(\lambda)$ for various waters can provide another source of information from which the above-water spectral signature may be obtained. Thus, $R_{\pm}$ provides the connection between the downwelling spectral irradiance and the upwelling spectral irradiance. It is now necessary to determine the coupling between the above surface and the below surface downwelling, irradiances, i.e., H_{tot} and H_{-}, and the relationship between N_u and H_{+}, to complete our development.

The two components of H_{tot}, i.e., $H_{\odot}$ and H_s, suffer different reflectance losses in passing through the water surface. The collimated light from the sun will be reduced by the fresnel reflectance of the surface associated with the sun zenith angle and the surface windspeed. Thus, the surface transmittance, t_d, for downwelling solar irradiance is

$$t_d = 1 - r_d ,$$

where values of r_d appropriate for various windspeed and zenith angles may be obtained from Table I.

The component of irradiance due to the sky, H_s, must be treated as an angularly distributed source and the contributions from the radiance of each portion of the sky individually propagated through the surface and summed. Because the contribution of H_s to the total irradiance is generally small we may assume the radiance of the sky to be uniformly distributed without introducing significant error in the final result. On this basis we may use values for the diffuse reflectance of the sea surface for computing the loss which the sky component suffers in being transmitted through the surface. Payne (1972) has found that the reflectance of the surface for a diffuse (heavily overcast) sky is 0.061 ±.005 which is in good agreement with Judd's (1942) calculation 0.0676 for the diffuse reflectance at an interface having a relative index of 1.34. We will, then, apply a diffuse transmittance for downwelling irradiance, $t'_d = 1 - r'_d$, of 0.94 to H_s.

The resulting H_{-} may now be taken as the sum of these two components, then

$$H_{-} = t'_d H_s + t_d H_{\odot} ,$$

or

$$H_{-} = [t'_d y + t_d (1 - y)] H_{tot} . \tag{8}$$

An estimate of the relationship between N_u and H_+ may be established on the basis of a set of measurements by Tyler (1960) in Lake Pend Oreille, Idaho. This lake, at the time of the measurements, was demonstrated to be vertically homogeneous in its physical properties. It thus provided an excellent medium for the exploration of the manner in which the apparent optical properties changed with depth. The primary measurements were of the angular distribution of radiance at 480 nanometers as a function of depth. These data were obtained on a sunny day ($\theta_s = 33.4°$) at seven depths from 4.24 meters to 66.1 meters. Figure 7 is a plot of the data obtained at a depth of 4.24 meters showing the relative upwelling radiance in three vertical planes intersecting through the vertical, at azimuth angles of 0° - 180°, 40° - 220°, and 90° - 270°. This plot shows a very significant departure from the uniform diffuse distribution which has been assumed to exist in some studies in the past.

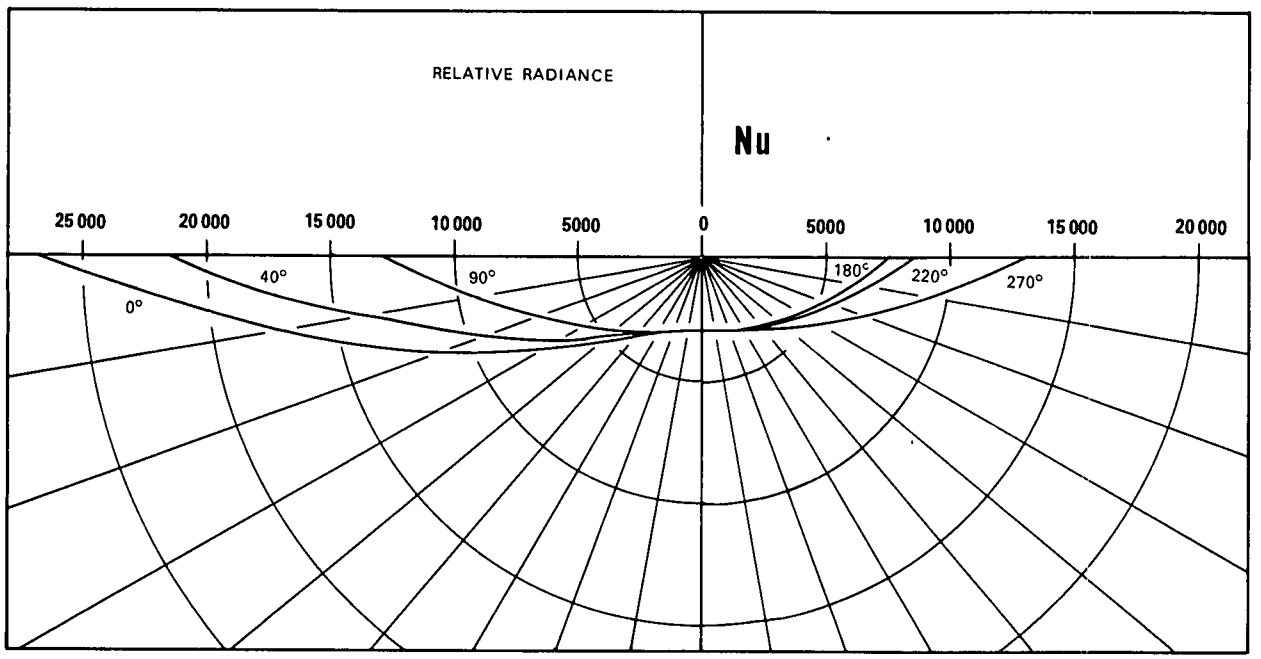

Fig. 7 Upwelling radiance distribution obtained at Lake Pend Oreille, Idaho (Tyler 1960), for 6 azimuth angles relative to the sun. Depth 4.24 meters, solar zenith angle 33.4°. The integrated upwelling irradiance H_+ for this distribution was 15 500 and the nadir radiance N_u was 3050, relative units.

By making the assumption that the distribution is uniform it follows that $N_u = H_+/\pi$. The actual distributions obtained by Tyler lead to a different result. The radiance distributions at six of the depths were integrated (Tyler *et al.* 1959) to obtain the irradiances corresponding to these distributions. The resulting ratios of irradiance to nadir radiance ranged from 5.08 to 5.40 as against the ratio of π resulting from the uniform diffuse assumption. The shape of the upwelling distribution may be expected to change

if the shape of the scattering function or the ratio of scattering to absorption coefficients in the water change significantly. The lower bound of the irradiance/radiance ratio in the absence of a highly reflective bottom is certain to be π, but the likelihood of the radiance distribution departing significantly from the Lake Pend Oreille data thus forcing the value of the ratio very far in that direction seems remote. As new data become available we are also prepared to expect that due to the spectral change in absorption the ratio may change somewhat with wavelength. For the present the best value for their H_+/N_u ratio would seem to be that calculated from the near surface (4.24 meters) case at Lake Pend Oreille, i.e., $H_+/N_u = 5.08$.

Based on the above and on Eq. (7) and (8) we can now write,

$$R_{\pm} = \frac{5.08\, N_u}{[t'_d\, y + t_d\,(1-y)]\, H_{tot}} \tag{9}$$

or alternatively,

$$N_u = \frac{R_{\pm}}{5.08}\,[t'_d\, y + t_d\,(1-y)]\, H_{tot}\,. \tag{10}$$

Using Eq. (3) to take N_u through the surface we find,

$$N_w = \frac{R_{\pm}}{5.08} \cdot \frac{t_e}{n^2}\,[t'_d\, y + t_d\,(1-y)]\, H_{tot}\,, \tag{11}$$

and finally combining Eqs. (2) and (11),

$$R_w = \frac{\pi}{5.08} \cdot \frac{t_e}{n^2}\,[t'_d\, y + t_d\,(1-y)]\, R_{\pm}\,. \tag{12}$$

The quantity in the square brackets, which will be called B, is common to Eqs. (9) through (12) and has been tabulated for two windspeeds, 0 and 16 meters per second, in Table III. Because t'_d and t_d are both close to 1.00 for all windspeeds and for all zenith angles out to 50° to 60°, there is little sensitivity to the value of y when the sun is above 60°, hence to the type of day or wavelength both of which affect y. When the sun is below 60°, i.e., nearer the horizon, B becomes significantly smaller and somewhat more dependent on the value of y.

Table III

Selected Values for Factor $B = [t'_d y + t_d(1 - y)]$ for Surface Windspeeds of 0 and 16 Meters Per Second

U = 0 m/s

θ_s / y	0°	40°	50°	60°	70°	80°
0 1	0.975	0.971	0 963	0.939	0 872	0.679
0 2	0.971	0.968	0.960	0 939	0 880	0 708
0.3	0.967	0.964	0 958	0.939	0 887	0 737
0.4	0.963	0.961	0.955	0.939	0 895	0 766

U = 16 m/s

θ_s / y	0°	40°	50°	60°	70°	80°
0.1	0.974	0.968	0.956	0.930	0.882	0.810
0.2	0.971	0.965	0 954	0.931	0 888	0 824
0.3	0.967	0 962	0.953	0 932	0 895	0 839
0.4	0.963	0.959	0 951	0 933	0.901	0 853

Note: $\theta_s = \theta_a$ is the solar zenith angle in air,

The term in front of the brackets in Eq. (12) is a constant having a value of 0.3365. Thus, the ratio of the above water to the underwater reflectances becomes

$$\frac{R_w}{R_{\pm}} = 0.3365\ B\ .$$

The credibility of these four equations can be demonstrated by comparing the values for $R_{\pm}$ computed from Eq. (9) with those obtained from measurements of H_- and H_+. Unfortunately, we do not have a case where H_{tot}, y, H_-, H_+, and N_u have been measured contemporaneously in the same ocean locations. We have, however, data from measurements obtained in different ocean locations at different times but at similar solar elevations which can be compared to show that we do find general agreement. One excellent source of data for underwater spectral irradiance data of the type required is the work of Tyler and Smith (1970). Data from three of their stations, one in the Gulf Stream and two in the Gulf of California, have been selected and computations made of the spectral irradiance reflectances, $R_{\pm}$, at 5 meters. These are plotted in Fig. 8. Note that the Gulf Stream data show a very high reflectance in the blue which is characteristic of the Gulf Stream water, and that the two stations in the Gulf of California show a marked reduction in the blue reflectance characteristic of the absorption found in biologically productive waters. The December 9, 1968 data obtained in water 160 meters deep near an island in the Gulf of California show a high green through yellow reflectance. The observed Munsell hue notation obtained at the station was 5G to 10GY, in agreement with the green-yellow computed underwater reflectance. A further observation made on-station was that the water was heavily silted. The station on May 9, 1969 was in the middle of the lower part of the Gulf of California in deep water away from the immediate effects of land. Whereas it showed the blue absorption noted earlier, it had about the same reflectance as the Gulf Stream water beyond 525 nanometers.

The solid curves are computed from the underwater radiance measurements obtained in August 1971 (Fig. 4) and the downwelling surface irradiance measurements obtained in August 1972 (two sets of data

from 28 August, shown in Fig. 5, and one set from 21 August). All days involved were cloud free at the times of the measurements. The solar zenith angles for the radiance and irradiance data sets were matched to within one degree. The general agreement between the $R_{\pm}$ curves derived from the disparate sources is excellent. The blue reflectance for curves I and III is slightly higher than that found in the Gulf of California, perhaps indicating there was less "yellow substance" in the San Pedro channel coastal waters. The "blue" water for Station 10 (curve II) was less blue than that of the Gulf Stream which, again, was not unexpected. The "green" water of Station 12 shows the same green-yellow maxima as the December 9, 1968 data. Certainly the two sets of reflectance data show sufficient similarity in their magnitudes, shapes, and features to provide confidence that the method is useful for remote sensing systems analysis.

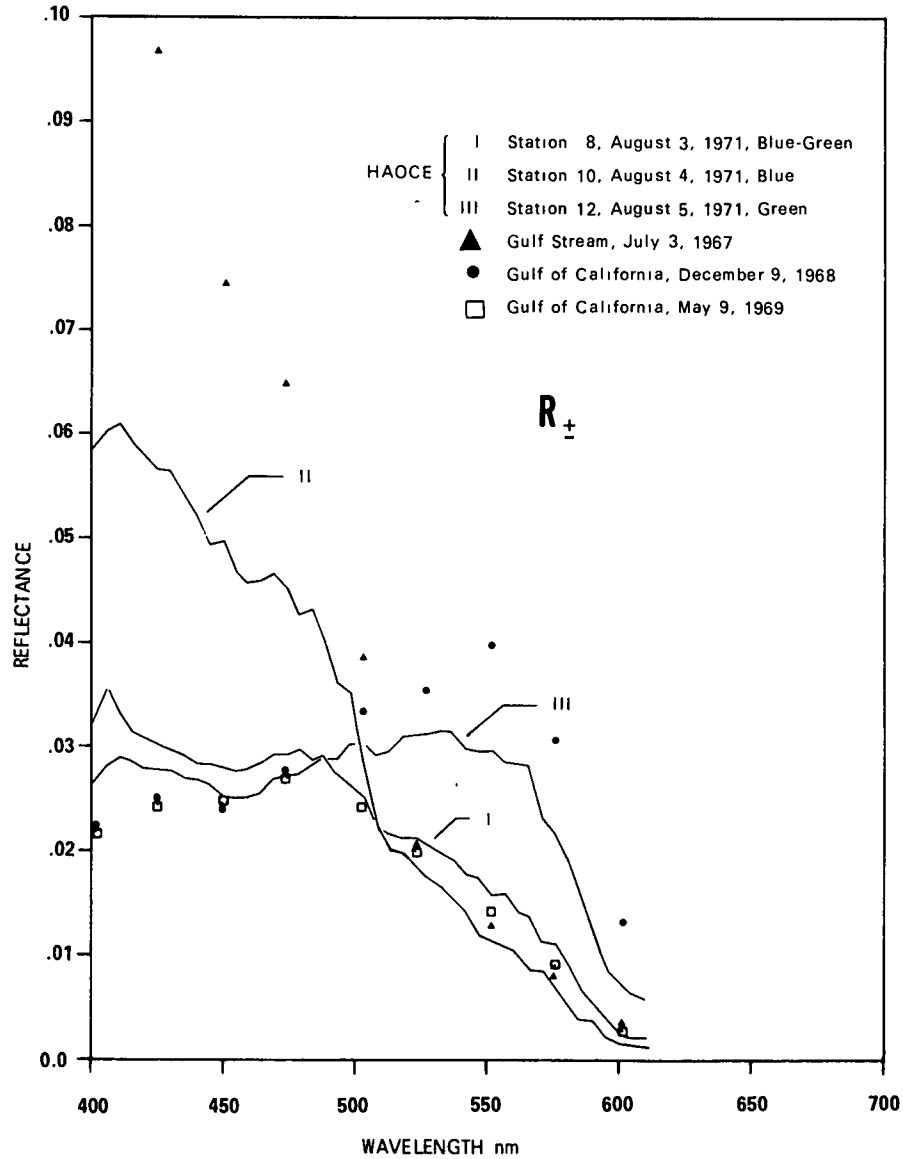

Fig. 8 Irradiance reflectance representing the ratio of upwelling to downwelling irradiance immediately below the ocean surface. Points from Tyler & Smith (1970).

SAMPLE INHERENT SPECTRAL RADIANCE SIGNALS

In Fig. 9 the upwelling spectral radiance of the water, N_w, as observed above the surface has been plotted for the three sub-surface cases shown in Fig. 4 by invoking the simple linear relationship of Eq. (3). Figure 10 shows zenith sky radiances, N_s, measured on occasions when the solar zenith angles were approximately the same as those occurring when the underwater radiance measurements were obtained. Note that the 21 August curve has a greater slope and falls appreciably below those for 28 August in consonance with the observation that the former day had a bluer sky and less haze (greater visibility). The lower curves show the spectral radiance of the sea surface, N_r, due to the reflection of the zenith sky. These latter three curves when added to the curves in Fig. 9 having corresponding sun positions provide the inherent nadir spectral radiance of the ocean surface, N_o. An example of this procedure is shown in Fig. 11 where the two components, radiances N_w and N_r, and their sum, N_o, are presented using the water radiance obtained on Station 10 (HAOCE), August 5, 1971.

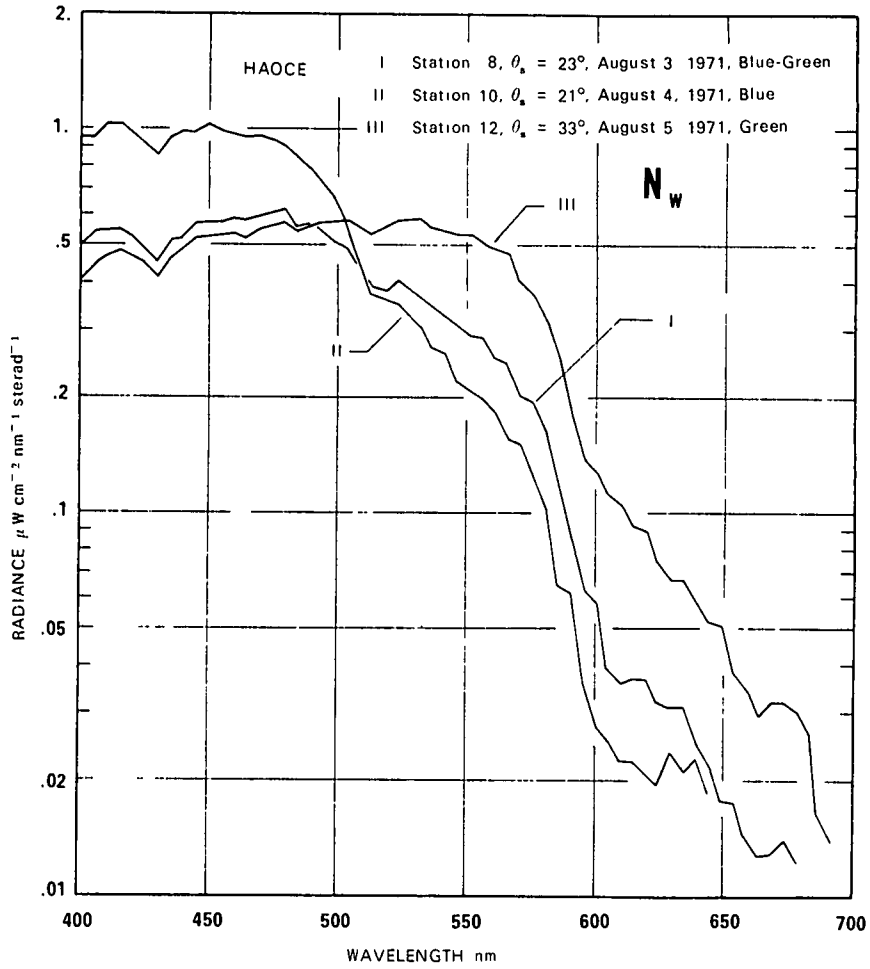

Fig. 9 Ocean surface radiance directed towards the zenith, due to the propagation of the underwater radiance N_u through the ocean surface. The two quantities are related as $N_w = t_e/n^2 N_u$.

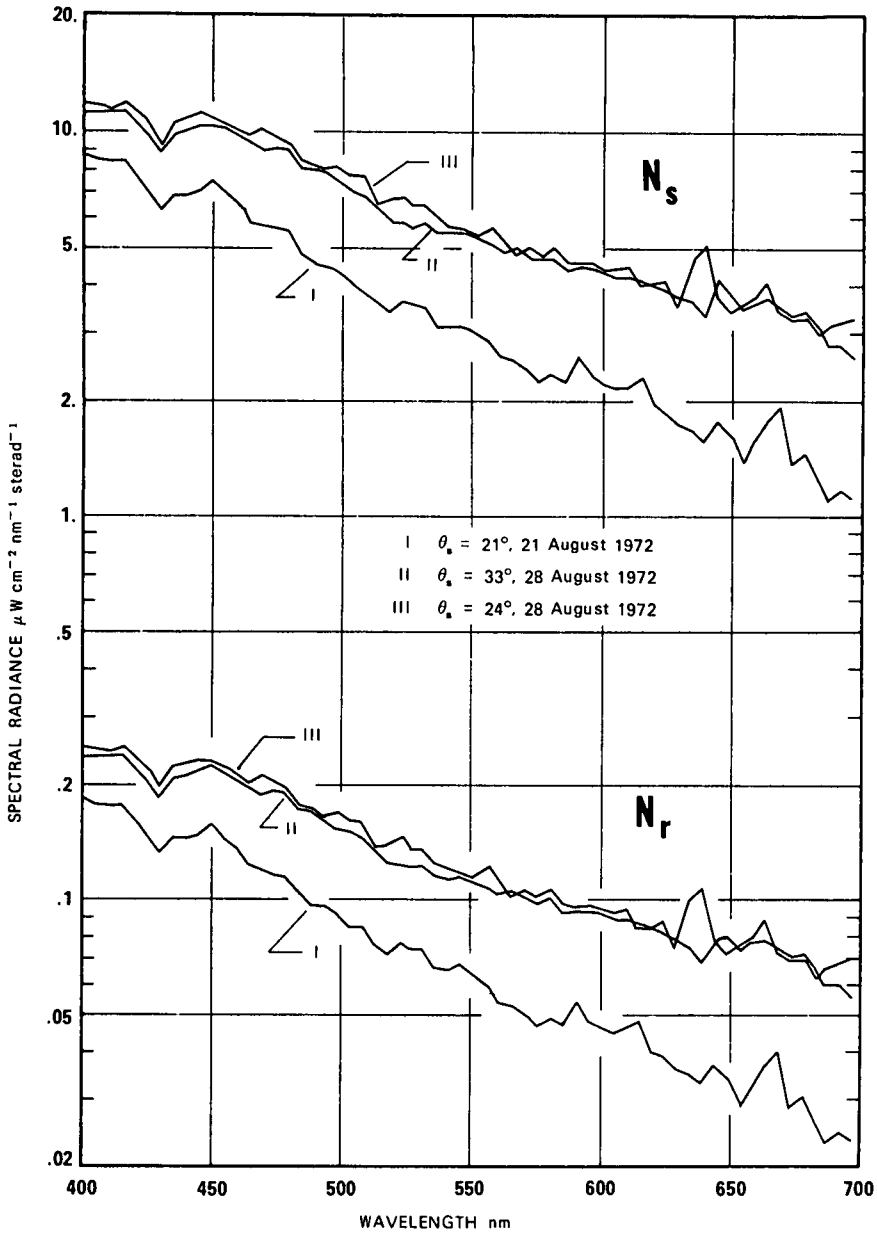

Fig. 10 Spectral radiance of the sky N_s at the zenith, and the reflected portion N_r at the sea surface for normal incidence. N_r has been computed from N_s through $N_r = 0.021 \cdot N_s$ where 0.021 is the Fresnel reflectance of the sea surface.

THE MODIFICATION OF THE SURFACE RADIANCE BY THE ATMOSPHERE

The last step in the process of determining the radiance reaching the remote sensor is accounting for the propagation of the inherent surface radiance through the atmosphere to the altitude of the sensor.

This topic will not be addressed here other than to provide the applicable basic equation of radiance transfer. The inherent radiance, N_o, leaving the surface will be reduced by the transmittance of the atmosphere, T_a, and augmented by the radiance of the path of sight, N^*. Thus, the apparent radiance, N_z, may be expressed as

$$N_z = N_o T_a + N^* ,$$

where T_a and N^* are functions of wavelength, the direction of the path of sight, and of course, the meteorological situation.

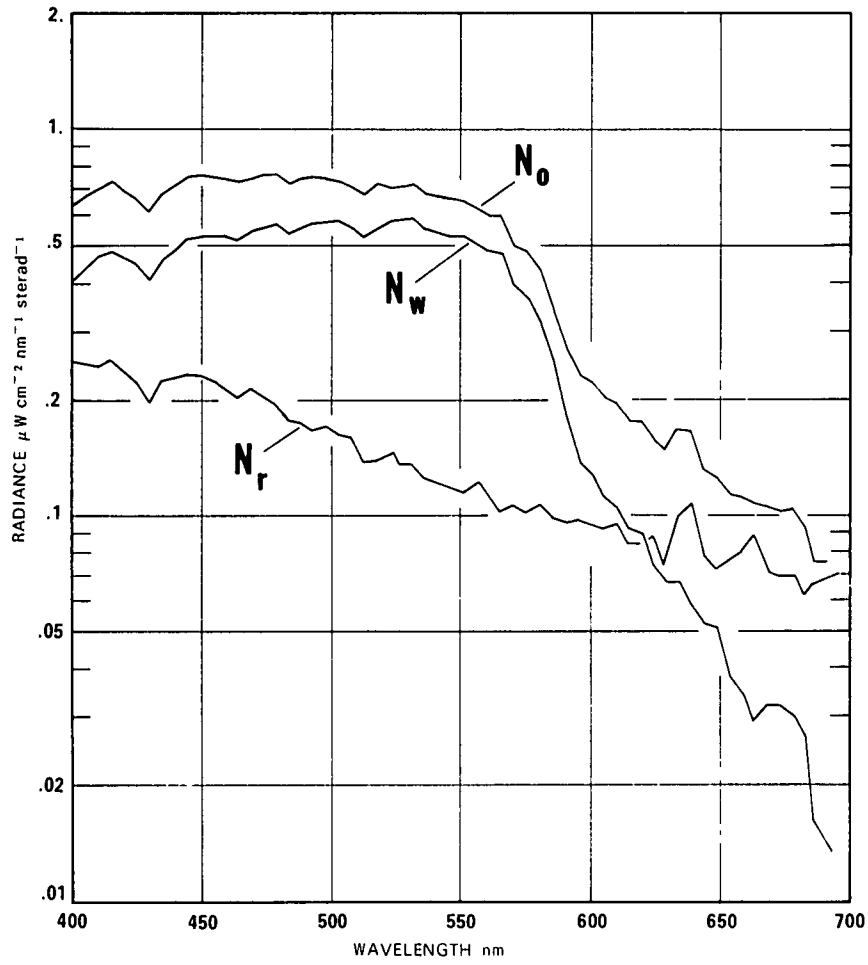

Fig. 11 Total zenith-directed radiance N_o of ocean surface, as a sum of the reflected zenith sky radiance N_r and the underwater nadir radiance transmitted through the surface N_w. Solar zenith angle, $\theta_s = 33°$.

2.3 SUMMARY

Inherent spectral radiance signatures for the ocean surface have been synthesized using data from measurements of the upwelling spectral radiance below the surface, N_u, and the zenith sky radiance, N_s. A second method was presented that relied on a knowledge of the underwater spectral irradiance reflectance, $R_{\pm}$, the total downwelling surface irradiance, H_{tot}, the ratio of sky to total irradiance, y, and the zenith sky radiance. The sensitivity of certain expressions to solar position have been shown. Data have been presented representative of the limited data bank of spectral measurements presently available. The accuracy of these data is generally satisfactory for most systems design or evaluation purposes. No significance should be attributed to the anomalous fluctuations which appear on some of the measured radiance and irradiance data which were due to temporary difficulties with instrument stability. Additional data for other conditions (e.g., solar elevation angles, atmospheric conditions, water properties, etc.) should be obtained. Some additional data is known to be available or is expected to become available from other studies and should be processed for presentation to interested users in the remote sensing community. The problems of paths of sight other than vertical, the solar glitter pattern and atmospheric effects should be similarly addressed in order to provide guidance on absolute magnitudes, and the spatial and spectral variability of these factors for the remote sensing problem.

REFERENCES

Brown, D. R. E. *Natural Illumination Charts.* Department of the Navy, Bureau of Ships, Wash. D. C., Report No. 374-1, Sept. 1952, PB 181522.

Clarke, G. L. and Gifford C. Ewing. "Application of Spectrometry to Biological Oceanography." Woods Hole Oceanographic Institution, WHOI-73-8, February 1973.

Gordon, J. I. *Directional Radiance (Luminance) of the Sea Surface.* University of California, San Diego, Scripps Institution of Oceanography, SIO Ref. 69-20, October 1969.

Judd, D. B. "Fresnel Reflection of Diffusely Incident Light." Department of Commerce, National Bureau of Standards, Research Paper RP1504, *Journal of Research of the National Bureau of Standards, Vol. 29,* Nov. 1942, pp. 329 - 332.

Payne, R. E. "Albedo of the Sea Surface. *"(Woods Hole Oceanographic Institution, Woods Hole, Mass., March 1972)." Journal of the Atmospheric Sciences, Vol. 29,* July 1972, pp. 959 - 970.

Tyler, J. E. "Radiance Distribution as a Function of Depth in an Underwater Environment." *Bulletin of the Scripps Institution of Oceanography of the University of California, La Jolla, California, Vol. 7, No. 5,* pp. 363 - 412. University of California Press, Berkeley and Los Angeles, California 1960.

Tyler, J. E., W. H. Richardson, and R. W. Holmes. "Method for Obtaining the Optical Properties of Large Bodies of Water." University of California, Scripps Institution of Oceanography, La Jolla, CA., *Journal of Geophysical Research, Vol.* **64**, *No. 6,* June 1959.

Tyler, J. E. and Raymond C. Smith. *Measurements of Spectral Irradiance Underwater.* New York: Gordon and Breach Science Publishers, 1970, 103 pp.

3. REFLECTANCE OF WHITECAPS, FOAM, AND SPRAY

R. W. Austin
Steve Moran

3.1 INTRODUCTION

This will be a brief report on the study of the reflectance of the ocean surface caused by wind-generated white water. Past photographic studies of the relationship between the fraction of the ocean surface covered by whitecaps have not had the benefit of good surface truth documentation (i.e., wind-speed,wave heights, etc.) or satisfactory means of processing the photographic data to remove the effects of the camera, the nonlinearities in the photographic process or the effects of the atmosphere. This project was initiated in 1969 to acquire, process, and analyze improved photographic data of the ocean surface with the objective of obtaining the reflectance statistics of the ocean surface as a function of wind-speed. Photography for the study was obtained by aircraft of the Earth Observations Aircraft Program Office of the NASA Manned Spacecraft Center on Missions 88, 119, and 156. The film processing has been handled by the Earth Resources Research Data Facility of MSC.

The material presented here shows, very briefly, the method of film data processing and the analysis technique used to convert the statistics of the densities on the film to the reflectances which were present in the scene. A sample analysis of a group of frames from Mission 88 is given as an illustration of the steps in the technique.

3.2 THEORY OF PROCESSING TECHNIQUE

The following is a description of the rationale and method used in the processing of the photographic data to obtain the reflectance statistics of the ocean surface.

The processing of ocean surface photography to yield surface reflectance data requires that one be able to accurately relate film density to inherent surface reflectance values. This relationship may be defined if the characteristic (H&D) curve for the film, the camera vignetting characteristics and the atmospheric properties between the target and photographic platform are known.

Reference may be made to Fig. 1 for an explanation of the terms used in the following development. If we let H be the irradiance on the ocean surface, N_o the inherent surface radiance, R the surface reflectance, T_r the atmospheric beam transmittance and N_r^* the atmospheric path radiance, then for a lambertian reflector

$$N_o(x,y) = \frac{R(x,y)H(x,y)}{\pi}. \tag{1}$$

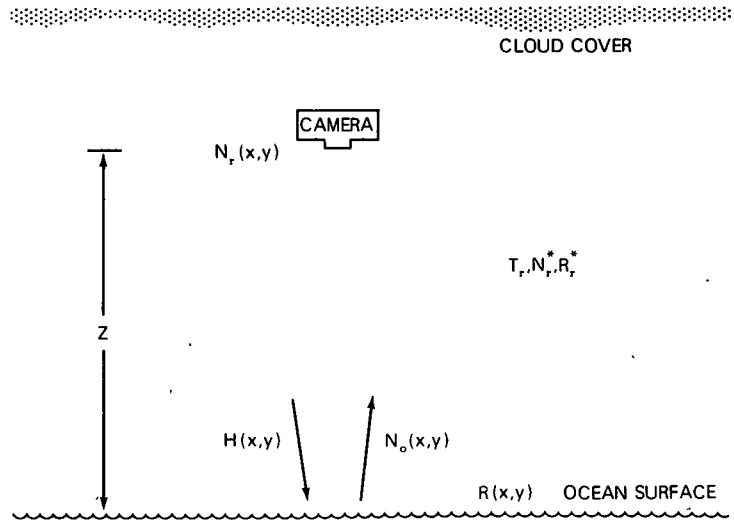

Z = Altitude of Camera Platform

θ = Zenith Angle of Path of Sight

$r = \frac{Z}{\cos\theta}$

H(x,y) = Surface Irradiance

R(x,y) = Surface Reflectance

$N_o(x,y)$ = Surface Radiance

$N_r(x,y)$ = Radiance at Altitude Z for Path of Sight r

T_r = Atmospheric Beam Transmittance for Vertical Path "r"

N_r^* = Atmospheric Path Radiance for Vertical Path "r"

R_r^* = Atmospheric Path Reflectance for Vertical Path "r"

$$N_o(x,y) = \frac{R(x,y)H(x,y)}{\pi} \qquad N_r(x,y) = N_o(x,y)T_r + N_r^* \qquad R_r^* = \frac{\pi N_r^*}{T_r H(x,y)}$$

Fig. 1. Definition of Variables Used in White Water Reflectance Study.

If N_r denotes the apparent surface radiance measured at the camera entrance pupil, then we have

$$N_r(x,y) = T_r N_o(x,y) + N_r^* . \tag{2}$$

The vignetting-corrected camera transmittance function $T_c(x,y)$ which relates apparent surface radiance at the camera entrance pupil to film exposure, $E(x,y)$, may be defined as follows

$$E(x,y) = t T_c(x,y) N_r(x,y) \tag{3}$$

where t is the exposure time. The variables x and y are coordinates at the camera film plane. Substituting (2) in (3) we have

$$\frac{E(x,y)}{t T_c(x,y)} = T_r N_o(x,y) + N_r^* \tag{4}$$

and

$$N_o(x,y) = \frac{E(x,y)}{t T_r T_c(x,y)} - \frac{N_r^*}{T_r} = \frac{R(x,y) H(x,y)}{\pi} . \tag{5}$$

Solving for R we obtain

$$R(x,y) = \frac{\pi}{H(x,y) T_r t T_c(x,y)} E(x,y) - \frac{\pi N_r^*}{T_r H(x,y)} . \tag{6}$$

Now defining the path reflectance R_r^* as

$$R_r^* = \frac{\pi N_r^*}{T_r H(x,y)} ,$$

equation (6) then becomes

$$R(x,y) = \frac{\pi}{H(x,y)T_r t T_c(x,y)} E(x,y) - R_r^*(x,y) \quad (7)$$

If the irradiance on the ocean surface is uniform, $H(x,y) = H = \text{const.}$

$$R(x,y) = \frac{\pi}{H T_r T_c(x,y) t} E(x,y) - R_r^*(x,y) \quad . \quad (8)$$

Equation (8) relates vignetting corrected film exposure values to inherent target reflectance values. The relationship is linear with slope

$$M = \frac{\pi}{H T_r T_c(x,y) t}$$

and intercept R_r^*.

The implementation of Equation (8) may be divided into three discrete tasks. First, the conversion of film density values to relative film exposure values. Second, correction of relative exposure values for camera vignetting and compiling exposure statistics. Third, conversion from corrected relative exposure statistics to inherent target reflectance statistics.

The conversion of film density values to relative exposure values is accomplished via a 21-point H&D curve which is obtained by scanning the duplicated sensitometric step tablet which was printed on the original negative before development. The film characteristic curve for Mission 88, RC-8, Roll 2 is shown in Fig. 2. Linear interpolation is used to convert density values which fall between the plotted values. This is swiftly done by computer using the table lookup technique.

Correction of the relative exposure values for camera vignetting is facilitated by a plot of camera transmittance isolines as a function of position in the film plane. In general, the transmittance function is not radially symmetric. However, a radially symmetric approximating function is fitted to the plot so that a single polynomial can provide transmittance data as a function of distance, R, from the center of the film plane. The camera transmittance curve used for the Wild RC-8 is shown in Fig. 3. The scanning subroutine calculates the distance of each data element from the center of the film. Vignetting effects are compensated for by dividing the relative exposure value at a given point by the transmittance polynomial evaluated at that point. Following this phase, the corrected log exposure statistics are compiled, and a card deck output of the cumulative distribution function (C.D.F.) of corrected relative exposures is punched.

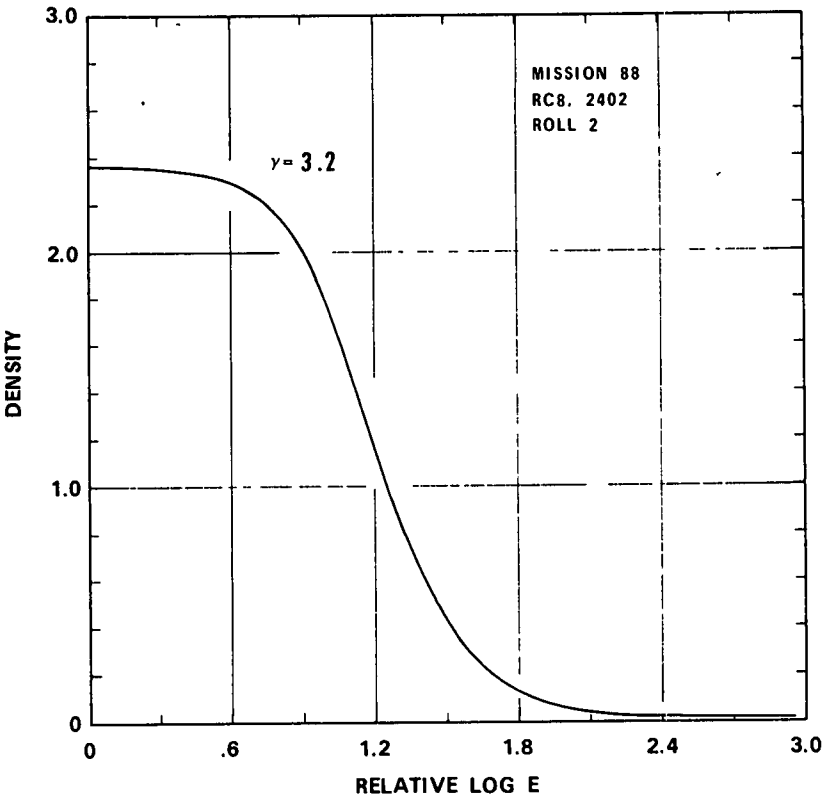

Fig. 2

Characteristic (H&D) Curve for Film Duplicate, i.e., Density of Duplicate vs Log Exposure on Original Negative.

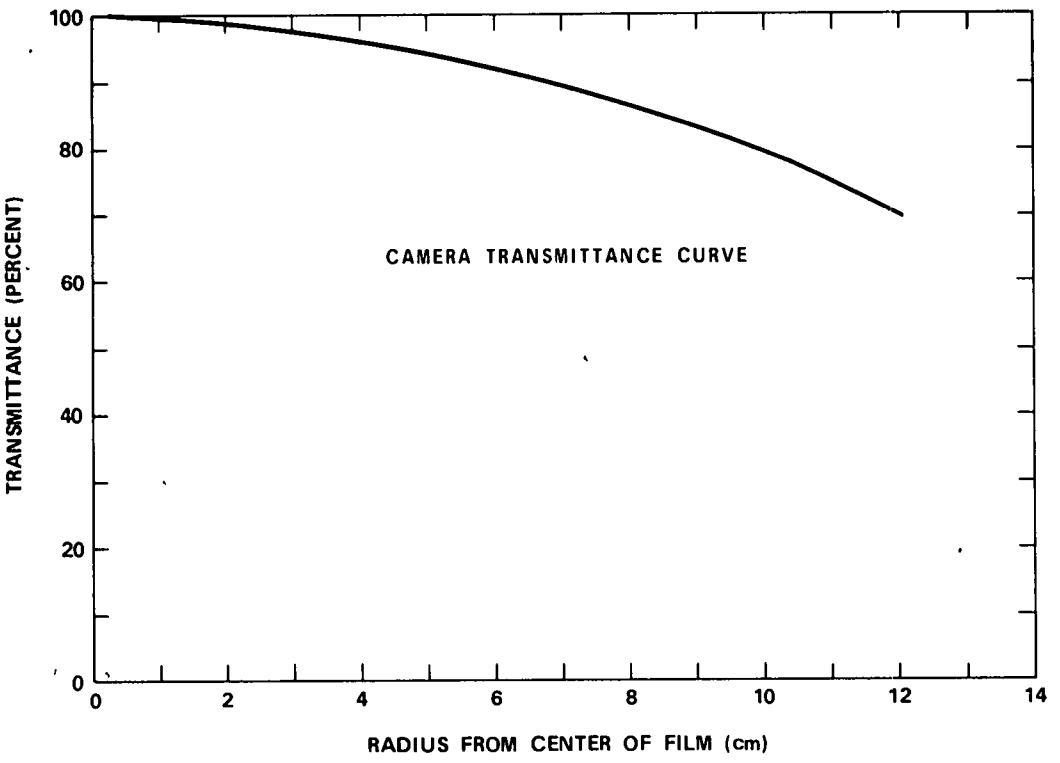

Fig. 3

The conversion of log exposure statistics to reflectance statistics requires that M and R_r^* be known. These values may be determined if the reflectance of two points in the target can be established. The fresnel reflectance of nonwhite areas of the sea surface is approximately 2 percent. The maximum diffuse reflectance of a typical whitecap is approximately 80 to 90 percent. By determining the relative exposure associated with each of these two regions the slope and intercept of the reflectance vs relative exposure line can be calculated. Given M and R_r^* and the log exposure C.D.F. card deck, a computer subroutine calculates, prints, and plots the reflectance statistics and punches the reflectance C.D.F. on cards.

3.3 MISSION 88 SAMPLE DATA ANALYSIS

A selection of eight frames of photography of the ocean surface obtained on Mission 88, Flight 6, line 53 over the North Sea on 14 March 1969 have been analyzed (using the technique described in 3.2). The results of this analysis are presented as a preview of the more general and complete report which will provide an analysis of photography obtained under a variety of windspeed conditions encountered on Missions 119 and 156 (JOSS I and JOSS II).

The particular photography obtained on this flight represents a unique body of data acquired under documented high windspeed conditions (48 to 50 knots). A total of 21 frames on line 53 show the appearance of the sea surface from 1500 feet with remarkable pictorial clarity. Unfortunately, some of the photometric controls desirable for a proper analysis of the data in order to obtain sea surface reflectance were lacking on this mission. Also, the initial quality of the black and white positive duplicate prints was inadequate to permit good photographic photometry. (A fourth copy has recently been received which appears to have suitable characteristics but it was not received in time to be used in this present analysis.)

The eight frames, representing an area on the ocean surface of 6.6×10^5 square meters, were scanned on a high speed electronic microdensitometer (Optronics International Model P1000). The scanning resolution was 50 micrometers on the film representing 0.15 meters on the ocean surface. The density data have been converted to surface reflectances in accordance with the procedure outlined in Section 3.2. The reflectance statistics for all eight frames have been combined and the combined cumulative distribution function for the sea surface reflectance is shown in Figs. 4 and 5. Figure 5 is an expanded version of Fig. 4 showing reflectances from approximately 17 to 47 percent. A histogram of reflectances is presented in Fig. 6. To facilitate the interpretation of the data depicted in Figs. 4 through 6, a reflectance profile of the ocean surface is presented in Fig. 7. The profile includes (1) a fresh whitecap, (2) foam from an older whitecap, and (3) nonwhite area. Figures 8 and 9 are expanded profiles of foam and whitecap, respectively. The regions they occupy in Fig. 7 are indicated in gray.

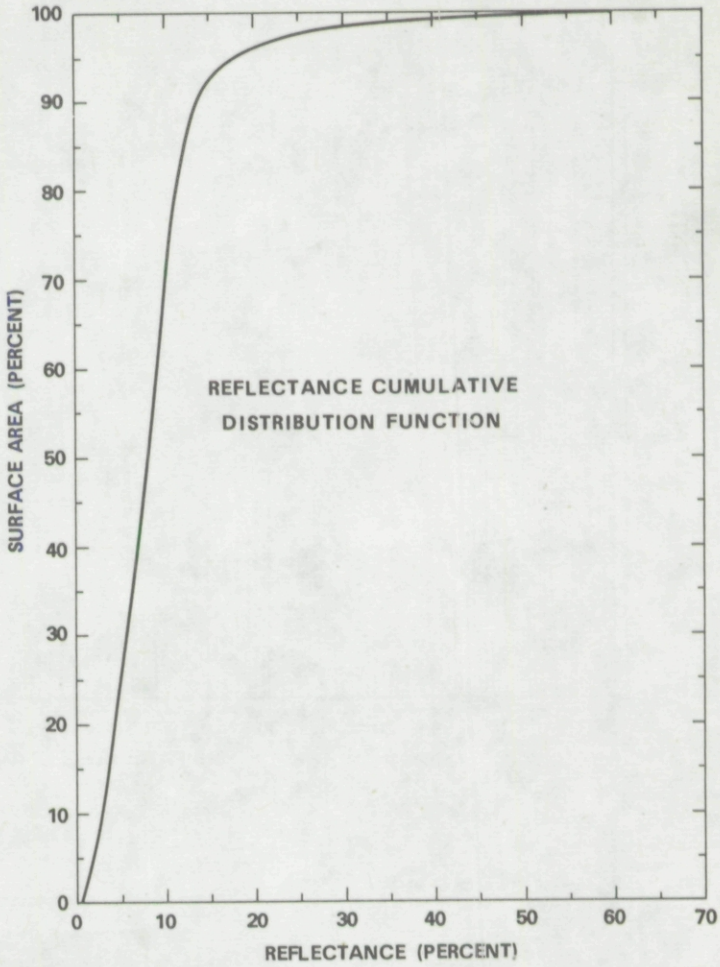
100
90
80
70
60
50
40
30
20
10
0
SURFACE AREA (PERCENT)
REFLECTANCE CUMULATIVE
DISTRIBUTION FUNCTION
0
10
20
30
40
50
60
70
REFLECTANCE (PERCENT)

Fig. 4

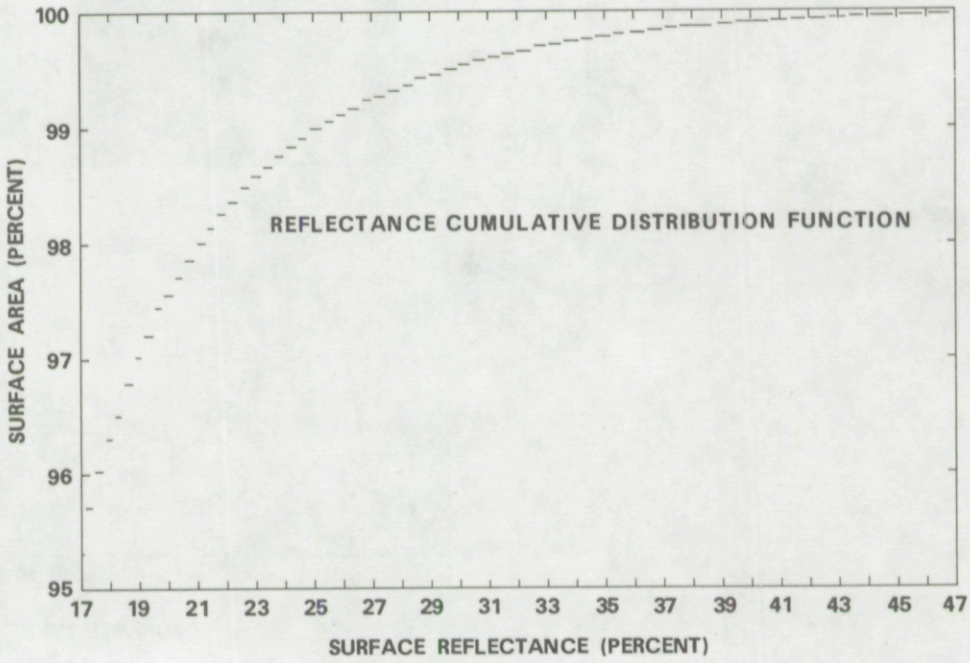
100
99
98
97
96
95
SURFACE AREA (PERCENT)
REFLECTANCE CUMULATIVE DISTRIBUTION FUNCTION
17
19
21
23
25
27
29
31
33
35
37
39
41
43
45
47
SURFACE REFLECTANCE (PERCENT)

Fig. 5

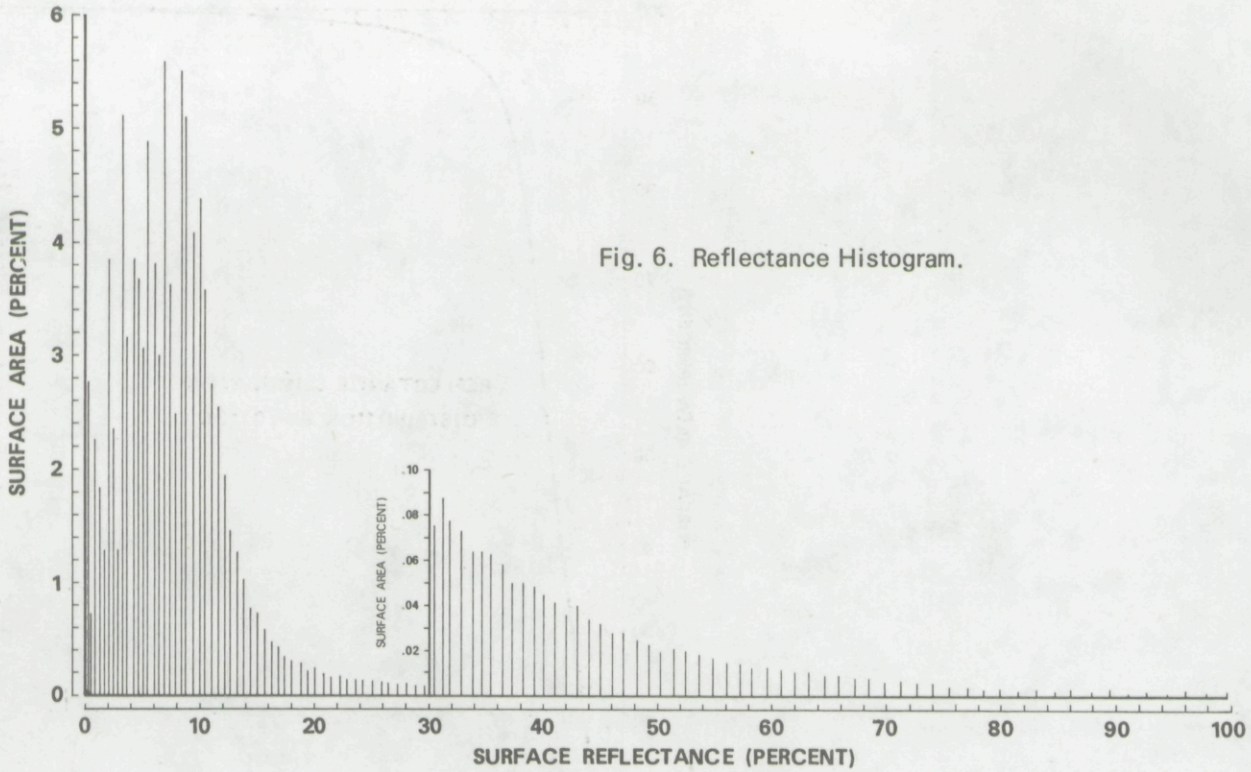

Fig. 6. Reflectance Histogram.

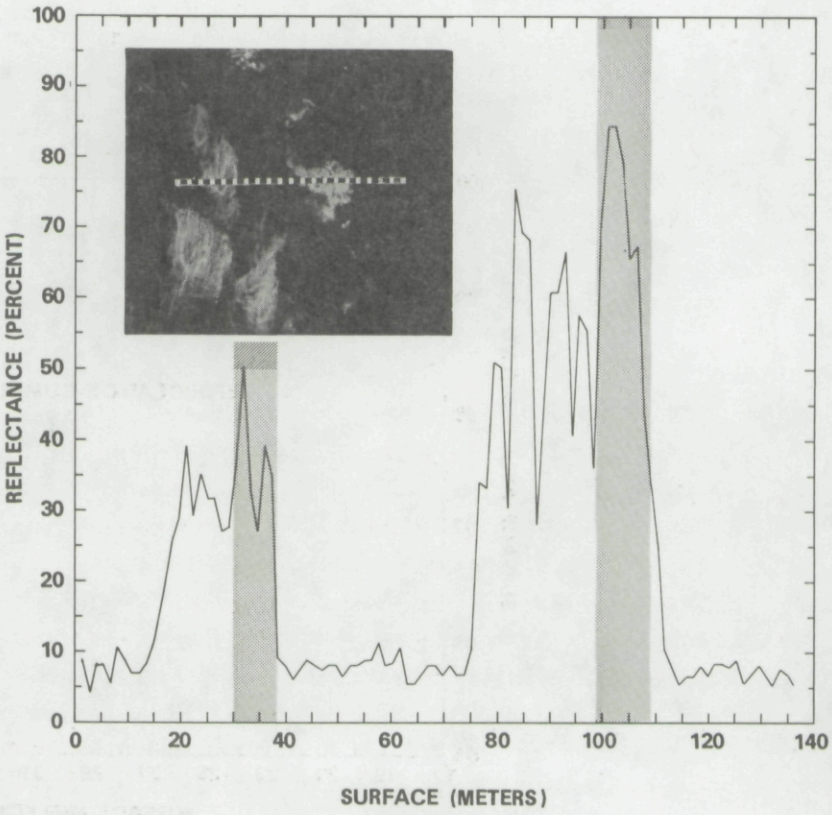

Fig. 7.
Surface Reflectance Profile.

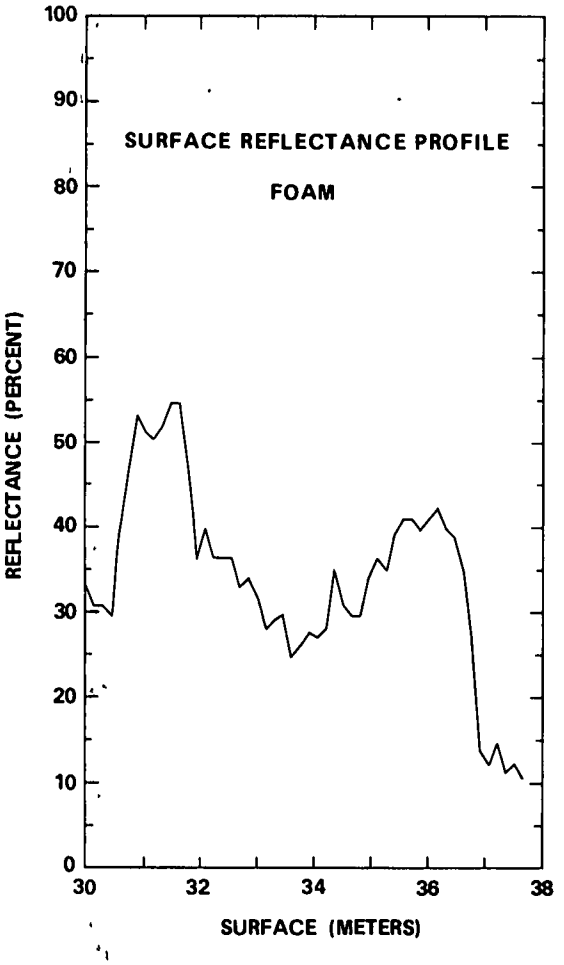

Fig. 8

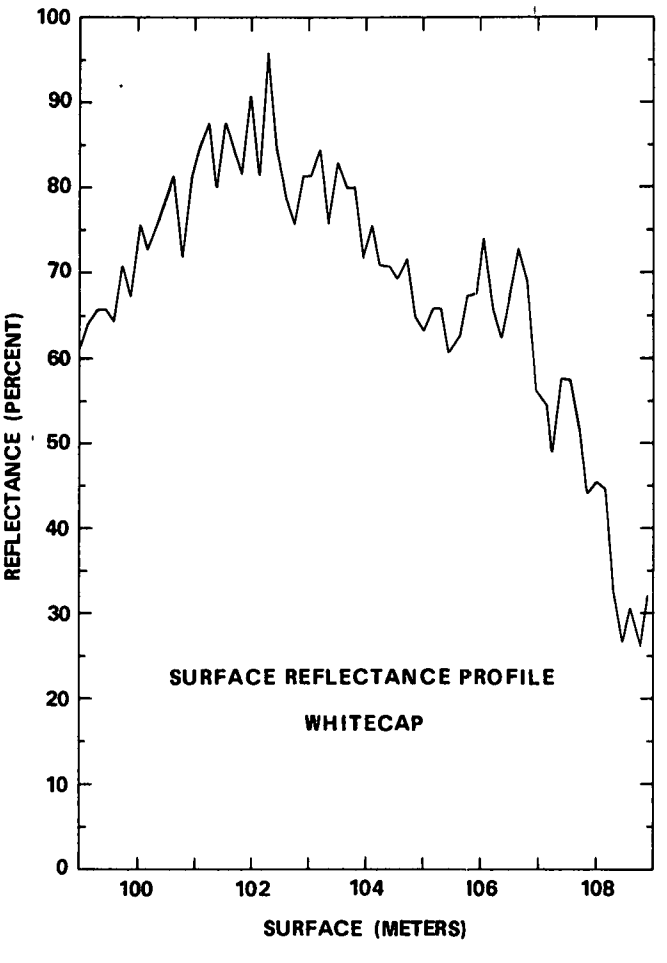

Fig. 9

3.4 SUMMARY

Most previous investigators have assessed the percentage of whitecap coverage using subjective outlining technique on photographs of the sea surface. This severely limits the information that can be obtained since it requires that the investigator impose a binary structure on the scene. Thus, the surface is divided into subregions that are deemed, in the judgment of the investigator, to contain "white water"—all other regions are consequently dark water. Furthermore, the decision is biased by transfer characteristics of the processed photographic materials used in the study. Information as to the reflectance properties of the water within the delineated subregion is not obtained nor is it possible, after the fact, to determine the threshold reflectance value that the investigator used as his decision criteria for "white." These become particularly important concerns at the higher sea states if one is interested in determining the effective reflectance of the total surface or if it becomes necessary to differentiate between the area covered with the dense white foam of a freshly formed whitecap and the area covered by the considerably less dense (and lower reflectance) foam of wind-generated streaks and older decaying whitecaps.

As opposed to the single number representing the fractional area covered with white water which is derived from the subjective outlining technique, the technique which we are using provides more complete reflectance statistics obtained from photographs obtained under known surface windspeed conditions and processed to a known transfer characteristic. Thus, it is difficult to compare our results directly with the findings of, say, Blanchard (1963) or Monahan (1971). The primary result is a histogram (Fig. 6) giving the fraction of the surface having a particular reflectance value (more correctly the fraction having reflectances falling within a small increment or range of values). A running summation of the histogram provides curves of the cumulative distribution function of reflectances (Figs. 4 and 5) which show as the ordinate the fraction of the surface having a reflectance less than the value shown as the abscissa.

Figure 7 shows a selected area from one of the eight Mission 88 frames which were scanned. This small area is not intended to be statistically representative of the group of frames but rather, to have within a small area both a new (right) and an old (left) whitecap. The reflectance profile shown in Fig. 7 (and much enlarged in Figs. 8 and 9) depicts the manner in which the reflectance of the whitecap varies with position and time (i.e., new and old whitecaps). The apparent variability of the background reflectance is due to the variations in sky (cloud) radiance in the particular direction being reflected by the wave facet being viewed. The average reflectance value of the background in this particular selected area is about 7 to 8 percent, whereas the value assigned to the minimum background reflectance found over the total area of each frame was 2 percent. Thus, the background in this selected region has approximately the same reflectance as the average for the entire area of the ensemble of eight frames (i.e., Fig. 4 shows that 50 percent of the area had a reflectance greater than 8 percent). Certainly in this region inspection of the profiles shown in Figs. 7, 8, and 9 indicates reflectances in excess of about 11 percent could be considered due to "white" water and from Fig. 4 we see that 75 percent of the surface had reflectances less than this value. Had we been using an outlining technique, then, and applied a threshold reflectance criteria of 11 percent we would have said that 25 percent of the surface was covered with whitecaps; however, we see in Fig. 5 that only 2.5 percent of the surface has a reflectance greater than 20 percent and a trivial portion has reflectance values in excess of 40 percent.

Additional scanning and analysis may show some changes in the exact placement of the reflectance scale and these present results should be treated as tentative until they can be combined with those from other windspeeds and the overall analysis completed.

REFERENCES

Blanchard, D. C. *The Electrification of the Atmosphere by Particles From Bubbles in the Sea.* Progress in Oceanography, Vol. 1, New York: Pergamon Press, pp. 71-202.

Monahan, E. C. "Oceanic Whitecaps." Journal of Physical Oceanography, **1**, 139 (1971).

UNCLASSIFIED
Security Classification

DOCUMENT CONTROL DATA - R&D

(Security classification of title, body of abstract and indexing annotation must be entered when the overall report is classified)

1 ORIGINATING ACTIVITY *(Corporate author)*
University of California, San Diego
Visibility Laboratory
San Diego, California 92152

2a. REPORT SECURITY CLASSIFICATION
UNCLASSIFIED

2b. GROUP

3 REPORT TITLE

OCEAN COLOR ANALYSIS

4 DESCRIPTIVE NOTES *(Type of report and inclusive dates)*
Final Technical

5 AUTHOR(S) *(Last name, first name, initial)*

Duntley, Siebert Q., Austin, Roswell W., Wilson, Wayne H.,
Edgerton, Catherine F., and Moran, Steven E.

6 REPORT DATE	7a TOTAL NO OF PAGES	7b NO OF REFS
April 1974	70	14

8a. CONTRACT OR GRANT NO	9a. ORIGINATOR'S REPORT NUMBER(S)
N00014-69-A-0200-6033 b. Grant No. 04-3-158-64	SIO Ref. 74-10
c.	9b. OTHER REPORT NO(S) *(Any other numbers that may be assigned this report)*
d.	

10 AVAILABILITY/LIMITATION NOTICES

Approved for public release; distribution unlimited.

11 SUPPLEMENTARY NOTES	12 SPONSORING MILITARY ACTIVITY
	Naval Research Laboratory, Washington, D. C. 20390 National Oceanographic and Atmospheric Agency, Washington, D. C. 20233

13 ABSTRACT

Three phases of the contract effort are summarized. The first is a study of the apparent spectral signal available to a remote sensor flying over ocean waters. The effect of solar zenith angle, atmospheric conditions, windspeed, spectral region, and direction of view on the sensitivity to small changes in chlorophyll concentration are considered. The second phase was the development of a method of synthesizing the inherent spectral radiance signature of the ocean surface. New measurements of the downwelling spectral irradiance at the ocean surface and the radiance of the zenith sky are presented. These measurements are used as inputs to the synthesis program. The third phase is the study of the reflectance characteristics of the ocean surface when wind-generated whitecaps, foam, and spray are present. A description of the methodology and some preliminary results are presented.

DD FORM 1 JAN 64 1473

UNCLASSIFIED
Security Classification

14 KEY WORDS	LINK A		LINK B		LINK C	
	ROLE	WT	ROLE		ROLE	WT
Ocean Color						
Remote Sensing						
Solar Glitter						
Sea Radiance						
Whitecaps						